A one-year ACSM source analysis of organic aerosol particle contributions from anthropogenic sources after long-range transport at the TROPOS research station Melpitz

Samira Atabakhsh[1], Laurent Poulain[1], Gang Chen[2,3], Francesco Canonaco[2,4], André Prévôt[2], Mira Pöhlker[1], Alfred Wiedensohler[1], Hartmut Herrmann[1]

[1]Leibniz Institute for Tropospheric Research, Leipzig, 04318, Germany
[2]Laboratory of Atmospheric Chemistry, Paul Scherrer Institute, Villigen, Aargau, 5232, Switzerland
[3]MRC Centre for Environment and Health, Environmental Research Group, Imperial College London, London, W12 0BZ, U.K.
[4]Datalystica Ltd., Park innovAARE, Villigen, Aargau, 5234,Switzerland

Correspondence to: Hartmut Herrmann (herrmann@tropos.de)

Abstract

Atmospheric aerosol particles are a complex combination of primary emitted sources (biogenic and anthropogenic) and secondary aerosol resulting from ~~the~~ aging processes such as condensation, coagulation,~~,~~ and cloud processing. To better understand their sources, investigations have been focused on urban areas in the past, while rural-background stations are normally less impacted by surrounding anthropogenic sources. Therefore, they are predisposed for studying the impact of long-range transport of anthropogenic aerosols. Here, the chemical composition and organic aerosol sources of submicron aerosol particles measured by an aerosol chemical speciation monitor (ACSM) and a multi-angle absorption photometer (MAAP) were investigated at Melpitz from September 2016 to August 2017. The location of the station at the frontier between Western and Eastern Europe makes it the ideal place to investigate the impact of long-range transport over Europe. Indeed, the station is under the influence of less polluted air masses from westerly directions and more polluted continental air masses from Eastern Europe~~To better understand their sources, investigations have been focused on source identification in urban areas in the past, while rural background stations are normally less impacted by surrounding anthropogenic sources. Therefore, they are predisposed for studying the impact of long range transport of anthropogenic aerosols. Moreover, long term measurements can help to study the potential temporal changes in the sources. Here, the chemical composition and organic aerosol sources of submicron aerosol particles were investigated at the Central European rural background research station, Melpitz, using a one yearlong dataset determined by an aerosol chemical speciation monitor (ACSM) and a multi angle absorption photometer (MAAP) from September 2016 to August 2017. Melpitz represents due to its location the Central European aerosol. It is an ideal location to investigate the impact of long range transport, since the location is influenced by less polluted air masses from westerly directions and more polluted continental air masses from Eastern Europe~~. The ~~organic aerosol (~~OA~~)~~ dominated the submicron particle mass concentration and showed strong seasonal variability ranging from 39 % (in winter) to 58 % (in

summer). It was followed by sulphate (15 % and 20 %) and nitrate (24 % and 11 %). The OA source identification was performed using the rolling positive matrix factorisation (PMF) approach to account for the potential temporal changes in the source profile (SoFi Pro). It was possible to split OA into five ~~-~~factors with a distinct temporal variability and mass spectral signature. Three were associated ~~to~~ with anthropogenic primary OA (POA) sources: hydrocarbon-like OA (HOA, 5.2 % of OA mass in winter and 6.8 % in summer), biomass burning OA (BBOA, 10.6 %, and 6.1 %) and coal combustion OA (CCOA, 23 %, and 8.7 %). Another two are secondary/processed oxygenated OA (OOA) sources: less-oxidized OOA (LO-OOA, 28.4 %, and 36.7 %) and more-oxidized OOA (MO-OOA, 32.8 %, and 41.8 %). Since equivalent black carbon (eBC~~eBC~~) was clearly associated with the identified POA factors (sum of HOA, BBOA, and CCOA, R^2= 0. 87), eBC~~eBC~~'s contribution to each of the POA factors was achieved using a multi-linear regression model. Consequently, CCOA represented the main anthropogenic sources of carbonaceous aerosol (sum of OA and eBC~~eBC~~) not only during winter (56 % of POA in winter) but also in summer (13 % of POA in summer), followed by BBOA (29 % and 69 % of POA in winter and summer, respectively) and HOA (15 % and 18 % of POA in winter and summer, respectively). A seasonal air mass cluster analysis was used to understand the geographical origins of the different aerosol types and showed that during both winter and summer time, PM_1 (PM with an aerodynamic diameter smaller than 1µm) air masses with eastern influence was always associated with the highest mass concentration and the highest coal combustion fraction. Since during winter time, CCOA is a combination of domestic heating and power plants emissions, the summer contribution of CCOA ~~emphasises~~ emphasizes the critical importance of coal power plants emissions to rural ~~-~~background aerosols and its impact on air quality, through long-range transportation.

1 Introduction

Human health effects of air pollution from particulate matter (PM) are well known, and efforts are being made across the world (*WHO, Expert Consultation*, 2019) to minimize both long-term exposures to harmful levels and air pollution peaks. ~~Throughout all the PMs, the~~ The submicronic particles known as PM_1 (particles with an aerodynamic diameter less than 1 µm), not only have a negative impact on human health (Pop and Dockery, 2016; Daellenbach et al., 2020) but also have a significant effect on visibility (Shi et al., 2014) and climate (Shrivastava et al., 2017). It is ability to penetrate to respiratory system make it more dangerous, therefore more relevant to mitigate adverse health impact ~~submicronic particles known as PM_1 (particles with an aerodynamic diameter less than 1 µm), not only have a negative impact on human health (Daellenbach et al., 2020) but also have a significant effect on visibility (Shi et al., 2014) and climate (Shrivastava et al., 2017)~~. Since the most numerous component of the atmospheric PM is the organic aerosol (OA) (Jimenez et al., 2009; Chen et al., 2022), contributions to OA and explanations of its chemical and physical characteristics remain challenging, whereas the large variety of OA can be attributed to primary emissions by various sources in different seasons, as well as different reactions to atmospheric dynamics and complicated chemical mechanisms depending on meteorological parameters and geographical locations.

In order to evaluate and recognize the sources of OA emission, aerosol mass spectrometers (AMS, Jayne et al., 2000) and aerosol chemical speciation monitors (ACSM) (Ng et al., 2011; Fröhlich et al., 2013) are widely deployed worldwide (Chen et al., 2022; Bressi et al., 2021; Fröhlich et al., 2015). AMS is commonly limited to short time periods due to the high maintenance of the AMS measurements and their high operating costs. As a result, only a few studies run AMS continuously (e.g., see Kumar et al., 2022 and O'Dowd et al., 2014). However, there was still a strong need for such a long-term analysis. ACSM is designated for long-term monitoring purposes due to its robustness and much less labour-intense compared to AMS. Therefore, the deployment of ACSM allows us to look at the long-term (more than one year) temporal changes and/or seasonal variability of OA sources.

Regarding the identification of OA sources, source apportionment analysis using positive matrix factorisation algorithm (PMF, Paatero ~~&~~ and Tappert, 1994) ~~was~~ has been intensively used over the past two decades on both AMS and ACSM measurements (e.g. see Crippa et al., 2014; Poulain et al., 2020). However, this algorithm faced two main limitations when used during a long time period: firstly, the factor profiles are static over the analyzing period (Paatero, 1997); and secondly, rotational ambiguity which provides non-unique solutions. To solve these issues, a multilinear engine (ME-2, Paatero, 1999) has been implemented in the PMF analysis, which allows to use of a priori knowledge to constrain the model to environmentally reasonable solutions (e.g., ~~Lanz et al., 2008;~~ Canonaco et al., 2013 and~~;~~ Crippa et al., 2014). To consider the temporal variation of the factor profiles, a rolling approach was suggested (Parworth et al., 2015; Canonaco et al., 2020). The rolling strategy involves advancing a smaller PMF window (i.e., 14 days) and moving/rolling it over the whole dataset to catch the temporal changes of the source profiles with a 1-day step.

Although several studies in Europe have already conducted source apportionment analyses of one year or more, most of them were associated with urban or suburban environments (e.g., for urban studies: Stavroulas et al., 2019; Vlachou et al., 2019; Huang et al., 2019; Qi et al., 2020; and for suburban studies: Katsanos et al., 2019; ~~Y.~~ Zhang et al., 2019), and only a few of them were studied in rural-background sites (Schlag et al., 2016; Crippa et al., 2014; Vlachou et al., 2018; Paglione et al., 2020; Dudoitis et al., 2016; Heikkinen et al., 2020; Chen et al., 2021; and Chen et al., 2022), although the rural-background sites represent the major advantage to be able to study the impact of long-range transport of anthropogenic emissions and their changes over a long time period. The Leibniz Institute for Tropospheric Research (TROPOS) Central European observatory Melpitz has been continuously measuring aerosol chemical compositions for 30 years. The station is a unique place in Europe, sitting at the border between marine-influenced Western Europe and continental Eastern Europe. A direct consequence is that the aerosol chemical compositions and mass concentrations strongly depend on the air mass origins, showing less polluted air masses coming from the West and more polluted air masses from the East (Birmili et al., 201~~0~~0~~1~~; Spindler et al., 2010). However, only a few studies were done on the source identification of the aerosol reaching the station by covering short time periods mostly during winter (van Pinxteren et al., 2016, ~~2020,~~ 2020~~2~~).

The current study comprehensively investigates the PM_1 aerosol particle chemical compositions and the various OA sources for Melpitz as a rural-background station, based on ACSM and multi-angle absorption photometer (MAAP) measurements from September 2016 to August 2017, using the most advanced rolling PMF with ME-2 implemented in the SoFi Pro package

(Datalystica Ltd., Villigen, Switzerland) (Parworth et al., 2015; Canonaco et al., 2013; Canonaco et al., 2020). Although previous papers already considered this dataset, they were focused on quality assurance (Poulain et al., 2020) to depict the European aerosol chemical composition (Bressi et al., 2021 and Chen et al., 2022) or the relationship between the CCN properties (Wang et al., 2022, Schmale et al., 2017), none of these papers were focused on carbonaceous source identification (OA and eBC) nor discussed the strong dependency of the aerosol chemical composition to the air mass origin. Therefore, a multi-linear regression model was used to estimate the contribution of equivalent black carbon (eBC) to the various primary organic PMF factors such as hydrocarbon-like organic aerosol, biomass burning organic aerosol, and coal combustion organic aerosol. Meanwhile, to better understand the emission area of PM_1 chemical composition and PMF factors, the influence of air mass origin was investigated based on self-developed back-trajectory cluster methods (BCLM).~~**The current study comprehensively investigates the PM1 aerosol particle chemical compositions and the various OA sources for Melpitz based on ACSM and multi-angle absorption photometer (MAAP) measurements from September 2016 to August 2017, using the most advanced rolling PMF with ME-2 implemented in the SoFi Pro package (Datalystica Ltd., Villigen, Switzerland) (Parworth et al., 2015; Canonaco et al., 2013; Canonaco et al., 2020). Moreover, a multi-linear regression model was used to estimate the contribution of equivalent black carbon (eBC) to the various PMF factors. Meanwhile, the influence of air mass origin was investigated to identify the emission area of the different PM1 sources.**~~

2 Methodology

2.1 Sampling site

The atmospheric aerosol measurements were carried out at the TROPOS research station Melpitz (51.54° N, 12.93° E, 86 m a.s.l.), located approximately 50 km northeast of Leipzig, Germany. The station itself is mainly encircled by agronomical pastures and forests within a rural area, ~~which~~ that is why the station is recognized as a rural-background station (Spindler et al., 2013). Since 1992, the station has been monitoring the influence of atmospheric long-range transport on the background air quality of Central European (e.g. Spindler et al., 2012 2013). The Melpitz station is part of EMEP (European Monitoring and Evaluation Programme; Level 3 station, Aas et al., 2012), ACTRIS (Aerosol, Clouds and Trace gases Research Infrastructure), GAW (Global Atmosphere Watch of the World Meteorological Organization), and GUAN (German Ultrafine Aerosol Network, Birmili et al., 2009, 2015, 2016). For a general description of the chemical and physical aerosol characterization analysis techniques, check e.g. Spindler et al., (2004, 2010, 2012, 2013); and Poulain et al., (2011, 2014, 2020).

2.2 ACSM

The chemical compositions and mass loadings of non-refractory PM_1 (NR-PM_1: organic, sulphate, nitrate, ammonium, and chloride) with a 30-minute time resolution were measured by an Aerodyne quadrupole ACSM. The ACSM sampling technique and operational information were previously detailed by Ng et al., (2011).

Briefly, after PM_1 transmits across a 100 µm critical orifice, the aerosols are centralized into a ~~slender~~ narrow beam in an aerodynamic lens (Liu et al., 2007). Non-refractory particulate material that evaporates at the oven temperature (generally 600°C) is recorded and chemically determined using electron impact quadrupole mass spectrometry at 70 eV (Ng et al., 2011). The ions are then detected using a quadrupole residual gas analyser (RGA, Pfeiffer Vacuum Prisma Plus). The ACSM takes 30 ~~-~~ second samples of both ambient and particle-free air. The difference in these measurements identifies the aerosol mass spectrum. To change the signal spectra into organic or inorganic species concentrations, the fragmentation table (Allan et al., 2004), the ion transmission correction, and the Response Factor (RF) are applied. To improve the particle loss as a result of bouncing off the vaporizer, the ACSM data were processed according to manufacturer guidelines ~~with~~ using a composition dependent collection efficiency (CDCE) correction relying on the algorithms suggested by Middlebrook et al. (2012). Calibrations of Ionization Efficiency (IE) and Relative Ion Efficiency (RIE) were performed using a 350 nm monodispersed ammonium nitrate and ammonium sulphate (Ng et al., 2011). The final mean value for IE was $4.93(\pm 1.45) \times 10^{-11}$ and the mean values for RIEs for ammonium and sulphate respectively were 6.48 ± 1.26, and 0.68 ± 0.13. The quality assurance of the ACSM measurements was performed by comparing them with collocated measurements including MPSS, and high-volume filter samples (PM_1 and $PM_{2.5}$) for the total particle mass concentration, water-soluble ions (nitrate, sulphate, and ammonium), as well as OC/EC. Details on the QA/QC and instrumental uncertainties can be found in Poulain et al., (2020).~~Details on the QA/QC for this dataset can be found in Poulain, et al., (2020).~~

The ACSM ammonium mass concentration mainly corresponds to ammonium nitrate and ammonium sulphate salts. Previously by Poulain et al. (2020), the neutralization state of the particles was estimated for datasets assuming complete neutralization by nitrate, sulphate, and chloride. Therefore, the particles are neutralized when considering nitrate, ammonium, and sulphate in this study. Furthermore, the significant role of organo-nitrate and organo-sulphate on signals of nitrate and sulphate is not negligible (Kiendler- Scharr et al. (2016). Since the Q-ACSM is working at a unit mass resolution (UMR), it is not possible to distinguish nitrate and sulphate from organic. Therefore, estimating the organo-nitrate would only introduce uncertainties to measurements, therefore, we did not consider to conduct this analysis in this study.

2.3 Additional measurements

In parallel to the ACSM, a MAAP was used to measure the mass concentrations of equivalent black carbon (eBC) (model 5012 Thermo Scientific; Petzold ~~&~~ and Schönlinner, 2004). ~~Conversion of the~~ The eBC mass concentration from the PM_{10} data was multiplied by a constant factor of 0.9 following Poulain et al (2011) to estimate the eBC mass concentration in the PM_1 fraction. Consequently, all the eBC mass concentrations reported and discussed here correspond to the eBC in the PM_1 fraction and are referred to as eBC-PM_1. ~~eBC mass concentration from the PM_{10} inlet to the ACSM PM_1 cut-off was made by applying a correction factor of 0.9 following Poulain et al (2011).~~ Furthermore, a dual mobility particle size spectrometer (TROPOS-type T-MPSS; Birmili et al., 1999) was used to measure the particle number size distribution (PNSD) from 3 to 800 nm (mobility diameter, d mob) at ambient and 300°C temperatures (Wehner et al., 2002). The MAAP was situated in the

same laboratory container as the ACSM and these instruments sampled the same PM_{10} inlet after a dryer, and the sampled air distribution among the instruments was equally assured by an isokinetic splitter (Poulain et al., 2020).

In addition to the online measurements, high-volume samplers (DIGITEL DHA-80, Digitel Elektronik AG, Hegnau, Switzerland) were utilized to capture daily $PM_{2.5}$ samples on a quartz filter (for 24 hours from midnight to midnight). For more details on the sample preparation and evaluation methods, see Spindler et al., (2013). Levoglucosan as a tracer for wood burning combustion was measured following Iinuma et al., (2009) using high performance anion exchange chromatography coupled with an electrochemical detector (HPAEC-PAD)~~Levoglucosan as a tracer for wood burning combustion was measured following Iinuma et al., (2009) using high performance anion exchange chromatography coupled with an electrochemical detector (HPAEC-PAD), that was used for the analysis of anhydro-monosaccharides (Iinuma et al., 2009).~~

Trace gas measurements were also carried out. Ozone was determined by a U.V. Photometric gas analyser mode 49C (Thermo Scientific, UK), SO_2 by an APSA-360A (Horiba, Kyoto, Japan), and NO and NO_2 using a customized Trace Level NOx Analysis Model 42i-TL (Thermo Scientific) equipped with a blue light converter. Standard meteorological parameters (temperature, relative humidity, solar radiation, precipitation, wind direction, and wind speed) were regularly measured.

2.4 Rolling PMF (ME-2) source apportionment of OA

This work conducted the most advanced source apportionment analysis following a standardized protocol developed by Chen et al., (2022). The PMF method was used to allocate the source of the OA (Paatero ~~&~~ and Tappert, 1994) through the Source Finder professional (SoFi Pro, version 8.0.3.1, Canonaco et al., 2021) software package (Datalystica Ltd., Villigen, Switzerland), within the Igor Pro software environment (Igor Pro, version 8.04, Wavemetrics, Inc., Lake Oswego, OR, USA). Two matrices of factor profiles *F* and factor contributions *G*, defined the dataset *X*, and the matrix *E* named the residual matrix is the fraction which cannot be described by the model. Time series and the chemical fingerprint of sources ~~respectively~~ have been represented by F_{kj} and G_{ik}, respectively. The dimension of F_{kj} and G_{ik} are based on the order *p*, which is the number of factors selected to represent the data ~~which is~~ defined by the user:

$$X_{ij} = \sum_{k=1}^{p} G_{ik} \times F_{kj} + E_{ij} \quad (1)$$

In this study, since the measurement covers a period of 12 months (full four seasons), four separate PMF inputs were prepared. Unconstrained PMF was applied with 4 to 6 factor~~s~~ runs for all the seasons; throughout the pre-result and while referring to previous studies (Crippa et al., 2014 and van Pinxteren et al., 2016) primary factors were separated as hydrocarbon-like OA (HOA), biomass burning OA (BBOA) and coal combustion OA (CCOA). However, unconstrained PMF did not result to separate the primary factor profiles. Introducing constraints based on prior knowledge is an efficient strategy for avoiding the mixing of primary factors (Canonaco et al., 2013; Crippa et al., 2014). For this reason, the multilinear engine (ME-2) algorithm (Paatero, 1999) enables the incorporation of time series and factor profiles constraints in form of the *a*-value approach. In

dealing with a profile constraint, the *a-value* specifies the variety of a factor that can deviate from the anchor profile during the PMF iteration:

$$f_{j,solution} = f_j \pm a \,.\, f_j \quad (2)$$

The constraints applied through ME-2 for HOA and BBOA sources used the anchor profile of Crippa et al., (2014), and Ng et al., (2010), respectively. The anchor profile used for CCOA was generated from our own winter data during this work (SI, 1.1). For each of the four seasons, primary profiles were subject to a sensitivity analysis with *a-values* ranging from 0-0.4 for HOA and BBOA, 0-0.5 for CCOA, and steps of 0.1 to choose the best *a-value* combination for these three factors.

In the PMF approach, there is the intrinsic property of static factor profiles during the period of PMF analysis. Even though for short-term measurements (like one/two season/s) this might be a sensible estimation, long-term observations as are typical for current ACSM study (one year and more), are expected to be subject to evolving factor profiles based on seasonality. To consider the temporal changes, the rolling PMF window method was developed (Canonaco et al., 2021b; Parworth et al., 2015). This technique is applied to a small window, which is slowly extended throughout the whole dataset. Based on the dataset, the user determines the width of the PMF window, the shift parameter, and the number of PMF repeats per window; for the current work, we set 14-day windows, 1-day shifts, and 100 repeats per window.

In addition, this rolling PMF analysis was coupled with the bootstrap re-sampling approach (*Bootstrap Methods: Another Look at the Jackknife on JSTOR*, 1979), which can randomly select a part of the original matrix and repeat a part of the rows to generate a new same-sized matrix to test the stability of solutions and to estimate the statistical error. Overall, we have combined rolling PMF with ME-2 and bootstrap to conduct the source apportionment investigation, and more information on this new approach was described in Canonaco et al., (2020). This approach for a yearlong dataset generates an enormous amount of PMF runs (N= 35800) and not all of the solutions are environmentally reasonable. Since it is practically impossible to manually inspect all PMF runs, the criterial-base selection was introduced in SoFi Pro to automatically and objectively select environmentally reasonable PMF solutions (Canonaco et al., 2020). Finally, the resulting factors were interpreted as HOA, BBOA, CCOA, and two oxidized OA (OOA) factors named less-oxygenated OOA (LO-OOA) and more oxygenated OOA (MO-OOA). The steps and setups utilized in the evaluation of this dataset are detailed in the supplement (Sect. 1).

2.5 eBC-PM_1 source apportionment

The eBC-PM_1 correlated with each of the three identified primary organic factors (HOA, BBOA, and CCOA) during the source apportionment analysis (Table. 1, which will be discussed later on in the result Sect.). The total amount of these primary factors (known as POA) was highly correlated with eBC-PM_1 (R^2= 0.87; Fig. 8a). As a result, the different sources of eBC-PM_1 were evaluated for each factor utilizing a multilinear regression model, as suggested by Laborde et al., (2013); Zhu et al., (2018) and Poulain et al., (2021), for instance. The following assumes that the eBC-PM_1 mass is associated with the separate contribution from each OA factor (i.e., eBC-PM_{1HOA}, eBC-PM_{1BBOA}, and eBC-PM_{1CCOA}) at any time:

$$eBC(t) = eBC_{HOA}(t) + eBC_{BBOA}(t) + eBC_{CCOA}(t) \quad (3)$$

The eBC-PM_1 emission from each source is expected to be proportionate to the separate source mass concentration generated in each season (m_{HOA}, m_{BBOA}, and m_{CCOA}, respectively). As a result, the multilinear regression model can be described as follows:

$$eBC(t) = am_{HOA} + bm_{BBOA} + cm_{CCOA} \quad (4)$$

where a, b, and c are the linear regression coefficients for m_{HOA}, m_{BBOA}, and m_{CCOA}, respectively, that will be applied to evaluate the contribution of eBC-PM_1 per each POA factor for each season (Table. S4).

2.6~~5~~ Air mass trajectory analysis

Non-parametric wind regressions (NWR) were used to approximate the OA source concentrations at a given wind direction and speed (Henry et al., 2009) in order to investigate not only the local but also the prevalent wind sector associated with transported emission sources (Marin, et al., 2019). ~~Non-parametric wind regressions (NWR) were used to approximate the OA source concentrations at a given wind direction and speed (Henry et al., 2009).~~ The NOAA HYbrid Single-Particle Lagrangian Integrated Trajectory (HYSPLIT-4) model was used to analyse 96 h backward trajectories at 500 m above the model ground of the sampling place (Draxler ~~&~~ and Hess, 1997~~2004~~). The trajectory results were used for two independent but complementary analyses to better depict the emission areas of the aerosol: by identifying the potential areas of aerosol sources ~~area~~ and by clustering the trajectories.

A cluster analysis of the different trajectories was performed. The synoptic-scale air mass condition, together with geographical locations and paths, is a crucial driver of local pollutant concentrations (e.g. Sun et al., 2020; Ma et al., 2014). Local particle mass concentrations and meteorological conditions can play a significant role and be associated with specific air mass trajectories. In addition, the trajectories of the air mass can influence aerosol compositions. For example, the stability of the atmosphere is also meaningful since it influences both the vertical dilution of pollutants and the overall particle mass concentrations. Therefore, the effects of inter-annual variations in air mass conditions and the stability of atmosphere on observed patterns were inspected using a self-developed back-trajectory cluster method (BCLM), concerning air mass backward trajectories, pseudo-potential temperature profiles, PM_{10} mass concentration profiles over Melpitz, and seasons (Birmili et al., 2010; Ma et al., 2014). ~~Descriptive analysis, cluster processing, and data processes and products are all described in detail by Sun et al., (2020) and Ma et al., (2014).~~

In this method, the different clusters can be divided according to the different seasons (CS: cold season; TS: transition season; and WS: warm season), and meteorological synoptic patterns (ST: stagnant; A1: anticyclonic with air mass coming from Eastern Europe; A2: anticyclonic with air mass coming from the west; C1: cyclonic with air mass coming from relatively

south; C2: cyclonic with air mass coming from the west and south west). However, the clustering approach did not consider spring and fall separately, and therefore the transition clusters correspond to both spring and fall. Finally, a total of fifteen clusters were identified, corresponding to different meteorological conditions over the course of the year. Descriptive analysis, cluster processing, and data processes and products are all described in detail by Sun et al., (2020) and Ma et al., (2014).

3 Results and discussion

3.1 PM_1 chemical composition

In this work, we investigate one-year ~~-~~long measurements of PM_1 for Melpitz, Germany. All the data ~~is~~ are presented in UTC, during the winter and summer, the time zone is one and two hours behind local time, respectively. Yearly time series, seasonal variation, and diurnal cycles of aerosol particle chemical compositions including mass concentrations and mass fractions, as measured by ACSM and MAAP, are shown in ~~figures~~ Figures 1, 2, and 3, respectively. Over the entire period, the chemical composition of PM_1 was basically made up of organic aerosol (46 % of the total mass; Fig. 1c), sulphate (16 %), nitrate (21 %), ammonium (11 %), eBC-PM_1~~eBC~~ (6 %), and chloride (close to 0 %). However, a mean mass concentration of 10.4~~97~~ µg/m^3 (Fig. 1) was obtained with an obvious seasonal trend which detected the highest total mass concentration~~s~~ (15.95 µg/m^3) during the winter time and lowest mass concentration during the summer time; 6.24 µg/m^3 (Fig. 1a and Fig. 2a). Compared to previous AMS measurements of Poulain et al., (2011) at the same station, a similar seasonal trend was observed in the period 2008/2009, while the absolute masses differed (Table. S1), which is at least partially related to the inter-annual changes of the meteorological conditions. Compared to previous ACSM long-term measurements of Poulain et al., (2021) at the same station, a similar mean mass concentration of PM_1 was observed in the period from June 2012 to November 2017 (Poulain et al., 2021: 10.23 µg/m^3 and this study: 10.49 µg/m^3; respectively), and presented same seasonal trends for all the chemical species (Table. S2) with a highest mass concentration in the winter and lowest mass concentration in the summer time (13.15 µg/m^3 and 7.64 µg/m^3, respectively; Table. S2). Consequently, the results obtained from the current study can be considered as a representative ACSM study for Melpitz station. Fig. ~~S2~~ S3 presents the coming high polluted air masses for total PM_1 to the measurement site in the current study; ~~the~~ polluted Eastern Europe flow with high mass concentration and south-west with lower mass concentration was more clearly found in winter time rather than in other seasons, which will be comprehensively discussed in the Sect. 3.4.

In comparison with other ACSM/AMS rural-background stations in Europe which can be divided into three parts Northern Europe (NE), Southern Europe (SE), and Mid-latitude Europe (ME) (Bressi et al., 2021), the annual PM_1 mean mass concentration measured at Melpitz is similar to the value obtained at other ME stations, such as Magadino 10.1 µg/m^3, Kosetice 8.5 µg/m^3 (Chen et al., 2022), 9.1 µg/m^3 on average of PM_1 mean mass concentration of 6 stations (Ispra, Melpitz, Magadino, Cabauw, Sirta, and Hohenpeissenberg, Bressi et al., 2021).

3.1.1 Inorganic

The seasonality of the inorganic species can be associated with their variations in emissions and/or the changes in their chemical atmospheric processes. Throughout the year, the mass concentration and their respective contribution to the total PM_1 mass of nitrate, ammonium, and chloride increased from a minimum value in summer (11 %, 7 %, and 0 %, respectively; Fig. 2b) and reached a maximum value in winter (24 %, 12 %, and 1 %, respectively; Fig. 2b). Moreover, the comparison between Bressi et al., (2021) and current study (Fig. S4 from Bressi et al 2021, Fig. 3 from the current study) for Melpitz station with different time coverage shows that the daily variation of ACSM sulphate, nitrate, and ammonium are similar in both winter and summer seasons. In comparison with other ACSM/AMS rural-background stations in Europe (Fig. S4, Bressi et al., 2021), the mean daily cycle of the PM_1 chemical components (sulphate, nitrate, and ammonium) does not show a similar pattern to the other stations (Bressi et al., 2021) due to the different geographical location and meteorological conditions.

Sulphate showed a slightly different behavior. Although the contribution of sulphate to the total PM_1 decreased slightly from summer (20 %) to winter (15 %), its mass concentration remained higher in winter compared to summer (2.38 µg/m^3 and 1.23 µg/m^3, respectively; Table. 1). The increment ~~enhancement~~ is not as drastic as other inorganic species since sulphate is least volatile, therefore, more fraction of sulphate stayed in particle phase even in summer. Moreover, the sulphate contribution to the total PM_1 was higher during the summer than winter time, since with enhanced irradiations in summer, sulphate formation from photochemistry could be enhanced as well. This sulphate higher contribution in summer over winter is consistent with the mean PM_1 mass concentration measured by AMS for the three periods during fall (16. September.2008 to 03. November.2008), winter (24. February.2009 to 25. March.2009), and summer (23. May.2009 to 09. June.2009) campaigns reported by Poulain et al., (2011). In comparison with previous ACSM long-term measurements of Poulain et al., (2021) at Melpitz station, a similar mean mass concentration of sulphate was observed in the period from June 2012 to November 2017 (Poulain et al., 2021: 1.54 µg/m^3 and this study: 1.67 µg/m^3; respectively; Table. S2). This comparison indicates the current study as a case study of ACSM for Melpitz station within 5-year ACSM data, with the best data coverage of time in a year. ~~Moreover, with enhanced irradiations in summer, sulphate formation from photochemistry could be enhanced as well. This result is consistent with the mean PM_1 mass concentration measured by AMS for the three periods during fall (16. September.2008 to 03. November.2008), winter (24. February.2009 to 25. March.2009), and summer (23. May.2009 to 09. June.2009) campaigns reported by Poulain et al., (2011).~~ The diurnal cycles of sulphate (Fig. 3) showed a different daily pattern in warm and cold seasons. In summer, sulphate mass concentration increased during the day and reached its maximum level at 12:00 UTC (Fig. 3) due to sulphur dioxide photochemical oxidation processes in the atmosphere, which also presented the highest mass concentration during the day, along with maximum temperature and sun radiation in summer time (Fig. S~~43~~). Furthermore, the NWR plots (Fig. S3) show that during the winter time, sulphate mostly comes from the north and east sectors with wind speeds above 5 m/s which can be associated with dominant transported sulphate sources. Although the eastern wind sector remains visible for the sulphate in the summer time, the high concentrations of sulphate can be observed during periods with low wind speed and without a specific wind sector; which corresponds to local sulphate formation. Sect. 3.4 will go into

detail about the long-range transported emissions later on). . Furthermore, the wind rose analysis showed a high mass concentration of sulphate at low wind speed (Fig S3). Although this locally formed emissions of sulphate (Fig. S32 and Fig. 9) can explain this peak during the day in summer, this photochemical process is not the only source of sulphate. It especially cannot explain the highest mass concentrations during the winter time with almost no diurnal variation (Fig. 3). For winter, the emission of domestic heating processes, which could be enhanced in the atmospheric boundary layer (Stieger et al., 2018), along with the long- range transported emissions, which came from north-east toward the measurement site (Fig. S32 and Fig. 9), and also high ammonium nitrate due to partitioning according to temperature, explain the high mass concentration but the low relative contribution of sulphate.

Nitrate is mostly found in the form of ammonium-nitrate (NH_4NO_3), which is reliant on the gas phase precursor concentrations, temperature, humidity, and aerosol chemical composition (Poulain et al. 2011; Stieger et al., 2018). Both nitrate and ammonium showed a minimum mass fraction and mass concentration in summer (11 %, 0.68 µg/m^3, 7 %, 0.43 µg/m^3, respectively; Fig. 2), an increasing trend toward the cold months and reached their maximum mass fraction and mass concentration in winter time (nitrate 24 %, 3.87 µg/m^3, ammonium 12 %, 2 µg/m^3, respectively; Fig. 2). The diurnal cycles of nitrate and ammonium (Fig. 3) showed a relatively similar daily pattern in all seasons, which means the highest values were reached in the morning, due to the beginning of vertical mixing and a reduction in the afternoon followed by an increase during the night, reflecting their night time production during every season. The volatile behaviour of ammonium-nitrate strongly affects its temporal variation during warm days leading to the formation of the gaseous nitric acid and ammonia compounds at higher temperatures and low humidity (Fig. S43, and S3S8). Nitrate profiles from NWR plots (Fig. S3) present two different wind directions for the whole period which might be associated with transported nitrate from Leipzig and Torgau (50 km in the south-west and 7 km in the north-east of Melpitz, respectively) with higher wind speed. Since the reaction pathway of OH and NO_2 can result in nitrate formation (Yang et al., 2022), this mechanism can be linked to traffic emissions in residential areas. These long-range transported sources together with locally formed emissions could describe higher mass concentrations for nitrate and ammonium due to e.g., meteorological conditions and abundant precursors in winter time. However, in winter, ammonium-nitrate remains mainly in the particle phase (Seinfeld and Pandis, 2006) since it can totally be changed from gas to particle phase at lower temperature (Spindler et al., 2010). High values of nitrate and ammonium in spring time are linked to agronomical fertilization (Stieger et al., 2018)). In winter, ammonium-nitrate remains mainly in the particle phase (Seinfeld and Pandis, 2006) and, like sulphate, arrived at the measurement site due to the long-range transported emissions which not only came from the north-eastern but also south-western flow, describing higher mass concentrations for nitrate and ammonium (Fig. S2). High values of nitrate and ammonium in spring time are linked to agronomical fertilization (Stieger et al., 2018). These seasonal contribution results for both, nitrate and ammonium, are consistent with the previous AMS study (Poulain et al., 2011), with minimum fraction to the total AMS-PM_1 during summer (nitrate 5 % and ammonium 8 %; Table. S1), and maximum fraction during winter time (nitrate 34 % and ammonium 17 %; Table. S1). However, it is known that a

fraction of the nitrate signal can be attributed to nitrogen containing organic species (Kiendler-Scharr et al., 2016), which can affect the overall nitrate mass concentration (Poulain et al., 2020).

Although chloride had the lowest annual mass concentration (0.05 µg/m^3) compared to all other PM_1 chemical components (Table. 1), it showed the highest mass concentration and mass fraction in winter (0.11 µg/m^3, 1 %, respectively; Fig. 2a&b; Table. 1) compared to ~~the~~ other seasons; as seen in the previous AMS study of Poulain et al., (2011) (2 %, Table. S1). It could be related to the surrounding and transported emissions which mass concentrations were high for air masses from north-easterly and south-westerly directions (Fig. S3~~2~~). In a multi-year analysis of the hourly PM_{10} chloride mass concentration measurements using a MARGA, Stieger et al., (2018) attributed the chloride sources of Melpitz during winter to the resuspension of road salt used for the de-icing of streets, mainly coming from the cities of Torgau and Leipzig. These sites are also located in the wind directions along with the coal and wood combustion emission region, which could explain the highest mass concentration of chloride during the winter. Furthermore, the existence of chloride might be due to low mass concentration marine influences consisting of sea-salt aerosols during all the seasons in the south-westerly direction (Fig. S3~~2~~) which ~~was~~ were previously studied by Stieger et al., (2018). However, it is known that the AMS ~~-~~technology cannot properly detect sea salt (~~S.~~ Huang et al., 2018; Ovadnevaite et al., 2014) because the majority of chloride is in the refractory part which cannot be flash vaporized at 600 ºC. Consequently, the chloride detected by the ACSM is mostly related to combustion processes (wood, coal combustion as well as trash burning; Li et al., 2012).

3.1.2 eBC-PM_1~~eBC~~ and organics

The eBC-PM_1~~eBC~~ showed its maximum mass concentration and mass fraction to PM mass during winter time at 1.38 µg/m^3 and 9 %, respectively (Fig. 2), and only 0.25 µg/m^3 and 4 %, respectively, during summer time (Fig. 2). This is consistent with the expected highest anthropogenic emissions from fossil fuel consumption (house heating and energy productions) in winter compared to summer (Spindler et al., 2010). Furthermore, considering measured eBC-PM_1 in regard to wind speed and wind direction from NWR plots (Fig. S3), eBC-PM_1 presented transported and local emissions. The highest mass concentrations for fall, winter, and spring seasons could be linked to north-easterly and south-westerly winds with higher wind speed (above 10 m/s). While in summer time it is mostly linked to the surrounding emissions regardless of wind direction with lower wind speed (Fig. S3). ~~Furthermore, considering measured eBC in regard to wind speed and wind direction (Fig. S2), the highest mass concentrations could be linked to north easterly and south westerly winds for fall, winter, and spring seasons, while in summer time it is mostly linked to the surrounding emissions (Fig. S2).~~ Significant changes in the diurnal profiles of eBC-PM_1~~eBC~~ for the different seasons can be found with the highest mass concentrations throughout the cold months compared to warm months owing to house heating (Fig. 3). It also showed morning and evening peaks during all seasons (Fig. 3). This is consistent with those observed for the nitrogen oxides (Fig. S4~~3~~), which might be attributed to liquid fuel emissions and possibly the impact of the traffic rush hours on the main street, B 87, located approximately 1 or 1.5 km north of the station, (Yuan et al., 2021). In the following chapter, diurnal patterns showed lower mass concentrations at noon, and increased in the

late afternoon to become nearly constant from 8 p.m. until midnight (Fig. 3). This ambient particulate pollution resulting from very surrounding sources in the village was reported by van Pinxteren et al., (20202). Diurnal increments of eBC-PM_1eBC were smaller in fall and spring compared to winter; the increment in summer is also correspondingly low due to the absence of house heating emissions, and the diurnal variation in the increment is determined by surrounding motor vehicle emissions in combination with the mixing layer height (van Pinxteren et al., 20200). Further discussions on the seasonal trend of the eBC-PM_1eBC can be found in Sect. 3.3.

Organic aerosol (OA) was the predominant species throughout the whole year, with a mean mass concentration of 4.84 µg/m^3 and a mass fraction of 46 % (Fig. 1c; Table. 1). The OA mass fraction decreased from the maximum value in summer and attained a minimum mass fraction in winter (58 %, 39 %, respectively; Fig. 2b). Similar to the comparison of previous inorganic AMS measurements performed at Melpitz (Poulain et al., 2011), AMS-OA contribution to total PM_1 showed maximum contribution during summer (59 %, Table. S1), and minimum contribution during winter (23 %) as well. However, the mass concentration of OA increased from its lowest value in summer and reached its highest value in winter time (3.67 µg/m^3, 6.21 µg/m^3 respectively; Fig. 2, Table. 1). Similar to eBC-PM_1eBC, by analyzing NWR plots, OA measured in according to wind direction and wind speed showed the highest average mass concentrations for north-easterly and south-westerly winds in winter (Fig. S32). In fall, polluted air masses came from the north-easterly direction, and in spring and summer OA, surrounding emissions closer to Melpitz were identified (Fig. S32). The diurnal cycle of the organic had an identical pattern across all seasons (Fig. 3), showing the highest mass concentration in night time, a small peak in the early hours of the morning related to rush hours, and the lowest mass concentrations around the early afternoon. The peak observed around 12:00 UTC in summer time (Fig.3) can be due to the local photochemical production that leads to the formation of secondary organic aerosol mass during the day, similar to the diurnal behavior of sulphate (previously discussed in Sect. 3.1.1). However, the reduction in total OA mass concentration throughout the day (Fig. 3), which was mostly observed during the warm seasons (spring and summer), could be clearly related to the dilution effect of increasing mixed layer height. During warm days, evaporation of semi-volatile organics from the particle phase cannot be completely excluded (Schaap et al., 2004; Keck and Wittmaack, 2005). In comparison between Bressi et al., (2021) and the current study for Melpitz station, the daily variation of organic are similar in both winter and summer seasons, while there are differences between Melpitz with other rural-background stations due to the different geographical location and meteorological conditions (Bressi et al., 2021).

Overall, eBC-PM_1eBC and OA can be composed of various sources with strong seasonal dependencies, as well as be influenced by different responses to atmospheric dynamics depending on meteorological parameters, geographical locations, and chemical processes. Therefore, a comprehensive analysis of the OA and eBC-PM_1eBC sources was performed using source apportionment techniques.

3.2 Source apportionment of OA

The chosen solution for the organic aerosol source apportionment contained five different factors based on their time series and mass spectra (Fig. 4). The source apportionment solution is based on a partly constrained rolling approach with three primary organic factors (POA), namely HOA (on average 0.30 µg/m^3 and 6 % of the total OA; Table.1 and Fig. 4), BBOA (on average 0.39 µg/m^3 and 7.9 % of the total OA) and CCOA (on average 0.77 µg/m^3 and 15.4 % of the total OA). In addition to these POA factors, two oxygenated organic aerosols (OOAs) were identified as LO-OOA (on average 1.62 µg/m^3 and 32.4 % of the total OA), and MO-OOA (on average 1.92 µg/m^3 and 38.4 % of the OA). The seasonal average mass concentrations and relative mass fractions of each OA factor to the total OA mass and their seasonal diurnal variation are presented in Figures 5 and 6; respectively. They will be discussed separately in the following sections.

3.2.1 POA factors

The HOA mass spectrum (Fig. 4b) is recognized by mass fragments at unsaturated and saturated hydrocarbon chain pairs *m/z* 41 (C_3H_5), 43 (C_3H_7), *m/z* 55 (C_4H_7) and 57 (C_4H_9) (Zhang et al., 2005; Canagaratna et al., 2004), which are representative of liquid fuel combustion emissions and are associated with either traffic emissions or domestic heating fuel (Wang et al., 2020). This result designates HOA as a minimal source of OA at the monitoring site, which is consistent with previous studies in the PM_1 range made in the same place: a) total average was 7 % of the organic mass concentration in a study by Crippa et al., (2014) total average was 3 % of PM size range between 0.05-1.2 µm mass concentration in a study by van Pinxteren et al., (2016) (Table. S3~~2~~). However, in comparison with other ACSM/AMS stations in Europe (22 stations; Chen et al., 2022), Kosetice with 9.7 % as a rural-background site, and Bucharest with 13.7 % as an urban-background site showed the minimum annual HOA mean contribution of total OA, which is similar to the contribution at Melpitz.

Mass concentration of HOA followed a slightly increasing seasonal pattern towards the cold months, from 0.23 µg/m^3 in summer to 0.36 µg/m^3 in the winter (Fig. 5a; Table. 1). HOA presented a low correlation with nitrogen oxides over the entire period (R^2= 0.17, Table. 1), but it correlated well with eBC-PM_1~~eBC~~ in winter (R^2= 0.52; Table. 1) and showed~~s~~ a weaker correlation in summer (R^2= 0.28; Table. 1). Possibly HOA is also associated with household heating (35 % by oil and 11 % by liquid petroleum gas, van Pinxteren et al., 202~~0~~2) rather than traffic emissions, especially during the cold months. Analyzing the NWR plots demonstrates the highest HOA mass concentration was observed at low wind speed during the warm period (Fig. 7) indicating, rather local emission sources. While during the cold period a clear increase of the mass concentration can be associated with the highest wind speed (> 10 m/s) mostly coming from the North to East sector. During periods with wind speeds below 10 m/s, the two dominant wind sectors (NE and SW) can be observed. The first one might be associated with emission plumes coming from either the surrounding traffic emissions (the federal street B 87), as well as the domestic emissions are associated not with house heating in summer but with hot water production (van Pinxteren et al., 2020), as well as the city of Torgau (with approx. 20,000 inhabitants, distance from 7 km). Although the SW sector shows a lower HOA mass concentration in comparison to the NE one, it corresponds to the direction of the city of Leipzig (above 600 000 inhabitants,

approx. 50 km). Therefore, it might be associated with the influence of the pollution plume of the city of Leipzig. ~~Analyzing the pollution wind rose, the highest winter HOA mass concentrations are associated with the north easterly wind direction regardless of the wind speed suggesting the influence of long range transported emissions (Fig. 7). During the warm months, the emissions were more from the surrounding area, still associated with a north easterly wind direction but only at low wind speed (Fig. 7), which might be associated with either the surrounding traffic emissions, as well as the domestic emissions associated not with house heating in summer but with hot water production (van Pinxteren et al., 2020).~~

The diurnal patterns of HOA reproduced two peaks in the morning and evening for all seasons (Fig. 6), which is related to traffic rush hours and linked to surrounding emissions from the main street (B 87, approx. 1.5 km north of the station), Melpitz village itself, and emissions coming from Leipzig and Torgau residential areas ~~The diurnal patterns of HOA reproduced two peaks in the morning and evening for all seasons (Fig. 6)~~. The small time shift for the start of the evening increase corresponds to the time shift of the sunrise between winter and summer. The diurnal cycles reached a systematic minimum during the day time probably not only owing to emission decrease but also emphasizing the effect of dynamic atmospheric processes (e.g. mixing layer height (MLH) and planetary boundary layer (PBL)) (Fig. 6, and S4). Oppositely to what can be seen during the day time, night time mass concentrations appeared to be unaffected by the seasons, showing similar mass concentrations all year round, i.e. their mass concentration rose continuously in the early evening and remained at a very similar mass concentration over the night, which supports the hypothesis of yearlong continuous rather surrounding emissions. Nevertheless, the differences between HOA mass concentration during the night time from summer to winter season (Fig. 6) are small and can be covered by the uncertainties of PMF result (± 32.5 %, Fig. S2), however, it can be explained by different emission sources, condensation of POA (Chen et al., 2022), evaporation, oxidation processes (Saha, et al., 2018), and potential night time aging process by high ozone concentration (Kodros, et al., 2020).

The mass spectra of BBOA are identified by ions at *m/z* 29, 43, 60, and 73 (Fig. 4b), known as fragments tracers of anhydro-sugars like levoglucosan (Alfarra et al., 2007), which have been ~~identified~~ recognized as indicators of wood combustion processes (Simoneit et al., 1999; Simoneit ~~&~~ and Elias, 2001). This is confirmed by the correlation between BBOA and levoglucosan over the whole period (R^2= 0.65; Table. 1). On average, BBOA mass concentration and contribution were 0.39 µg/m^3 and 7.9 %, respectively (Table. 1 and Fig. 4a). However, its contribution is highest during winter time (10.6 %; Fig. 5), which is similar to previous studies in different PM ranges for the Melpitz station during the cold months: a) in PM_1 range, 14 % of OA mass concentration in fall (Crippa et al., 2014); b) in 0.05-1.2 µm range, highest contribution with 10 % of PM mass concentration in winter (van Pinxteren et al., 2016); and c) in PM_{10} range, highest contribution with 16 % of PM mass concentration in winter (van Pinxteren et al., 202~~2~~).

By analyzing the NWR model, the high mass concentration of BBOA in cold months, regardless of wind speed can be observed with two wind sectors coming from north-east and south-west directions. These BBOA emissions are mainly attributed to residential heating in Melpitz village and also indicate the effect of transported biomass burning emissions to the sampling site with higher wind speed (> 10 m/s, Fig. 7). ~~The high value of BBOA is mainly attributed to residential heating, and indicates~~

~~the effect of transported biomass burning emissions to the sampling site in cold months (Fig. 7),~~ W~~w~~hile in summer time, it is still observable as surrounding emissions during periods of low wind speed (Fig. 7 and Fig. S4) with a mass concentration of 0.21 µg/m^3 and a contribution of 6.1 % to total OA (Fig. 5). The presence of BBOA in the summer can be linked to water heating systems using wood briquettes and logs (estimated at 32 % of total central heating in this area, van Pinxteren et al., 2020~~0~~). Moreover, it can also be related to recreational open fires and/or barbecue activities (van Pinxteren et al., 2020~~2~~). This result is similar to other ACSM/AMS rural-background stations in Europe (22 stations; Chen et al., 2022); both Magadino and Kosetice showed the highest contribution of BBOA during winter time (27.4 % and 15.5 % respectively).

The diurnal cycles, peaking from early evening to early morning in winter (Fig. 6), match the expectations for a factor related to domestic heating activities, along with a better eBC-PM$_1$~~eBC~~ correlation during winter than during summer time (R^2= 0.81, and R^2= 0.42, respectively; Table. 1). Finally, in opposition to HOA, the night time BBOA mass concentration showed a strong seasonal variation, having its highest mass concentration during winter nights and lowest during summer time, the influence of the impact of house heating emissions on the BBOA emissions. However, the day time behavior reflects the influence of enhanced vertical mixing during day time (higher temperature, Fig. S4~~3~~) combined with high wind speeds ~~(Fig. 11)~~ can readily cause dilution and thus low pollutant concentrations near the ground (Chen et al., 2021; Via et al., 2020; Paglione et al., 2020).

The mass spectrum of CCOA is characterized by fragments at *m/z* 77, 91, and 115 (Fig. 4b) as previously reported by Dall'Osto et al., (2013); Xu et al., (2020); Tobler et al., (2021) and Chen et al., (2022). These specific fragments can be associated with unsaturated hydrocarbons, particularly ion peaks related to polycyclic aromatic hydrocarbon (PAH). The CCOA time series showed the strongest correlation with eBC-PM$_1$~~eBC~~ (R^2= 0.9; Table. 1). In addition, several studies reported that coal combustion emissions are often accompanied by high chloride mass concentrations (e.g; Iapalucci et al., 1969; Yudovich ~~&~~ and Ketris, 2006 and Tobler et al., 2021). Here, the correlation between CCOA and chloride was higher during winter than during summer time (R^2= 0.41, 0.15 respectively; Table. 1), as the gas-particle phase equilibrium dramatically changes with rising temperatures (Tobler et al., 2021). Although chloride is almost observable in the particle phase as ammonium chloride (NH_4Cl) at lower temperatures, chloride is typically observable in the gas phase as hydrogen chloride (HCl) at higher temperatures (Tobler et al., 2021).

CCOA represented on average 15.4 % of the total OA (0.77 µg m^{-3}), (Table. 1; Fig. 4a) and is the most important POA over the entire period. No CCOA factor was identified in the previous AMS measurements made at Melpitz (Crippa et al., 2014). Most likely this factor was not properly resolved and/or it was not possible to properly separate it from the other factors since no reference mass spectra for CCOA ~~was~~ were reported in the literature at that time. CCOA showed the highest mass concentration and mass fraction during the winter (1.58 µg/m^3, 23 %, respectively; Fig. 5a; Table. 1). By analyzing the NWR plots, this high mass concentration during winter time can be related to the surrounding emissions and long-range transported air masses coming from two different directions, north-easterly and south-westerly (Fig. 7).~~CCOA showed the highest mass concentration and mass fraction during the winter (1.58 µg/m^3, 23 %, respectively; Fig. 5a; Table. 1), which is related to the surrounding emissions and long-range transported air masses coming from two different directions, north-easterly and south-~~

~~westerly (Fig. 7).~~ Not surprisingly, the lowest mass concentration and contribution were observed during the summer time (0.30 µg/m^3, 8.7 %, respectively; Fig. 5a; Table. 1,) which most probably correspond to only long-range transport as later discussed in Sect. 3.4 (Fig. 9). Moreover, this result is consistent with previous measurements made in the same place. For the size range 0.05-1.2 µm van Pinxteren et al., (2016) reported a contribution of 29 % and 21 % of the PM in winter and summer respectively, and a contribution of 7 % and 0 % for winter and summer respectively for the PM_{10} range was found (van Pinxteren et al., 202~~02~~). From all ~~ASCM~~ACSM/AMS stations (22 stations; Chen et al., 2022) only Melpitz as a rural-background site and Krakow as an urban-background site showed the coal combustion emissions with the maximum contribution during winter for both sites (Krakow: 18.2 % and Melpitz: 23 %) compared to summer (Krakow: 4.5 % and Melpitz: 8.7%). The drastic seasonal changes in Krakow are attributed to the common use of coal burning for residential heating reasons during the winter time (~~Casotto et al., 2022;~~ Tobler et al., 2021), while in Melpitz, as discussed above, coal combustion is affected by both surrounding and transported emissions from other sites.

Mass concentrations of CCOA during night time were much higher than during day time throughout all seasons (Fig. 6), further verifying the increased coal combustion emissions from coal heat generation at night in winter time ~~night~~ and the potential decrease in emissions during the day due to a strong influence of atmospheric dynamics.

3.2.2 OOA factors

The two OOAs (Fig. 4) referred to as LO-OOA and MO-OOA are known to be characterized by the different ratios of their *m/z* 43 and *m/z* 44 fragments (Fig. 4b), ~~that~~ which represent the oxidation level (Canagaratna et al., 2015). While *m/z* 43 could be derived from $C_2H_3O^+$ (a signature of the semi-volatile) and/or C_3H7^+ (a signature of the primary emissions of the hydrocarbon-like), *m/z* 44 is mainly derived from the fragment of CO_2^+ (a signature of oxygenated, particularly acids) (Canonaco et al., 2015; Ng et al., 2010). As presented in Fig. 4b, MO-OOA mass spectra showed a notable peak at *m/z* 44. This spectrum has been extensively recognized as low volatility OOA (LV-OOA) and described to be made~~-~~up of aged secondary OA (SOA) and highly oxidized OA (~~Lanz et al., 2007;~~ Ulbrich et al., 2009; ~~Q.~~ Zhang et al., 2011; Ng et al., 2011~~b~~); while the mass spectra of LO-OOA in this study presented a higher *m/z* 43 (Figs. 4b) compared to MO-OOA, which is similar to the mass spectral pattern of the previously reported freshly formed semi~~-~~volatile OOA (SV-OOA) (Jimenez et al., 2009; Ng et al., 2010). To differentiate the variations of the OOAs factor, the *f*44 vs *f*43 space was used which is a typical diagnostic tool based on atmospheric aging (Ng et al., 2010).

The seasonal *f*44/ *f*43 for OOAs measured points and the *f*44/ *f*43 for modelled factor profiles (LO-OOA and MO-OOA) are presented in Fig. S5~~4~~. The data points in Fig. S5~~4~~ are distributed differently according to the season (Chen et al., 2021; Canonaco et al., 2015; Crippa et al., 2014; Chazeau et al., 2022). Furthermore, the modelled factor profile points represent a high variability in space, especially for LO-OOA. This assumes how an annual or seasonal PMF solution, unless a larger number of factors are used, would perform poorly in capturing all of the variations of SOA. In order to capture time-dependent changes, in particular for LO-OOA, it is, therefore, advantageous to perform rolling PMF analysis. The triangle plot defined by Ng et al. (2010) is also shown in Fig. S5~~4~~. As assumed the LO-OOA points were concentrated in the lower part of the space,

whereas more aged MO-OOA points relocated to the upper part of the space during the aging process. The fall, spring, and summer data points were all located on the right side of the triangle (Fig. S5~~4~~), however, the winter data points were located near the top and inside the triangle. The data points on the right side of the triangle correspond to the time exposed to higher temperatures more than those that are within the triangle. This could be attributed to an increase in biogenic SOA emissions if the temperature increased, as biogenic OOA appears to be dispersed all along the right ~~the~~ side of the triangle. Furthermore, as the temperature is reduced, the increased biomass emissions cause the OOA points to lie vertically inside the triangle, as seen in the winter data.

The two OOAs were the two most significant contributors to the total OA fraction (Fig. 4) over the entire period. The seasonal mean mass concentrations of MO-OOA varied from higher mass concentrations during winter (2.25 µg/m^3) and lower during summer time (1.44 µg/m^3, Table. 1). However, the highest MO-OOA mass concentrations found during the cold periods are similar to the seasonal patterns in POA. This high mass concentration in cold seasons can be seen from the NWR plot (Fig. 7) presenting local emissions with low wind speed (> 5 m/s) and transported emissions from east, north-east, and south-west directions with high wind speed (< 5 m/s). ~~-~~Furthermore, high mass concentrations of MO-OOA are generally found at high relative humidity (RH > 80 %) and low temperature (< 0 °C), i.e., conditions during winter time (Fig. S6~~5~~). This low air temperature condition can be linked to a possible scenario for an increase in the MO-OOA precursor emissions from biomass burning and coal combustion as a result of residential heating activities during winter time. Therefore, significant enhancement appears to be an effect of RH during winter, proposing that the aqueous-phase heterogeneous mechanisms could also play a crucial way in the regional MO-OOA formation through winter as suggested by Gilardoni et al., (2016). In contrast, no RH-temperature-dependent trends for the MO-OOA were found in the other seasons (Fig. S6~~5~~), indicating more complex formation processes during other seasons. Meanwhile, MO-OOA diurnal cycles presented a seasonal variation as well, with a remarkable enhancement in the evening and night time during winter (Fig. 6), indicating a potential regional formation mechanism containing night time chemistry (Tiitta et al., 2016), and descending pattern from night time to day time due to planetary boundary layer effect~~Meanwhile, MO-OOA diurnal cycles presented a seasonal variation as well, with a remarkable enhancement in the evening and night time during winter (Fig. 6), indicating a potential regional formation mechanism containing night time chemistry (Tiitta et al., 2016).~~ While in fall, spring, and summer, MO-OOA displayed a considerable increase during the day (Fig. 6), indicating that higher temperatures result in considerable regional photochemical production of SOA particles (Fig. S4~~3~~) and enhanced solar radiation (Petit et al., 2015). Furthermore, regarding the correlation of mass concentration of MO-OOA with sulphate, the latter is regarded as a local secondary production indicator (Petit et al., 2015, and Table. 1). Consequently, alongside almost stable mass spectra throughout the year, MO-OOA seems to be derived from a variety of seasonal-dependent formation mechanisms and sources (such as aged background, biomass burning, coal combustion, and biogenic sources).

The seasonal mean mass concentrations of LO-OOA varied from higher mass concentrations during fall (2.13 μg/m^3) and lower mass concentrations during spring time (1.24 μg/m^3, Table. 1). Temperature had a significant effect on LO-OOA, and showed a distinguishable seasonal variation pattern. The temperature-RH dependence of the LO-OOA was not quite similar depending on the season (Fig. S65). The highest winter time LO-OOA mass concentrations were found mostly at low temperatures and high RH environments, indicating that gas-particle partitioning might have a key role in LO-OOA formation throughout this season. The freshly formed SOA deriving from primary biomass burning and coal combustion emissions, as found in previous studies (Crippa et al., 2013; Zhang et al., 2015; Y. Sun et al., 2018; Stavroulas et al., 2019) can also affect the LO-OOA during the cold months. Furthermore, since nitrate could be originated locally or arrived from a long distance to Melpitz (Sect. 3.1.1), with a good correlation between LO-OOA and nitrate (R^2= 0.59) during winter, the long-range transported LO-OOA from different directions reaching to measuring site could be explained (Fig. 7). ~~Furthermore, during winter time the correlations between LO-OOA and nitrate (R^2= 0.59) were found.~~ Different LO-OOA daily cycles were also found in different seasons (Fig. 6). The daily changes in LO-OOA displayed higher mass concentrations in night time compared to day time in fall, spring, and summer (Fig. 6), highlighting the significant roles of night time chemistry and/or gas-particle partitioning in the LO-OOA formation~~,~~ while the decrease during the day is partly linked to the atmospheric dilution effect (Fig. S43), evaporation and photochemical aging into MO-OOA (Fig. 6). For winter night increments, lower temperature in favor of condensation; and more abundant precursors present considering increased BBOA emission, therefore enhanced night-chemistry activities, leads to higher LO-OOA; moreover, shallow boundary layer in winter and night time inversion caused pollutants to accumulate.

3.3 ~~eBC s~~Source apportionment of eBC-PM$_1$

By applying a multilinear regression model, ~~The~~ during the source apportionment analysis, eBC-PM$_1$ correlated with every one of the three identified primary organic factors (HOA, BBOA, and CCOA, ~~eBC correlated with each of the three identified primary organic factors (HOA, BBOA, and CCOA) during the source apportionment analysis (~~Table. 1~~)). The total amount of these primary factors (known as POA) was highly correlated with eBC (R^2= 0.87; Fig. 8a). As a result, the different sources of eBC were evaluated for each factor utilizing a multilinear regression model, as suggested by Laborde et al., (2013); Zhu et al., (2018) and Poulain et al., (2021), for instance. The following assumes that the eBC mass is associated with the separate contribution from each OA factor (i.e., eBC_{HOA}, eBC_{BBOA}, and eBC_{CCOA}) at any time:~~

~~$$eBC(t) = eBC_{HOA}(t) + eBC_{BBOA}(t) + eBC_{CCOA}(t) \quad (3)$$~~

~~The eBC emission from each source is expected to be proportionate to the separate source mass concentration generated in each season (m_{HOA}, m_{BBOA}, and m_{CCOA}, respectively). As a result, the multilinear regression model can be described as follows:~~

~~$$eBC(t) = am_{HOA} + bm_{BBOA} + cm_{CCOA} \quad (4)$$~~

where a, b, and c are the linear regression coefficients for m_{HOA}, m_{BBOA}, and m_{CCOA}, respectively, that will be applied to evaluate the contribution of eBC per each POA factor for each season (Table. S3).

CCOA appeared to have be the largest source of eBC-PM_1eBC, contributing half of it (eBC-PM_1eBC-CCOA 55 %, Table. 1), followed by eBC-PM_1eBC associated with BBOA 37 % (eBC-PM_1eBC-BBOA), while the lowest contribution was found for eBC-PM_1eBC-HOA (8 %). However, the contribution of sources to the total eBC-PM_1eBC strongly depends on the season. Looking at each individual source, the hydrocarbon-like emissions contributed most to the eBC-PM_1eBC fraction in the fall (eBC-PM_1eBC-HOA with 22 %, Table. 1; Fig. 8b), while biomass burning emissions dominated the eBC-PM_1eBC in summer and coal combustion emission dominated in winter (eBC-PM_1eBC-BBOA and eBC-PM_1eBC-CCOA with 69 % and 56 %, Table. 1). In the diurnal cycle, contribution to the total eBC-PM_1eBC of eBC-PM_1eBC-HOA showed two peaks in the morning and evening for fall, spring, and summer (Fig. S76), reflecting the impact of the traffic rush hours as mentioned in Sect. 3.2.1, and the minimum contributions during the day time due to the effect of lowest emissions and PBL effect (Fig. S43). However, winter time did not show a strong variation in the diurnal cycle (Fig. S76). This indicates the potential influence of continuous emissions at the measurement site. Biomass burning combustion with its maximum contribution during the day in summer (Fig. S76) can be related to a variety of different eBC-PM_1eBC-POA mass concentrations (Fig. S76b), while the BBOA mass concentration was almost constant, the other POA mass concentration decreased during the day. Coal combustion showed an increasing contribution during night time in all the seasons (Fig. S7S6), especially during the winter time, which further confirms the enhanced coal combustion emission in winter nights (Fig. S76b).

3.4 Impact of airSeasonal air mass clustering mass origin and trajectory analysis

As mentioned before, the geographical origin of the PM_1 chemical species and also PMF components are not only emitted from the surrounding area but also transported. Therefore, to better identify the origin of their sources, trajectory analysis, and their clustering analysis were applied using the self-developed back-trajectory cluster method (BCLM) (Sun et al., 2020; Ma et al., 2014; Hussein et al., 2006). A total of fifteen clusters were identified, corresponding to different meteorological conditions over the course of the year at Melpitz (Fig. 9a). The different clusters can be divided according to the different seasons (CS: cold season; TS: transition season; and WS: warm season), and meteorological synoptic patterns (ST: stagnant; A1: anticyclonic with air mass coming from Eastern Europe; A2: anticyclonic with air mass coming from the west; C1: cyclonic with air mass coming from relatively south; C2: cyclonic with air mass coming from the west and south west). However, the clustering approach did not consider spring and fall separately, and therefore the transition clusters correspond to both spring and fall. Regarding this cluster approach, six air masses were identified at Melpitz station for the winter season, four air masses for the transition seasons, and five air masses for the summer season (Fig. 9a). The number of clusters with their corresponding mean mass concentration of PM_1 chemical species and PMF factors of organics are summarized in Table. 2 and with more details in Tables S3 S4 and S4S5.

3.4.1 Winter

Fig. 9b and 9c illustrate the mass concentration and contribution of PM_1 chemical species and PMF factors of organic for each air mass type at Melpitz based on the type of air masses. For the winter season, the cluster CS-ST corresponds to more surrounding emission origin with a PM mean value of 21.95 µg/m^3, which occurred during 14 % of the total measurement period. These surrounding emissions refer to the emissions from Melpitz station directly, Melpitz village, and short distance transported particles like particles from Leipzig and Torgau. ~~Thi~~. This cluster presented the highest mass concentration of LO-OOA to the PM mass (2.73 µg/m^3). In fact, SOA is considered to be formed by biomass burning as well as coal combustion, particularly during the winter when biogenic emissions and UV radiation are low (Lanz et al., 2010; Kodros, et al., 2020). In this condition and in the presence of NO_2 and O_3, the biomass burning emissions could age rapidly and produce SOA. In conclusion, this cluster could confirm the role of freshly formed SOA which originated from the primary biomass burning and coal combustion emission (mass concentrations of 0.97 µg/m^3 and 1.89 µg/m^3, respectively). ~~s cluster with the highest mass concentration of LO-OOA to the PM mass (2.73 µg/m3) could confirm the role of freshly formed SOA originating around the station from primary biomass burning and coal combustion emissions (mass concentration of 0.97 µg/m3 and 1.89 µg/m3, respectively).~~ Furthermore, nitrate showed a high mass concentration and contribution in this air mass (5.38 µg/m^3 and 25 %, respectively) due to e.g., meteorological conditions and abundant precursors.

The cluster CS-A1 with the highest mass concentration of PM (29.14 µg/m^3) represented Eastern European continental air masses (passing Poland and the Czech Republic) during anticyclonic flow which occurred during 18 % of the total measurement period, meaning that Melpitz was under their influence during winter. This air mass, with the highest POA mass concentration (5.56 µg/m^3), especially coal combustion emissions (CCOA and eBC-PM_1 ~~eBC~~-CCOA with an average mass concentration of 4.01 µg/m^3 and 1.93 µg/m^3, respectively), highlight the importance of long-range transported emissions. This cluster also contained the highest mass concentration of sulphate (5.39 µg/m^3) and ~~can~~ could support the importance of coal combustion on sulphate formation, which is known to be strongly emitted by coal power plants (Wierońska-Wiśniewska et al., 2022).

The air mass CS-A2 identified as marine-influenced air mass with a mean value of 13.39 µg/m^3 of PM came from the United Kingdom with the anticyclonic flow, which occurred during 8 % of the total measurement period. This cluster presented a low mass concentration of POA and for two OOAs almost the same mass concentration and contribution (Table. ~~S3~~ S5 and Table. ~~S4~~S6). Since Melpitz is placed away from the coast, therefore the sampling location is affected by aged maritime air masses (Poulain et al., 2011). Inorganics are dominated by nitrate in this cluster with the high mass concentration (3. 86 µg/m^3) ~~and~~ which represents the highest mass fraction (50 % of the total inorganic species).

The CS-C1 air mass with a mean value of 15.99 µg/m^3 characteristic of Southern European air mass, came from an industrial and polluted area starting from Spain and partly crossing Italy with the cyclonic flow, which occurred during 10 % of the total measurement period. POA mass concentration and contribution were low in this cluster, while SOA, especially MO-OOA, showed the highest mass concentration of PM over the entire period (3.77 µg/m^3) and the highest contribution during the winter

season (24 %). This can be linked to the high sulphate in this air mass (2.99 µg/m^3), which showed that the regional influence by contribution from aged BBOA and CCOA might be manifested in MO-OOA (as discussed in Sect. 3.2.2).

Finally, CS-C2a and CS-C2b were both associated with cyclonic and marine influence conditions which only occurred for a short time (3 % and 2 % of the total measurements, respectively), showing the lowest PM mean value (4.09 µg/m^3 and 2.60 µg/m^3, respectively). Both of them showed almost the same mass concentration and contribution of POA (Fig. 8a and b; and Table. ~~S3~~ S5 and ~~S4~~S6). However, similar~~ly~~ to CS-A2, cluster CS-C2a contained a marine component at the beginning point of the air masses, and in the following time it was dominated by continental areas (France and southern Germany), where due to the longer time transferring over continent and aging process, it showed more nitrate mass concentration and contribution than CS-C2b (1.35 µg/m^3, 16 µg/m^3; and 28 % 14 %, respectively). Whereas CS-C2b started near Iceland with same history of the air mass over the continent, and in comparison, with CS-C2a, it presented a higher contribution of sulphate (29 % and 19 %, respectively), which could be associated with aged marine air mass due to the higher contribution of MO-OOA (21 % and 18 %, respectively).

3.4.2 Transition seasons

For transition seasons (fall and spring), whereas the four clusters showed ~~a~~ quite similar PM mass concentrations (Fig. 9) which might be linked to the overall weather situation during these two times of the year, their chemical composition strongly depended on their origins. TS-A1 and TS-A2 corresponded to two different types of anticyclonic air masses with respective mean PM mass concentrations of 6.06 µg/m^3 and 5.86 µg/m^3. Cluster TS-A1 which occurred during 4 % of the total measurements period, started from Finland, crossing the Estonian, Latvian, Lithuanian, and Polish coasts before arriving at Melpitz. Although it might contain a certain marine component, this cluster mostly followed coastal areas, which means that in this cluster OA mass concentration dominated PM (2.95 µg/m^3). Furthermore, this cluster showed continental and polluted aspects with the highest LO-OOA mass concentration and contribution during transition seasons (1.03 µg/m^3 and 17 % respectively), which is linked to originating from freshly formed SOA from primary biomass burning and coal combustion emissions around coastal areas. On the other hand, cluster TS-A2 (4 % of the measurement~~s~~ period) is characterized as a marine cluster and started from the south of Iceland/Greenland. This cluster showed inorganics as the dominant components in PM with a high mass concentration and a mass fraction (3.35 µg/m^3 and 58 % respectively). Since Melpitz is influenced by aged marine air masses, this cluster showed a maximum nitrate mass concentration during the transition seasons (1.54 µg/m^3 and a contribution of 26 %, respectively).

Finally, two other clusters TS-C1 and TS-C2 were two different types of cyclonic air masses in fall and spring time, with mean PM mass concentrations of 4.69 µg/m^3 and 4.94 µg/m^3 respectively. These trajectories with different types of marine influenced air masses occurred for a very short period of time (3 % and 4 % of the total measurements period, respectively). The first one, TS-C1, started from the Atlantic Ocean near Spain and is associated with a more continental influence, which is why organic mass concentration and contribution were higher than inorganics. However, The LO-OOA contribution of this cluster was the highest during this time period (26 %) due to the aging processes of primary organic aerosols especially CCOA, which had a

maximum mass concentration (0.31 µg/m^3 and mass fraction of 7 %, respectively). While the second one, TS-C2, was almost a pure marine cluster, coming from the Norwegian Sea. In opposition to TS-C1, PM was dominated by inorganics in TS-C2, with a high mass concentration of nitrate (1.35 µg/m^3) representing the aging effect due to the long-time transfer over the continents.

3.4.3 Summer

During the summer season, the different clusters showed strong changes in both chemical compositions and total mass concentrations. Cluster WS-ST was identified as the local air mass with a mean value of 8.97 µg/m^3, which occurred for a short period, 6 % of the measurement. However, this cluster contained a low POA mass concentration but a maximum contribution of MO-OOA (32 %), assuming important regional photochemical roles of SOA particles with higher temperatures (Fig. ~~11~~S4) and enhanced solar radiation (Petit et al., 2015).

Air masses WS-A1 and WS-A2 were two different types of anticyclonic air masses with different directions and different mean PM mass concentrations. Cluster WS-A1, known as the highest mass concentration during summer time, (16.95 µg/m^3 and contribution of 11 % of the measurement period) was the continental air mass which was coming from Eastern Europe during the anticyclonic flow (starting from Belarus, crossing Poland and the Czech Republic). This air mass included maximum inorganics and organics especially CCOA mass concentration (1.28 µg/m^3) during summer time, which can explain the existing higher CCOA during summer, and showed the role of long-range transported emissions in the summer season. However, WS-A2 air mass, with a mean value of 9.48 µg/m^3 was a marine-influenced air masse and was coming from the North Sea, which only occurred for a short period (6 % of the total measurement period).

Moreover, two cyclonic air masses, WS-C1 and WS-C2, were also identified as two different marine clusters. These trajectories did not occur very often, only 5 % and 3 % of the total measurement period, respectively. The starting point of WS-C1 with a mean value of 8.41 µg/m^3 was the Celtic Sea, but in the following time, it predominantly passed over continental areas (France and southern Germany), which means it could be aged and the result can be shown in the high mass concentration of nitrate and sulphate in this cluster (1.63 µg/m^3 and 1.86 µg/m^3, respectively). Finally, the starting point of WS-C2 with a mean value of 4.46 µg/m3, was near Iceland, with the lowest PM mass concentration during summer. However, it showed the highest sulphate contribution (27 %) at this time which could be associated with aged marine air mass like other marine air masses.

3.4.4 Cluster seasonality

A parallel comparison can be made between the winter and summer clusters. Clusters CS-A1 and WS-A1 both show the highest POA contribution dominated by coal combustion, which emphasizes that the origin of this source could be associated with the transport of the coal power plants emissions from Eastern Europe (e.g. Eastern part of Germany, Poland, Czech Republic and further countries located in the East). ~~They~~ These clusters were not only affected by the winter air quality but also the summer air quality.

Clusters CS-ST and WS-ST, which were known as local air masses, showed the seasonal effect on the chemical component. First, the volatility of ammonium nitrate at higher summer temperatures could explain their lower value in summer. Then, atmospheric photochemical oxidation processes affected the sulphate locally formed emission in summer, which its highest value over inorganic components during summer can be confirmed. Not surprisingly, due to the residential heating effect, POA mass concentration was very high during winter; however, freshly formed SOA originating from biomass and coal emissions can explain the higher LO-OOA mass concentration in winter.

During the whole period, some marine air masses with cyclonic and anticyclonic flow showed the important roles of aged marine air masses over the measurement site: a) clusters CS-A2 and WS-A2 with anticyclonic pattern starting from the North and/or Norwegian Sea, and b) CS-C2a, WS-C1, and TS-C1 starting from the Celtic Sea near Spain, and also CS-C2b and WS-C2 starting from Iceland, all with cyclonic patterns contain nitrate and sulphate during the transferring over the continental areas in different seasons.

4 Conclusion

The chemical compositions of non-refractory fine aerosol (NR-PM_1) at the German rural-background observatory Melpitz were investigated in this study over a one-year period between September 2016 and August 2017. Overall, the averaged total PM_1 mass concentration is 10.49 $\mu g/m^3$ and follows a clear seasonal pattern, with the highest mass concentration during winter (15.95 $\mu g/m^3$) and the lowest mass concentration during summer time (6.24 $\mu g/m^3$). The organic aerosol was the most significant component, accounting for 46% of total PM_1 and showing significant seasonal dependency (39 % in winter to 58 % in summer). It was followed by sulphate (15 % and 20 %) and nitrate (24 % and 11 %). For OA source apportionment, PMF in a rolling fashion has been applied using the SoFi Pro, which provided the decomposition of time-dependent factor profiles that were able to better capture the variability of OA sources across seasons in comparison with the conventional seasonal PMF. The final solution enabled the identification of five factors throughout the one-year measurements of OA; HOA, BBOA, CCOA, LO-OOA, and MO-OOA. Using the correlation between HOA, BBOA, and CCOA with eBC-PM_1, a multilinear regression approach was applied to perform the source apportionment of eBC-PM_1.

Generally, in Melpitz, HOA as a minor source of OA (6 % of the contribution of total organic mass) and eBC-PM_1 (8 % of the total eBC-PM_1) was associated with: a) low traffic emissions, b) household heating in winter, and c) the central heating for hot water production for all the seasons which uses multiple fuel types in the Melpitz area. BBOA representing 7.9 % of the contribution of total organic mass and 37 % of the total eBC-PM_1, showed a seasonal effect, emphasizing the impact of house heating during winter. Similar to HOA, the presence of BBOA during summer was due to central heating which uses multiple fuel types in the Melpitz area. The most dominant anthropogenic source was associated with CCOA with a 15.4 % contribution of total organic mass and 55 % of the total eBC-PM_1 with the highest mass concentration and contribution of PM during winter rather than summer. Although a certain fraction of CCOA could be linked to surrounding domestic heating (van Pinxteren et

al., 2020), it is rather associated with power plant emissions and long-range transport all year round which is supported by cluster and back-trajectory analysis. LO-OOA and MO-OOA referred to oxidized oxygenated organic aerosol (32.4 % and 38.4 % of the contribution of total organic mass, respectively), were identified as a secondary organic aerosol with the highest mass concentration during the cold months and the lowest mass concentration during the warm months. LO-OOA mass concentration decreased during the day due to dilution, and the evaporation process resulted in aging into MO-OOA.

A combination of the NWR model and cluster analysis was used to better understand the origin of the aerosol reaching the station. Overall, Melpitz is influenced by fifteen types of air masses, such as long-range continental, marine, and surrounding emissions. During winter and summer time, easterly continental air masses, CS-A1 and WS-A1 with an anticyclonic pattern come from Eastern Europe and showed a significant particle mass concentration, especially high POA (and CCOA) mass concentration at the measurement site. Marine clusters, mostly coming from the south/west/north side with aged marine air masses including nitrate and sulphate, also have important roles in the PM mass concentration at the Melpitz site over the entire period (winter: CS-A2, CS-C2b, and CS-C2a, transition: TS-C, TS-A2 and TS-C2, and summer: WS-Ca, WS-C2, and WS-A2). However, the surrounding emissions are recognized as another important source of emissions which include high organic and inorganic components during winter and summer (CS-ST and WS-ST, respectively).~~Within this study, the change in chemical compositions of non-refractory fine aerosol (NR-PM_1) at the German rural-background observatory Melpitz was investigated during a one-year period between September 2016 and August 2017, by applying PMF in a rolling fashion with 14 days window length and a 1-day shift using the SoFi Pro. This method provided the decomposition of time-dependent factor profiles that were able to better capture the variability of OA sources across seasons, in particular for LO-OOA. Overall, the averaged total PM_1 mass concentration is 10.47 $\mu g/m^3$ and follows a clear seasonal pattern, with the highest mass concentration during winter (15.95 $\mu g/m^3$) and lowest mass concentration during summer time (6.24 $\mu g/m^3$). The organic aerosol was the major component accounting for 46 % of total PM_1 and showing a strong seasonal variability ranging from 39 % (in winter) to 58 % (in summer). It was followed by sulphate (15 % and 20 %) and nitrate (24 % and 11 %). The final solution of the PMF rolling approach for OA source apportionment enabled the identification of five factors throughout the one-year measurements of OA; HOA, BBOA, CCOA, LO-OOA, and MO-OOA.~~

~~Generally, in Melpitz, HOA as a minor source of OA (6 % of the contribution of total organic mass) was associated with: a) low traffic emissions, b) household heating in winter, and c) the central heating for hot water production for all the seasons which showed a small increasing mass concentration pattern toward cold months (winter and summer: 0.36–0.23 $\mu g/m^3$). The HOA night time mass concentration was not affected by the seasons, which indicates the presence of a continuous emission source. Biomass burning emissions (BBOA) representing 7.9 % of the contribution of total organic mass showed a seasonal effect, emphasizing the impact of house heating during winter (winter and summer: 23 % and 8.7 %). This highest mass concentration during the winter time showed the descending pattern from night time to day time due to domestic heating~~

activities and the planetary boundary layer effect; however similar to HOA, the presence of BBOA during summer was due to central heating which uses multiple fuel types in the Melpitz area. The most dominant anthropogenic source was associated with coal combustion (CCOA) with a 15.4 % contribution of total organic mass and 55 % of eBC with the highest mass concentration and contribution of PM during winter rather than summer (1.58 0.30 μg/m^3). Although a certain fraction of CCOA could be linked to surrounding domestic heating (van Pinxteren et al., 2022), it is rather associated with power plant emissions and long range transport all year round. Using the correlation between HOA, BBOA, and CCOA with eBC, a multilinear regression approach was applied to perform the source apportionment of eBC. This analysis highlighted eBC contribution related to the source of HOA (8 % of the total eBC), BBOA (37 % of the total eBC), and CCOA (55 % of the total eBC), which showed the CCOA as the largest source of eBC during the measurement period. Moreover, from the seasonal source apportionment, CCOA presented the largest fraction (56 % of the total eBC) during winter, while the highest fraction is attributed to BBOA for summer time (69% of the total eBC). LO-OOA and MO-OOA referred to oxidized oxygenated organic aerosol (32.4 % and 38.4 % of the contribution of total organic mass, respectively), were identified as a secondary organic aerosol with the highest mass concentration during the cold months (fall: 2.13 μg/m^3 and winter: 2.25 μg/m^3, respectively) and the lowest mass concentration during the warm months (spring: 1.24 μg/m^3 and summer: 1.44 μg/m^3, respectively). LO-OOA mass concentration decreased during the day due to dilution, and the evaporation process resulted in aging into MO-OOA.

A combination of pollution wind rose and cluster analysis was used to better understand the origin of the aerosol reaching the station. Overall, Melpitz is influenced by fifteen types of air masses, such as long-range continental, marine, and surrounding emissions. During winter and summer time, easterly continental air masses, CS-A1 and WS-A1 with an anticyclonic pattern come from Eastern Europe and showed a significant particle mass concentration, especially high POA (and CCOA) mass concentration at the measurement site. Marine clusters, mostly coming from the south/west/north side with aged marine air masses including nitrate and sulphate, also have important roles in the PM mass concentration at the Melpitz site over the entire period (winter: CS-A2, CS-C2b, and CS-C2a, transition: TS-C, TS-A2 and TS-C2, and summer: WS-Ca, WS-C2, and WS-A2). However, the surrounding emissions are recognized as another important source of emissions which include high organic and inorganic components during winter and summer (CS-ST and WS-ST, respectively).

Our results emphasize the importance of the long-range transported emissions of coal combustion related aerosol particles regardless of the season, which supports that the main CCOA source is related to coal power plants emissions. However, coal power plants emissions not only affect the surrounding air quality but can also be transported over long distances. It is important to note that the overall coal combustion mass concentration presented here can certainly be underestimated since the identified CCOA factor is associated with freshly emitted organic aerosol and no factor associated with potential aged coal combustion was identified. Because coal still is an important energy source in the European energy mix (68.4 % of all energy in the EU was produced from coal, crude oil, and natural gas, Energy Statistics - an Overview - Statistics Explained, 2022) as well as on

a global scale and also that it still will be in used for the coming decades (until 2040, Europe's Coal Exit - Europe Beyond Coal : Europe Beyond Coal, 2022), further researches should be done on the identification of coal emissions across Europe in order to better understand its atmospheric aging processes.

Acknowledgements

This work is supported by the COST action CA16109 Chemical On-Line cOmpoSition and Source Apportionment of fine aerosoLs (COLOSSAL), the SNF COST project SAMSAM IZCOZO_177063., by the infrastructure projects ACTRIS (EU FP7, grant 262254), the RI-URBANS project under grant NO. 101036245, the ERA-PLANET, and transnational projects SMURBS and iCUPE (grant agreement NO. 689443), and ACTRIS-2 (Grant 654109).

References

Aas, W., Tsyro, S., Bieber, E., Bergström, R., Ceburnis, D., Ellermann, T., Fagerli, H., Frölich, M., Gehrig, R., Makkonen, U., Nemitz, E., Otjes, R., Perez, N., Perrino, C., Prévôt, A. S. H., Putaud, J. P., Simpson, D., Spindler, G., Vana, M., and Yttri, K. E.: Lessons learnt from the first EMEP intensive measurement periods, Atmos. Chem. Phys., 12(17), 8073–8094, https://doi.org/10.5194/acp-12-8073-2012, 2012.

Alfarra, M. R., Prevot, A. S. H., Szidat, S., Sandradewi, J., Weimer, S., Lanz, V. A., Schreiber, D., Mohr, M., and Baltensperger, U.: Identification of the mass spectral signature of organic aerosols from wood burning emissions, Environ. Sci. Technol., 41(16), 5770–5777, https://doi.org/10.1021/es062289b, 2007.

Allan, J. D., Delia, A. E., Coe, H., Bower, K. N., Alfarra, M. R., Jimenez, J. L., Middlebrook, A. M., Drewnick, F., Onasch, T. B., Canagaratna, M. R., Jayne, J. T., and Worsnop, D. R.: A generalised method for the extraction of chemically resolved mass spectra from Aerodyne aerosol mass spectrometer data, J. Aerosol Sci., 35(7), 909–922, https://doi.org/10.1016/j.jaerosci.2004.02.007, 2004.

Birmili, W., Heinke, K., Pitz, M., Matschullat, J., Wiedensohler, A., Cyrys, J., Wichmann, H. E., and Peters, A.: Particle number size distributions in urban air before and after volatilisation, Atmos. Chem. Phys., 10(10), 4643–4660, https://doi.org/10.5194/acp-10-4643-2010, 2010.

Birmili, W., Schepanski, K., Ansmann, A., Spindler, G., Tegen, I., Wehner, B., Nowak, A., Reimer, E., Mattis, I., M ¨ Uller, K., Brüggemann, E., Brüggemann, B., Gnauk, T., Herrmann, H., Wiedensohler, A., Althausen, D., Schladitz, A., Tuch, T., and Löschau, G.: A case of extreme particulate matter concentrations over Central Europe caused by dust emitted over the southern Ukraine, Atmos. Chem. Phys., 8, www.atmos-chem-phys.net/8/997/2008/, 2008.

Birmili, W., Stratmann, F., and Wiedensohler, A.: Technical note design of a DMA-based size spectrometer for a large particle size range and stable operation, J. Aerosol Sci., 30, Issue 4, 1999.

Birmili, W., Sun, J., Wiedensohler, A., Birmili, W., Sun, J., Weinhold, K., Merkel, M., Rasch, F., Spindler, G., Wiedensohler, A., Bastian, S., Löschau, G., Schladitz, A., Quass, U., Kuhlbusch, T. A. J., Kaminski, H., Cyrys, J., Pitz, M., Gu, J., Peters, A., Flentje, H., Meinhardt, F., Schwerin, A., Bath, O., Ries, L., Gerwig, H., Wirtz, K., and Weber, S.: Enhanced Land Use Regression models for urban fine dust and ultrafine particle concentrations View project Radon parallel measurements, View project Atmospheric aerosol measurements in the German Ultrafine Aerosol Network (GUAN), https://www.researchgate.net/publication/330910927, 2015.

Birmili, W., Weinhold, K., Rasch, F., Sonntag, A., Sun, J., Merkel, M., Wiedensohler, A., Bastian, S., Schladitz, A., Löschau, G., Cyrys, J., Pitz, M., Gu, J., Kusch, T., Flentje, H., Quass, U., Kaminski, H., Kuhlbusch, T. A. J., Meinhardt, F., Schwerin, A., Bath, O., Ries, L., Gerwig, H., Wirtz, K., and Fiebig, M.: Long-term observations of tropospheric particle number size distributions and equivalent black carbon mass concentrations in the German Ultrafine Aerosol Network (GUAN), Earth System Science Data, 8(2), 355–382, https://doi.org/10.5194/essd-8-355-2016, 2016.

Birmili, W., Wiedensohler, A., Mueller, K., Birmili, W., Weinhold, K., Nordmann, S., Wiedensohler, A., Spindler, G., Müller, K., Herrmann, H., Gnauk, T., Pitz, M., Cyrys, J., Flentje, H., Nickel, C., J Kuhlbusch, T. A., Löschau, G., Haase, D., Meinhardt, F., F., Schwerin, A., Ries, L., and Wirtz, K.: Atmospheric aerosol measurements in the German Ultrafine Aerosol Network (GUAN) Korngrößendifferenzierte Feinstaubbelastung in Straßennähe in Ballungsgebieten Sachsens (2003-2005) View project Chemistry, Air Quality and Climate View project Atmospheric aerosol measurements in the German Ultrafine Aerosol Network (GUAN) Part 1: Soot and particle number size distributions, https://www.researchgate.net/publication/232089057, 2009.

Bootstrap Methods: Another Look at the Jackknife on JSTOR, https://www.jstor.org/stable/2958830?origin=JSTOR-pdf, 1979.

Bressi, M., Cavalli, F., Putaud, J. P., Fröhlich, R., Petit, J. E., Aas, W., Äijälä, M., Alastuey, A., Allan, J. D., Aurela, M., Berico, M., Bougiatioti, A., Bukowiecki, N., Canonaco, F., Crenn, V., Dusanter, S., Ehn, M., Elsasser, M., Flentje, H., M., Flentje, H., Graf, P., Green, D. C., Heikkinen, L., Hermann, H., Holzinger, R., Hueglin, C., Keernik, H., Kiendler-Scharr, A., Kubelova, L., Lunder, C., Maasikmets, M., Makes, O., Malaguti, A., Mihalopoulos, N., Nicolas, J.B., O'Dowd, C., Ovadnevaite, J., Petralia, E., Poulain, L., Priestman, M., Riffault, V., Ripoll, A., Schlag, P., Schwarz, J., Sciarec,, J., Slowik, J., Sosedova, Y., Stavroulas, I., Teinemaa, E., Via, M., Vodickar, P., Williams, P.I., Wiedensohler, A., Young, D.E., Zhang, S., Favez, O., Minguillon, M.C., and Prevot, A. S. H.: A European aerosol phenomenology - 7: High-time resolution chemical characteristics of submicron particulate matter across Europe, Atmos. Environ, X, 10, https://doi.org/10.1016/j.aeaoa.2021.100108, 2021.

Canagaratna, M. R., Jayne, J. T., Ghertner, D. A., Herndon, S., Shi, Q., Jimenez, J. L., Silva, P. J., Williams, P., Lanni, T., Drewnick, F., Demerjian, K. L., Kolb, C. E., and Worsnop, D. R.: Chase studies of particulate emissions from in-use New York City vehicles, Aerosol Sci Technol., 38(6), 555–573, https://doi.org/10.1080/02786820490465504, 2004.

Canagaratna, M. R., Jimenez, J. L., Kroll, J. H., Chen, Q., Kessler, S. H., Massoli, P., Hildebrandt Ruiz, L., Fortner, E., Williams, L. R., Wilson, K. R., Surratt, J. D., Donahue, N. M., Jayne, J. T., and Worsnop, D. R.: Elemental ratio measurements of organic compounds using aerosol mass spectrometry: Characterization, improved calibration, and implications, Atmos. Chem. Phys., 15(1), 253–272, https://doi.org/10.5194/acp-15-253-2015, 2015.

Canonaco, F., Crippa, M., Slowik, J. G., Baltensperger, U., and Prévôt, A. S. H.: SoFi, an IGOR-based interface for the efficient use of the generalized multilinear engine (ME-2) for the source apportionment: ME-2 application to aerosol mass spectrometer data, Atmos. Meas. Tech., 6(12), 3649–3661, https://doi.org/10.5194/amt-6-3649-2013, 2013.

Canonaco, F., Slowik, J. G., Baltensperger, U., and Prévôt, A. S. H.: Seasonal differences in oxygenated organic aerosol composition: Implications for emissions sources and factor analysis, Atmos. Chem. Phys., 15(12), 6993–7002, https://doi.org/10.5194/acp-15-6993-2015, 2015.

Canonaco, F., Tobler, A., Chen, G., Sosedova, Y., Gates Slowik, J., Bozzetti, C., Rudolf Daellenbach, K., el Haddad, I., Crippa, M., Huang, R. J., Furger, M., Baltensperger, U., and Prévôt, A. S. H.: A new method for long-term source apportionment with time-dependent factor profiles and uncertainty assessment using SoFi Pro: Application to 1 year of organic aerosol data. Atmos. Meas. Tech., 14(2), 923–943, https://doi.org/10.5194/amt-14-923-2021, 2021.

Canonaco, F., Tobler, A., Chen, G., Sosedova, Y., Slowik, J. G., Bozzetti, C., Daellenbach, K. R., ElHaddad, I., Crippa, M., Huang, R.-J., Furger, M., Baltensperger, U., and Prévôt, A. S. H.: A new method for long-term source apportionment with time-dependent factor profiles and uncertainty assessment using SoFi Pro: application to one year of organic aerosol data, Atmos. Meas. Tech., 1–39, https://doi.org/10.5194/amt-2020-204, 2020.

Chazeau, B., el Haddad, I., Canonaco, F., Temime-Roussel, B., D'Anna, B., Gille, G., Mesbah, B., Prévôt, A. S. H., Wortham, H., and Marchand, N.: Organic aerosol source apportionment by using rolling positive matrix factorization: Application to a Mediterranean coastal city, Atmos. Environ., X, 14, https://doi.org/10.1016/j.aeaoa.2022.100176, 2022.

Chen, G., Canonaco, F., Tobler, A., Aas, W., Alastuey, A., Allan, J., Atabakhsh, S., Aurela, M., Baltensperger, U., Bougiatioti, A., de Brito, J. F., Ceburnis, D., Chazeau, B., Chebaicheb, H., Daellenbach, K. R., Ehn, M., el Haddad, I., Eleftheriadis, K., Favez, O., Flentje, H., Font, A., Fossum, K., Freney, E., Gini, M., Green, D.C., Heikkinen, L., Herrmann, H., Kalogridis, A., Keernik, H., Lhotka, R., Lin, C., Lunder, C., Maasikmets, M., Manousakas, M.I., Marchand, N., Marin, C., Marmureanu, L., Mihalopoulos, N., Mocnika, G., Nęckia, J., O'Dowd, C., Ovadnevaite, J., Petera, T., Petita, J.E., Pikridasa, M., Matthew Platt, S., Pokorna, P., Poulain, L., Priestman, M., Riffault, V., Rinaldia, M., Rozanskia, K., Schwarz, J., Sciarea, J., Simon, L., Skiba, A., Slowik, J.G., Sosedova, Y., Stavroulas, I., Styszkoa, K., Teinemaa, E., Timonen, H., Tremper, A., Vasilescu, J., Via, M., Vodicka, P., Wiedensohler, A., Zografou, O., Cruz Minguillon, M., and Prévôt, A. S. H.: European aerosol phenomenology –

8: Harmonised source apportionment of organic aerosol using 22 Year-long ACSM/AMS datasets, Environ. Int., 166, https://doi.org/10.1016/j.envint.2022.107325, 2022.

Chen, G., Sosedova, Y., Canonaco, F., Fröhlich, R., Tobler, A., Vlachou, A., Daellenbach, K., Bozzetti, C., Hueglin, C., Graf, P., Baltensperger, U., Slowik, J., el Haddad, I., and Prévôt, A.: Time dependent source apportionment of submicron organic aerosol for a rural site in an alpine valley using a rolling PMF window, Atmos. Chem. Phys., 1–52, https://doi.org/10.5194/acp-2020-1263, 2020.

Chen, G., Sosedova, Y., Canonaco, F., Fröhlich, R., Tobler, A., Vlachou, A., Daellenbach, K. R., Bozzetti, C., Hueglin, C., Graf, P., Baltensperger, U., Slowik, J. G., el Haddad, I., and Prévôt, A. S. H.: Time-dependent source apportionment of submicron organic aerosol for a rural site in an alpine valley using a rolling positive matrix factorisation (PMF) window, Atmos. Chem. Phys., 21(19), 15081–15101, https://doi.org/10.5194/acp-21-15081-2021, 2021.

Crippa, M., Canonaco, F., Lanz, V. A., Äijälä, M., Allan, J. D., Carbone, S., Capes, G., Ceburnis, D., Dall'Osto, M., Day, D. A., DeCarlo, P. F., Ehn, M., Eriksson, A., Freney, E., Ruiz, L. H., Hillamo, R., Jimenez, J. L., Junninen, H., Kiendler-Scharr, A., Kortelainen, A.-M., Kulmala, M., Laaksonen, A., Mensah10, A.A., Mohr1, C., Nemitz, E., O'Dowd, C., Ovadnevaite, J., Pandis, S. N., Petäjä, T., Poulain, L., Saarikoski, S., Sellegri, K., Swietlicki, E., Tiitta, P., Worsnop, D. R., Baltensperger, U., and Prévôt, A. S. H.: Organic aerosol components derived from 25 AMS data sets across Europe using a consistent ME-2 based source apportionment approach. Atmos. Chem. Phys., 14(12), 6159–6176, https://doi.org/10.5194/acp-14-6159-2014, 2014.

Crippa, M., Decarlo, P. F., Slowik, J. G., Mohr, C., Heringa, M. F., Chirico, R., Poulain, L., Freutel, F., Sciare, J., Cozic, J., di Marco, C. F., Elsasser, M., Nicolas, J. B., Marchand, N., Abidi, E., Wiedensohler, A., Drewnick, F., Schneider, J., Borrmann, S., Nemitz, E., Zimmermann, R., Jaffrezo, J.-L., Prevot, A. S. H., and Baltensperger, U. Wintertime aerosol chemical composition and source apportionment of the organic fraction in the metropolitan area of Paris, Atmos. Chem. Phys., 13(2), 961–981, https://doi.org/10.5194/acp-13-961-2013, 2013.

Daellenbach, K. R., Uzu, G., Jiang, J., Cassagnes, L. E., Leni, Z., Vlachou, A., Stefenelli, G., Canonaco, F., Weber, S., Segers, A., Kuenen, J. J. P., Schaap, M., Favez, O., Albinet, A., Aksoyoglu, S., Dommen, J., Baltensperger, U., Geiser, M., el Haddad, I., Jaffrezo, J.L., and Prévôt, A. S. H.: Sources of particulate-matter air pollution and its oxidative potential in Europe, Nature, 587(7834), 414–419, https://doi.org/10.1038/s41586-020-2902-8, 2020.

Dall'Osto, M., Ovadnevaite, J., Ceburnis, D., Martin, D., Healy, R. M., O'Connor, I. P., Kourtchev, I., Sodeau, J. R., Wenger, J. C., and O'Dowd, C.: Characterization of urban aerosol in Cork city (Ireland) using aerosol mass spectrometry. Atmos. Chem. Phys., 13(9), 4997–5015, https://doi.org/10.5194/acp-13-4997-2013, 2013.

Draxler, R.R. and Hess, G.D.: Description of the HYSPLIT-4 Modeling System, NOAA Technical Memorandum ERL ARL-224, NOAA Air Resources Laboratory, Silver Spring, 1-24, 1997.

Dudoitis, V., Byčenkiene, S., Plauškaite, K., Bozzetti, C., Fröhlich, R., Mordas, G., and Ulevičius, V.: Spatial distribution of carbonaceous aerosol in the southeastern Baltic Sea region (event of grass fires), Acta Geophysica, 64(3), 711–731, https://doi.org/10.1515/acgeo-2016-0018, 2016.

Energy statistics - an overview - Statistics Explained, https://ec.europa.eu/eurostat/statistics-explained/index.php?title=Energy_statistics_-_an_overview, 2022.

Europe's coal exit - Europe Beyond Coal: Europe Beyond Coal, https://beyond-coal.eu/europes-coal-exit/, 2022.

Fröhlich, R., Crenn, V., Setyan, A., Belis, C. A., Canonaco, F., Favez, O., Riffault, V., Slowik, J. G., Aas, W., Aijälä, M., Alastuey, A., Artiñano, B., Bonnaire, N., Bozzetti, C., Bressi, M., Carbone, C., Coz, E., Croteau, P. L., Cubison, M. J., Esser-Gietl, J. K., Green, D. C., Gros, V., Heikkinen, L., Herrmann, H., Jayne, J. T., Lunder, C. R., Minguillón, M. C., Mocnik, G., O'Dowd, C. D., Ovadnevaite, J., Petralia, E., Poulain, L., Priestman, M., Ripol, Sarda-Estève, A., R., Wiedensohler, A., Baltensperger, U., Sciare, J., and Prévôt, A. S. H., ACTRIS ACSM intercomparison - Part 2: Intercomparison of ME-2 organic source apportionment results from 15 individual, co-located aerosol mass spectrometers, Atmos. Meas. Tech., 8(6), 2555–2576, https://doi.org/10.5194/amt-8-2555-2015, 2015.

Fröhlich, R., Cubison, M. J., Slowik, J. G., Bukowiecki, N., Prévôt, A. S. H., Baltensperger, U., Schneider, J., Kimmel, J. R., Gonin, M., Rohner, U., Worsnop, D. R., and Jayne, J. T.: The ToF-ACSM: A portable aerosol chemical speciation monitor with TOFMS detection. Atmos. Meas. Tech., 6(11), 3225–3241, https://doi.org/10.5194/amt-6-3225-2013, 2013.

Gilardoni, S., Massoli, P., Paglione, M., Giulianelli, L., Carbone, C., Rinaldi, M., Decesari, S., Sandrini, S., Costabile, F., Gobbi, G. P., Pietrogrande, M. C., Visentin, M., Scotto, F., Fuzzi, S., and Facchini, M. C.: Direct observation of aqueous secondary organic aerosol from biomass-burning emissions, Proceedings of the National Academy of Sciences of the United States of America, 113(36), 10013–10018, https://doi.org/10.1073/pnas.1602212113, 2016.

Heikkinen, L., Äijälä, M., Daellenbach, K., Chen, G., Garmash, O., Aliaga, D., Graeffe, F., Räty, M., Luoma, K., Aalto, P., Kulmala, M., Petäjä, T., Worsnop, D., and Ehn, M.: Eight years of sub-micrometre organic aerosol composition data from the boreal forest characterized using a machine-learning approach, Atmos. Chem. Phys., 1–47, https://doi.org/10.5194/acp-2020-868, 2020.

Henry, R., Norris, G. A., Vedantham, R., and Turner, J. R.: Source region identification using kernel smoothing, Environ. Sci. Technol., 43(11), 4090–4097, https://doi.org/10.1021/es8011723, 2009.

Huang, S., Wu, Z., Poulain, L., van Pinxteren, M., Merkel, M., Assmann, D., Herrmann, H., and Wiedensohler, A.: Source apportionment of the organic aerosol over the Atlantic Ocean from 53°N to 53°S: Significant contributions from marine emissions and long-range transport, Atmos. Chem. Phys., 18(24), 18043–18062, https://doi.org/10.5194/acp-18-18043-2018, 2018.

Huang, W., Saathoff, H., Shen, X., Ramisetty, R., Leisner, T., and Mohr, C.: Seasonal characteristics of organic aerosol chemical composition and volatility in Stuttgart, Germany, Atmos. Chem. Phys., 19(18), 11687–11700, https://doi.org/10.5194/acp-19-11687-2019, 2019.

Hussein, T., Karppinen, A., Kukkonen, J., Härkönen, J., Aalto, P. P., Hämeri, K., Kerminen, V. M., and Kulmala, M.: Meteorological dependence of size-fractionated number concentrations of urban aerosol particles, Atmos. Environ., 40(8), 1427–1440, https://doi.org/10.1016/j.atmosenv.2005.10.061, 2006.

Iapalucci, T. L., Demski, R. J., and Bienstock, D.: Chlorine in Coal Combustion. United States Department of the Interior, Bureau of Mines Report of Investigation 7260s, 1969.

Iinuma, Y., Engling, G., Puxbaum, H., and Herrmann, H.: A highly resolved anion-exchange chromatographic method for determination of saccharidic tracers for biomass combustion and primary bio-particles in atmospheric aerosol, Atmos. Environ., 43(6), 1367–1371, https://doi.org/10.1016/j.atmosenv.2008.11.020, 2009.

Jayne, J. T., Leard, D. C., Zhang, X., Davidovits, P., Smith, K. A., Kolb, C. E., and Worsnop, D. R.: Development of an Aerosol Mass Spectrometer for Size and Composition Analysis of Submicron Particles, Aerosol Sci Technol., 33:1-2, 48-70, https://doi.org/10.1080/027868200410840, 2000.

Jimenez, J. L., Canagaratna, M. R., Donahue, N. M., Prevot, A. S. H., Zhang, Q., Kroll, J. H., DeCarlo, P. F., Allan, J. D., Coe, H., Ng, N. L., Aiken, A. C., Docherty, K. S., Ulbrich, I. M., Grieshop, A. P., Robinson, A. L., Duplissy, J., Smith, J. D., Wilson, K. R., Lanz, V. A., Hueglin, C., Sun, Y. L., Tian, J., Laaksonen, A., Raatikainen, T., Rautiainen, J., Vaattovaara, P., Ehn, M., Kulmala, M., Tomlinson, J. M., Collins, D. R., Cubison, M. J., Dunlea, E. J., Huffman, J. A., Onasch, T. B., Alfarra, M. R., Williams, P. I., Bower, K., Kondo, Y., Schneider, J., Drewnick, F., Borrmann, S., Weimer, S., Demerjian, K., Salcedo, D., Cottrell, L., Griffin, R., Takami, A., Miyoshi, T., Hatakeyama, S., Shimono, A., Sun, J. Y, Zhang, Y. M., Dzepina, K., Kimmel, J. R., Sueper, D., Jayne, J. T., Herndon, S. C., Trimborn, A. M., Williams, L. R., Wood, E. C., Middlebrook, A. M., Kolb, C. E., Baltensperger, U., and Worsnop, D. R.: Evolution of organic aerosols in the atmosphere. Science, 326(5959), 1525–1529, https://doi.org/10.1126/science.1180353, 2009.

Katsanos, D., Bougiatioti, A., Liakakou, E., Kaskaoutis, D. G., Stavroulas, I., Paraskevopoulou, D., Lianou, M., Psiloglou, B. E., Gerasopoulos, E., Pilinis, C., and Mihalopoulos, N.: Optical properties of near-surface urban aerosols and their chemical tracing in a mediterranean city (Athens), Aerosol and Air Quality Research, 19(1), 49–70, https://doi.org/10.4209/aaqr.2017.11.0544, 2019.

Keck, L. and Wittmaack, K.: Effect of filter type and temperature on volatilisation losses from ammonium salts in aerosol matter, Atmos. Environ., 39, 4093–4100, https://doi.org/10.1016/j.atmosenv.2005.03.029, 2005.

Kiendler-Scharr, A., Mensah, A. A., Friese, E., Topping, D., Nemitz, E., Prevot, A. S. H., Äijälä, M., Allan, J., Canonaco, F., Canagaratna, M., Carbone, S., Crippa, M., Dall Osto, M., Day, D. A., de Carlo, P., di Marco, C. F., Elbern, H., Eriksson, A., Freney, E., Hao, L., Herrmann, H., Hildebrandt, L.,. Hillamo, R., Jimenez, J. L., Laaksonen, A., McFiggans, G., Mohr, C., O'Dowd, C., Otjes, R., Ovadnevaite, J., Pandis, S. N., Poulain, L., Schlag, P., Sellegri,

K., Swietlicki, E., Tiitta, P., Vermeulen, A., Wahner, A., Worsnop, D. and Wu, H. C.: Ubiquity of organic nitrates from night time chemistry in the European submicron aerosol, Geophysical Research Letters, 43(14), 7735–7744, https://doi.org/10.1002/2016GL069239, 2016.

Kodros, J., Papanastasiou, D., Paglionea, M., Masiol, M., Squizzato, S., Florou, K., Skyllakou, K., Kaltsonoudis, C., Nenesa, A., and Pandisa, S.: Rapid dark aging of biomass burning as an overlookedsource of oxidized organic aerosol, PNAS, https://doi.org/10.1073/pnas.1602212113, 2020.

Kumar, V., Giannoukos, S., Haslett, S. L., Tong, Y., Singh, A., Bertrand, A., Lee, C. P., Wang, D. S., Bhattu, D., Stefenelli, G., Dave, J. S., Puthussery, J. v., Qi, L., Vats, P., Rai, P., Casotto, R., Satish, R., Mishra, S., Pospisilova, V., C., Bell, D.M., Ganguly, D., Verma, V., Rastogi, N., Baltensperger, U., Tripathi, S.N., Prévôt, A.S.H., and Slowik, J. G.: Highly time-resolved chemical speciation and source apportionment of organic aerosol components in Delhi, India, using extractive electrospray ionization mass spectrometry, Atmos. Chem. Phys., 22(11), 7739–7761, https://doi.org/10.5194/acp-22-7739-2022, 2022.

Laborde, M., Crippa, M., Tritscher, T., Jurányi, Z., Decarlo, P. F., Temime-Roussel, B., Marchand, N., Eckhardt, S., Stohl, A., Baltensperger, U., Prévôt, A. S. H., Weingartner, E., and Gysel, M.: Black carbon physical properties and mixing state in the European megacity Paris, Atmos. Chem. Phys., 13(11), 5831–5856, https://doi.org/10.5194/acp-13-5831-2013, 2013.

Lanz, V., Prevot, A., Alfarra, M., Weimer, S., Mohr, C., DeCarlo, P., Gianini, M., Hueglin, C., Schneider, J., Favez, O., D'Anna, B., George, C., and Baltensperger, U.: Characterization of aerosol chemical composition with aerosol massspectrometry in Central Europe: an overview, Atmos. Chem. Phys., 10, 10453–10471, 2010.

Li, G., Lei, W., Bei, N., and Molina, L. T.: Contribution of garbage burning to chloride and PM 2.5 in Mexico City, Atmos. Chem. Phys., 12(18), 8751–8761, https://doi.org/10.5194/acp-12-8751-2012, 2012.

Lin, C., Ceburnis, D., Hellebust, S., Buckley, P., Wenger, J., Canonaco, F., Prévôt, A. S. H., Huang, R. J., O'Dowd, C., and Ovadnevaite, J.: Characterization of Primary Organic Aerosol from Domestic Wood, Peat, and Coal Burning in Ireland, Environ. Sci. Technol., 51(18), 10624–10632, https://doi.org/10.1021/acs.est.7b01926, 2017.

Liu, P. S. K., Deng, R., Smith, K. A., Williams, L. R., Jayne, J. T., Canagaratna, M. R., Moore, K., Onasch, T. B., Worsnop, D. R., and Deshler, T.: Transmission efficiency of an aerodynamic focusing lens system: Comparison of model calculations and laboratory measurements for the aerodyne aerosol mass spectrometer, Aerosol Sci Technol., 41(8), 721–733, https://doi.org/10.1080/02786820701422278, 2007.

Ma, N., Birmili, W., Müller, T., Tuch, T., Cheng, Y. F., Xu, W. Y., Zhao, C. S., and Wiedensohler, A.: Tropospheric aerosol scattering and absorption over central Europe: A closure study for the dry particle state. Atmos. Chem. Phys., 14(12), 6241–6259, https://doi.org/10.5194/acp-14-6241-2014, 2014.

Marin, C., Marmureanu, L., Rado, C., Dodosci, A., Stan, C., Toanca, F., Preda, L., and Antonescu, B.: Wintertime Variations of Gaseous Atmospheric Constutuents in Bucharest Peri-Urban Area, Atmosphere, 10(8), 478; https://doi.org/10.3390/atmos10080478, 2019.

Middlebrook, A. M., Bahreini, R., Jimenez, J. L., and Canagaratna, M. R.: Evaluation of composition-dependent collection efficiencies for the Aerodyne aerosol mass spectrometer using field data. Aerosol Sci Technol., 46(3), 258–271, https://doi.org/10.1080/02786826.2011.620041, 2012.

Ng, N. L., Canagaratna, M. R., Zhang, Q., Jimenez, J. L., Tian, J., Ulbrich, I. M., Kroll, J. H., Docherty, K. S., Chhabra, P. S., Bahreini, R., Murphy, S. M., Seinfeld, J. H., Hildebrandt, L., Donahue, N. M., Decarlo, P. F., Lanz, V. A., Prévôt, A. S. H., Dinar, E., Rudich, Y., and Worsnop, D. R.: Organic aerosol components observed in Northern Hemispheric datasets from Aerosol Mass Spectrometry, Atmos. Chem. Phys., 10(10), 4625–4641, https://doi.org/10.5194/acp-10-4625-2010, 2010.

Ng, N. L., Herndon, S. C., Trimborn, A., Canagaratna, M. R., Croteau, P. L., Onasch, T. B., Sueper, D., Worsnop, D. R., Zhang, Q., Sun, Y. L., and Jayne, J. T.: An Aerosol Chemical Speciation Monitor (ACSM) for routine monitoring of the composition and mass concentrations of ambient aerosol, Aerosol Sci Technol., 45(7), 780–794, https://doi.org/10.1080/02786826.2011.560211, 2011.

O'Dowd, C., Ceburnis, D., Ovadnevaite, J., Vaishya, A., Rinaldi, M., and Facchini, M. C.: Do anthropogenic, continental or coastal aerosol sources impact on a marine aerosol signature at Mace Head? Atmos. Chem. Phys., 14(19), 10687–10704, https://doi.org/10.5194/acp-14-10687-2014, 2014.

Ovadnevaite, J., Ceburnis, D., Leinert, S., Dall'Osto, M., Canagaratna, M., O'Doherty, S., Berresheim, H., and O'Dowd, C.: Submicron NE Atlantic marine aerosol chemical composition and abundance: Seasonal trends and air mass categorization, J. Geophys. Res., 119(20), 11,850-11,863, https://doi.org/10.1002/2013JD021330, 2014.

Paatero, P.: Least squares formulation of robust non-negative factor analysis, In Chemometrics and Intelligent Laboratory Systems, 37, 1997.

Paatero, P.: The Multilinear Engine- A Table-Driven, Least Squares Program for Solving Multilinear Problems, Including the n-Way Parallel Factor Analysis Model, J Comput Graph Stat., 8(4), 854–888, https://doi.org/10.1080/10618600.1999.10474853, 1999.

Paatero, P., and Tappert, U.: Positive matrix factorization: A non-negative factor model with optimal utilization of error estimates of data values *, ENVIRONMETRICS, 5, 111-126, 1994.

Paglione, M., Gilardoni, S., Rinaldi, M., Decesari, S., Zanca, N., Sandrini, S., Giulianelli, L., Bacco, D., Ferrari, S., Poluzzi, V., Scotto, F., Trentini, A., Poulain, L., Herrmann, H., Wiedensohler, A., Canonaco, F., Prévôt, A. S. H., Massoli, P., Carbone, C., C., Bell, D.M., Ganguly, D., Verma, V., Rastogi, N., Baltensperger, U., Tripathi, S.N., Prévôt, A.S.H., and Fuzzi, S.: The impact of biomass burning and aqueous-phase processing on air quality: A multi-year source apportionment study in the Po Valley, Italy, Atmos. Chem. Phys., 20(3), 1233–1254, https://doi.org/10.5194/acp-20-1233-2020, 2020.

Parworth, C., Fast, J., Mei, F., Shippert, T., Sivaraman, C., Tilp, A., Watson, T., and Zhang, Q.: Long-term measurements of submicrometer aerosol chemistry at the Southern Great Plains (SGP) using an Aerosol Chemical

Speciation Monitor (ACSM), Atmos. Environ., 106, 43–55, https://doi.org/10.1016/j.atmosenv.2015.01.060, 2015.

Petit, J.-E., Favez, O., Sciare, J., Crenn, V., Sarda-Esteve, R., Bonnaire, N., Mocnik, G., Dupont, J. C., Haeffelin, M., Leoz-Garziandia, E., Sarda, R., Petit, J.-E., Favez, O., Sciare, J., Crenn, V., Sarda-Estève, R., Bonnaire, N., Močnik, G., Dupont, J.-C., Haeffelin., M., and Leoz-Garziandia, E.: Two years of near real-time chemical composition of submicron aerosols in the region of Paris using an Aerosol Chemical Speciation Monitor (ACSM) and a multi-wavelength Aethalometer, European Geosciences Union, 15(6), 2985–3005, https://doi.org/10.5194/acpd-14-24221-2014ï, 2015.

Petzold, A., and Schönlinner, M.: Multi-angle absorption photometry - A new method for the measurement of aerosol light absorption and atmospheric black carbon, J. Aerosol Sci., 35(4), 421–441, https://doi.org/10.1016/j.jaerosci.2003.09.005, 2004.

Pope, C. A., and Dockery, D. W., Health Effects of Fine Particulate Air Pollution: Lines that Connect, J. Air & Waste Manage. Assoc 56, 35, https://doi.org/10.1080/10473289.2006.10464485 2006.

Poulain, L., Birmili, W., Canonaco, F., Crippa, M., Wu, Z. J., Nordmann, S., Spindler, G., Prévôt, A. S. H., Wiedensohler, A., and Herrmann, H.: Chemical mass balance of 300 °c non-volatile particles at the tropospheric research site Melpitz, Germany, Atmos. Chem. Phys., 14(18), 10145–10162, https://doi.org/10.5194/acp-14-10145-2014, 2014.

Poulain, L., Fahlbusch, B., Spindler, G., Müller, K., van Pinxteren, D., Wu, Z., Iinuma, Y., Birmili, W., Wiedensohler, A., and Herrmann, H.: Source apportionment and impact of long-range transport on carbonaceous aerosol particles in central Germany during HCCT-2010, Atmos. Chem. Phys., 21(5), 3667–3684, https://doi.org/10.5194/acp-21-3667-2021, 2021.

Poulain, L., Spindler, G., Birmili, W., Plass-Dülmer, C., Wiedensohler, A., and Herrmann, H.: Seasonal and diurnal variations of particulate nitrate and organic matter at the IfT research station Melpitz. Atmos. Chem. Phys., 11(24), 12579–12599, https://doi.org/10.5194/acp-11-12579-2011, 2011.

Poulain, L., Spindler, G., Grüner, A., Tuch, T., Stieger, B., Pinxteren, D. van, Petit, J. E., Favez, O., Herrmann, H., and Wiedensohler, A.: Multi-year ACSM measurements at the central European research station Melpitz (Germany)-Part 1: Instrument robustness, quality assurance, and impact of upper size cutoff diameter, Atmos. Meas. Tech., 13(9), 4973–4994, https://doi.org/10.5194/amt-13-4973-2020, 2020.

Qi, L., Vogel, A. L., Esmaeilirad, S., Cao, L., Zheng, J., Jaffrezo, J. L., Fermo, P., Kasper-Giebl, A., Daellenbach, K. R., Chen, M., Ge, X., Baltensperger, U., Prévôt, A. S. H., and Slowik, J. G.: A 1-year characterization of organic aerosol composition and sources using an extractive electrospray ionization time-of-flight mass spectrometer (EESI-TOF), Atmos. Chem. Phys., 20(13), 7875–7893, https://doi.org/10.5194/acp-20-7875-2020, 2020.

Saha, P., Kylystov, A., and Grieshop, A.: Downwind evolution of the volatility and mixing state of near-road aerosols near a US interstate highway, ACP, https://doi.org/10.5194/acp-18-2139, 2018.

Schaap, M., Spindler, G., Schulz, M., Acker, K., Maenhaut, W., Berner, A., Wieprecht, W., Streit, N., Muller, K., Bruggemann, E., Chi, X., Putaud, J. P., Hitzenberger, R., Puxbaum, H., Baltensperger, U., and ten Brink, H.: Artefacts in the sampling of nitrate studied in the "INTERCOMP" campaigns of EUROTRAC-AEROSOL, Atmos. Environ., 38, 6487–6496, https://doi.org/10.1016/j.atmosenv.2004.08.026, 2004.

Schlag, P., Kiendler-Scharr, A., Johannes Blom, M., Canonaco, F., Sebastiaan Henzing, J., Moerman, M., Prévôt, A. S. H., and Holzinger, R.: Aerosol source apportionment from 1-year measurements at the CESAR tower in Cabauw, the Netherlands, Atmos. Chem. Phys., 16(14), 8831–8847, https://doi.org/10.5194/acp-16-8831-2016, 2016.

Schmale, J., Henning, S., Henzing, B., Keskinen, H., Sellegri, K., Ovadnevaite, J., Bougiatioti, A., Kalivitis, N., Stavroulas, I., Jefferson, A., Park, M., Schlag, P., Kristensson, A., Iwamoto, Y., Pringle, K., Reddington, C., Aalto, P., Äijälä, M., Baltensperger, U., Bialek, J., Birmili, W., Bukowiecki, N., Ehn, M., Fjæraa, A., Fiebig, M., Frank, G., Fröhlich, R., Frumau, A., Furuya, M., Hammer, E., Heikkinen, L., Herrmann, E., Holzinger, R., Hyono, H., Kanakidou, M., Kiendler-Scharr, A., Kinouchi, K., Kos, G., Kulmala, M., Mihalopoulos, N., Motos, G., Nenes, A., O'Dowd, C., Paramonov, M., Petäjä, T., Picard, D., Poulain, L., Prévôt, A., Slowik, J., Sonntag, A., Swietlicki, E., Svenningsson, B., Tsurumaru, H., Wiedensohler, A., Wittbom, C., Ogren, J., Matsuki, A., Yum, S., Myhre, G., Carslaw, K., Stratmann F., and Gysel, M.: Collocated observations of cloud condensation nuclei, particle size distributions, and chemical composition. Sci Data 4, 170003, https://doi.org/10.1038/sdata.2017.3, 2017.

Seinfeld, J. H., and Pandis, S. N.: Atmospheric Chemistry and Physics: From Air Pollution to Climate Change, 3rd Edition, 1152, ISBN 9781118947401, 2006.

Shi, Y., Chen, J., Hu, D., Wang, L., Yang, X., and Wang, X.: Airborne submicron particulate (PM1) pollution in Shanghai, China: Chemical variability, formation/dissociation of associated semi-volatile components and the impacts on visibility, Science of the Total Environment, 473–474, 199–206, https://doi.org/10.1016/j.scitotenv.2013.12.024, 2014.

Shrivastava, M., Cappa, C. D., Fan, J., Goldstein, A. H., Guenther, A. B., Jimenez, J. L., Kuang, C., Laskin, A., Martin, S. T., Ng, N. L., Petaja, T., Pierce, J. R., Rasch, P. J., Roldin, P., Seinfeld, J. H., Shilling, J., Smith, J. N., Thornton, J. A., Volkamer, R., Wang, J., Worsnop, D.R., Zaveri, R.A., Zelenyuk, A., and Zhang, Q.: Recent advances in understanding secondary organic aerosol: Implications for global climate forcing, Reviews of Geophysics, 55(2), 509–559, https://doi.org/10.1002/2016RG000540, 2017.

Simoneit, B. R. T., and Elias, V. O.: Detecting Organic Tracers from Biomass Burning in the Atmosphere, Marine Pollution Bulletin, 42, 10, 805-810, DOI: 10.1016/s0025-326x(01)00094-7, 2001.

Simoneit, B. R. T., Schauer, J. J., Nolte, C. G., Oros, D. R., Elias, V. O., Fraser, M. P., Rogge, W. F., and Cass, G. R.: Levoglucosan, a tracer for cellulose in biomass burning and atmospheric particles, Atmos. Environ., 33, 173-182, https://doi.org/10.1016/S1352-2310(98)00145-9, 1999.

Spindler, G., Brüggemann, E., Gnauk, T., Grüner, A., Müller, K., and Herrmann, H.: A four-year size-segregated characterization study of particles PM10, PM2.5 and PM1 depending on air mass origin at Melpitz, Atmos. Environ., 44(2), 164–173, https://doi.org/10.1016/j.atmosenv.2009.10.015, 2010.

Spindler, G., Gnauk, T., Grüner, A., Iinuma, Y., Müller, K., Scheinhardt, S., and Herrmann, H.: Size-segregated characterization of PM10 at the EMEP site Melpitz (Germany) using a five-stage impactor: A six-year study, J. Atmos. Chem., 69(2), 127–157, https://doi.org/10.1007/s10874-012-9233-6, 2012.

Spindler, G., Grüner, A., Müller, K., Schlimper, S., and Herrmann, H.: Long-term size-segregated particle (PM10, PM2.5, PM1) characterization study at Melpitz - Influence of air mass inflow, weather conditions and season, J. Atmos. Chem., 70(2), 165–195, https://doi.org/10.1007/s10874-013-9263-8, 2013.

Spindler, G., Müller, K., Brüggemann, E., Gnauk, T., and Herrmann, H.: Long-term size-segregated characterization of PM 10, PM 2.5, and PM_1 at the IfT research station Melpitz downwind of Leipzig (Germany) using high and low-volume filter samplers, Atmos. Environ., 38(31), 5333–5347, https://doi.org/10.1016/j.atmosenv.2003.12.047, 2004.

Stavroulas, I., Bougiatioti, A., Grivas, G., Paraskevopoulou, D., Tsagkaraki, M., Zarmpas, P., Liakakou, E., Gerasopoulos, E., and Mihalopoulos, N.K: Sources and processes that control the submicron organic aerosol composition in an urban Mediterranean environment (Athens): A high temporal-resolution chemical composition measurement study, Atmos. Chem. Phys., 19(2), 901–919, https://doi.org/10.5194/acp-19-901-2019, 2019.

Stieger, B., Spindler, G., Fahlbusch, B., Müller, K., Grüner, A., Poulain, L., Thöni, L., Seitler, E., Wallasch, M., and Herrmann, H.: Measurements of PM10 ions and trace gases with the online system MARGA at the research station Melpitz in Germany – A five-year study, J. Atmos. Chem., 75(1), 33–70, https://doi.org/10.1007/s10874-017-9361-0, 2018.

Sun, J., Birmili, W., Hermann, M., Tuch, T., Weinhold, K., Merkel, M., Rasch, F., Müller, T., Schladitz, A., Bastian, S., Löschau, G., Cyrys, J., Gu, J., Flentje, H., Briel, B., Asbach, C., Kaminski, H., Ries, L., Sohmer, R., Gerwig, H., Wirtz, K., Meinhardt, F., Schwerin, A., Bath, O., Ma, N., and Wiedensohler, A.: Decreasing trends of particle number and black carbon mass concentrations at 16 observational sites in Germany from 2009 to 2018, Atmos. Chem. Phys., 20(11), 7049–7068, https://doi.org/10.5194/acp-20-7049-2020, 2020.

Sun, Y., Xu, W., Zhang, Q., Jiang, Q., Canonaco, F., Prévôt, A. S. H., Fu, P., Li, J., Jayne, J., Worsnop, D. R., and Wang, Z.: Source apportionment of organic aerosol from 2-year highly time-resolved measurements by an aerosol chemical speciation monitor in Beijing, China, Atmos. Chem. Phys., 18(12), 8469–8489, https://doi.org/10.5194/acp-18-8469-2018, 2018.

Tiitta, P., Leskinen, A., Hao, L., Yli-Pirilä, P., Kortelainen, M., Grigonyte, J., Tissari, J., Lamberg, H., Hartikainen, A., Kuuspalo, K., Kortelainen, A. M., Virtanen, A., Lehtinen, K. E. J., Komppula, M., Pieber, S., Prévôt, A. S. H., Onasch, T. B., Worsnop, D. R., Czech, H., Zimmermann, R., Jokiniemi, J., and Sippula, O.: Transformation of logwood combustion emissions in a smog chamber: Formation of secondary organic aerosol and changes in the

primary organic aerosol upon daytime and night time aging, Atmos. Chem. Phys., 16(20), 13251–13269, https://doi.org/10.5194/acp-16-13251-2016, 2016.

Tobler, A., Skiba, A., Canonaco, F., Močnik, G., Rai, P., Chen, G., Bartyzel, J., Zimnoch, M., Styszko, K., Nęcki, J., Furger, M., Różański, K., Baltensperger, U., Slowik, J., and Prévôt, A.: Characterization of NR-PM1 and source apportionment of organic aerosol in Krakow, Poland, Atmos. Chem. Phys., 1–22, https://doi.org/10.5194/acp-2021-197, 2021.

Ulbrich, I. M., Canagaratna, M. R., Zhang, Q., Worsnop, D. R., and Jimenez, J. L.: Interpretation of organic components from Positive Matrix Factorization of aerosol mass spectrometric data, Atmos. Chem. Phys., 9, www.atmos-chem-phys.net/9/2891/2009/, 2009.

van Pinxteren, D., Fomba, K. W., Spindler, G., Müller, K., Poulain, L., Iinuma, Y., Löschau, G., Hausmann, A., and Herrmann, H.; Regional air quality in Leipzig, Germany: Detailed source apportionment of size-resolved aerosol particles and comparison with the year 2000, Faraday Discussions, 189, 291–315, https://doi.org/10.1039/c5fd00228a, 2016.

van Pinxteren, D., Mothes, F., Spindler, G., Fomba, K. W., Cuesta, A., Tuch, T., Müller, T., Wiedensohler, A., and Herrmann, H.: Zusatzbelastung aus Holzheizung, Sächsisches Landesamt für Umwelt, Landwirtschaft und Geologie (LfULG), Dresden, https://publikationen.sachsen.de/bdb/artikel/36106, 2020.

Via, M., Minguillón, M. C., Reche, C., Querol, X., and Alastuey, A.: Increase of secondary organic aerosol over four years in an urban environment, Atmos. Chem. Phys., 1–20, https://doi.org/10.5194/acp-2020-1244, 2020.

Vlachou, A., Daellenbach, K., Bozzetti, C., Chazeau, B., Salazar, G., Szidat, S., Jaffrezo, J.-L., Hueglin, C., Baltensperger, U., Haddad, I. el, Daellenbach, K. R., Salazar, G. A., and Prévôt, A. S. H.: Advanced source apportionment of carbonaceous aerosols by coupling offline AMS and radiocarbon size-segregated measurements over a nearly 2-year period, Atmos. Chem. Phys., 18(9), 6187–6206, https://doi.org/10.5194/acp-18-6187-2018ï, 2018.

Vlachou, A., Tobler, A., Lamkaddam, H., Canonaco, F., Daellenbach, K. R., Jaffrezo, J. L., Minguillón, M. C., Maasikmets, M., Teinemaa, E., Baltensperger, U., el Haddad, I., and Preávôt, A. S. H.: Development of a versatile source apportionment analysis based on positive matrix factorization: a case study of the seasonal variation of organic aerosol sources in Estonia, Atmos. Chem. Phys., 19(11), 7279–7295, https://doi.org/10.5194/acp-19-7279-2019, 2019.

Wang, Y., Henning, S., Poulain, L., Lu, C., Stratmann, F., Wang, Y., Niu, S., Pöhlker, M., Herrmann, H., and Wiedensohler, A.: Aerosol activation characteristics and prediction at the central European ACTRIS research station of Melpitz, Germany, https://doi.org/10.5194/acp-22-15943, 2022.

Wang, T., Fu, T., Chen, K., Cheng, R., Chen, S., Liu, J., Mei, M., Li, J., and Xue, Y.: Co-combustion behavior of dyeing sludge and rice husk by using TG-MS: Thermal conversion, gas evolution, and kinetic analyses, Bioresource Technology, 311, https://doi.org/10.1016/j.biortech.2020.123527, 2020.

Watson, J. G.: Visibility: science and regulation, J. Air Waste Manage., 52, 628-713, https://doi.org/10.1080/10473289.2002.10470813, 2002.

Wehner, B., Philippin, S., and Wiedensohler, A.: Design and calibration of a thermodenuder with an improved heating unit to measure the size-dependent volatile fraction of aerosol particles, Aerosol Science, 33, www.elsevier.com/locate/jaerosci, 2002.

WHO, Expert Consultation: https://www.who.int/news-room/events/detail/2019/02/12/default-calendar/expert-consultation-risk-communication-and-intervention-to-reduce-exposure-and-to-minimize-the-health-effects-of-air-pollution, 2019.

Wierońska-Wiśniewska, F., Makowska, D., and Strugała, A.: Arsenic in polish coals: Content, mode of occurrence, and distribution during coal combustion process, Fuel, 312, https://doi.org/10.1016/j.fuel.2021.122992, 2022.

Xu, W., He, Y., Qiu, Y., Chen, C., Xie, C., Lei, L., Li, Z., Sun, J., Li, J., Fu, P., Wang, Z., Worsnop, D. R., and Sun, Y.: Mass spectral characterization of primary emissions and implications in source apportionment of organic aerosol, Atmos. Meas. Tech., 13(6), 3205–3219, https://doi.org/10.5194/amt-13-3205-2020, 2020.

Yang, S., Yuan, B., Peng, Y., Huang, S., Chen, W., Hu, W., Pei, C., Zhou, J., Parrish, D., Wang, W., He, X., Cheng, C., Li, X., Yang, X., Song, Y., Wang, H., Qi, J., Wang, B., Wang, C., Wang, C., Wang, Z., Li, T., Zheng, E., Wang, S., Wu, C., Cai1, M., Ye, C., Song, W., Cheng, P., Chen, D., Wang, X., Zhang, Z., Wang, X., Zheng, J., and Shao, M.: The formation and mitigation of nitrate pollution: comparison between urban and suburban environments, ACP, https://doi.org/10.5194/acp-22-4539, 2022.

Yuan, J., Lewis Modini, R., Zanatta, M., Herber, A. B., Müller, T., Wehner, B., Poulain, L., Tuch, T., Baltensperger, U., and Gysel-Beer, M.: Variability in the mass absorption cross section of black carbon (BC) aerosols is driven by BC internal mixing state at a central European background site (Melpitz, Germany) in winter, Atmos. Chem. Phys., 21(2), 635–655, https://doi.org/10.5194/acp-21-635-2021, 2021.

Yudovich, Y. E., and Ketris, M. P.: Chlorine in coal: A review, In International Journal of Coal Geology, 67, Issues 1–2, pp. 127–144, https://doi.org/10.1016/j.coal.2005.09.004, 2006.

Zhang, Q., Jimenez, J. L., Canagaratna, M. R., Ulbrich, I. M., Ng, N. L., Worsnop, D. R., and Sun, Y.: Understanding atmospheric organic aerosols via factor analysis of aerosol mass spectrometry: A review, In Analytical and Bioanalytical Chemistry, 401, Issue 10, pp. 3045–3067, https://doi.org/10.1007/s00216-011-5355-y, 2011.

Zhang, Q., Rami Alfarra, M., Worsnop, D. R., Allan, J. D., Coe, H., Canagaratna, M. R., and Jimenez, J. L.: Deconvolution and quantification of hydrocarbon-like and oxygenated organic aerosols based on aerosol mass spectrometry, Environ. Sci. Technol., 39(13), 4938–4952, https://doi.org/10.1021/es048568l, 2005.

Zhang, Y., Favez, O., Petit, J. E., Canonaco, F., Truong, F., Bonnaire, N., Crenn, V., Amodeo, T., Prévôt, A. S. H., Sciare, J., Gros, V., and Albinet, A.: Six-year source apportionment of submicron organic aerosols from near-continuous highly time-resolved measurements at SIRTA (Paris area, France), Atmos. Chem. Phys., 19(23), 14755–14776, https://doi.org/10.5194/acp-19-14755-2019, 2019.

Zhang, Y. J., Tang, L. L., Wang, Z., Yu, H. X., Sun, Y. L., Liu, D., Qin, W., Canonaco, F., Prévôt, A. S. H., Zhang, H. L., and Zhou, H. C.: Insights into characteristics, sources, and evolution of submicron aerosols during harvest seasons in the Yangtze River delta region, China, Atmos. Chem. Phys., 15(3), 1331–1349, https://doi.org/10.5194/acp-15-1331-2015, 2015.

Zhu, Q., Huang, X. F., Cao, L. M., Wei, L. T., Zhang, B., He, L. Y., Elser, M., Canonaco, F., Slowik, J. G., Bozzetti, C., El-Haddad, I., and Prévôt, A. S. H.: Improved source apportionment of organic aerosols in complex urban air pollution using the multilinear engine (ME-2), Atmos. Meas. Tech., 11(2), 1049–1060, https://doi.org/10.5194/amt-11-1049-2018, 2018.

Aas, W., Tsyro, S., Bieber, E., Bergström, R., Ceburnis, D., Ellermann, T., Fagerli, H., Frölich, M., Gehrig, R., Makkonen, U., Nemitz, E., Otjes, R., Perez, N., Perrino, C., Prévôt, A. S. H., Putaud, J. P., Simpson, D., Spindler, G., Vana, M., & Yttri, K. E. (2012). Lessons learnt from the first EMEP intensive measurement periods. *Atmospheric Chemistry and Physics*, *12*(17), 8073–8094. https://doi.org/10.5194/acp-12-8073-2012

Alfarra, M. R., Prevot, A. S. H., Szidat, S., Sandradewi, J., Weimer, S., Lanz, V. A., Schreiber, D., Mohr, M., & Baltensperger, U. (2007). Identification of the mass spectral signature of organic aerosols from wood burning emissions. *Environmental Science and Technology*, *41*(16), 5770–5777. https://doi.org/10.1021/es062289b

Allan, J. D., Delia, A. E., Coe, H., Bower, K. N., Alfarra, M. R., Jimenez, J. L., Middlebrook, A. M., Drewnick, F., Onasch, T. B., Canagaratna, M. R., Jayne, J. T., & Worsnop, D. R. (2004). A generalised method for the extraction of chemically resolved mass spectra from Aerodyne aerosol mass spectrometer data. *Journal of Aerosol Science*, *35*(7), 909–922. https://doi.org/10.1016/j.jaerosci.2004.02.007

Birmili, W., Heinke, K., Pitz, M., Matschullat, J., Wiedensohler, A., Cyrys, J., Wichmann, H. E., & Peters, A. (2010). Particle number size distributions in urban air before and after volatilisation. *Atmospheric Chemistry and Physics*, *10*(10), 4643–4660. https://doi.org/10.5194/acp-10-4643-2010

Birmili, W., Schepanski, K., Ansmann, A., Spindler, G., Tegen, I., Wehner, B., Nowak, A., Reimer, E., Mattis, I., M ¨ Uller, K., Brüggemann, E., Brüggemann, B., Gnauk, T., Herrmann, H., Wiedensohler, A., Althausen, D., Schladitz, A., Tuch, T., & Löschau, G. (2008). Atmospheric Chemistry and Physics A case of extreme particulate matter concentrations over Central Europe caused by dust emitted over the southern Ukraine. In *Atmos. Chem. Phys* (Vol. 8). www.atmos-chem-phys.net/8/997/2008/

Birmili, W., Stratmann, F., & Wiedensohler, A. (1999). TECHNICAL NOTE DESIGN OF A DMA BASED SIZE SPECTROMETER FOR A LARGE PARTICLE SIZE RANGE AND STABLE OPERATION. In *J. Aerosol Sci* (Vol. 30, Issue 4).

Birmili, W., Sun, J., Wiedensohler, A., Birmili, W., Sun, J., Weinhold, K., Merkel, M., Rasch, F., Spindler, G., Wiedensohler, A., Bastian, S., Löschau, G., Schladitz, A., Quass, U., Kuhlbusch, T. A. J., Kaminski, H., Cyrys, J., Pitz, M., Gu, J., Peters, A., Flentje, H., Meinhardt, F., Schwerin, A., Bath, O., Ries, L., Gerwig, H., Wirtz, K., Weber, S. (2015). *Enhanced Land Use Regression models for urban fine dust and ultrafine particle concentrations*

View project Radon parallel measurements. View project Atmospheric aerosol measurements in the German Ultrafine Aerosol Network (GUAN). https://www.researchgate.net/publication/330910927

Birmili, W., Weinhold, K., Rasch, F., Sonntag, A., Sun, J., Merkel, M., Wiedensohler, A., Bastian, S., Schladitz, A., Löschau, G., Cyrys, J., Pitz, M., Gu, J., Kusch, T., Flentje, H., Quass, U., Kaminski, H., Kuhlbusch, T. A. J., Meinhardt, F., Schwerin, A., Bath, O., Ries, L., Gerwig, H., Wirtz, K., Fiebig, M. (2016). Long-term observations of tropospheric particle number size distributions and equivalent black carbon mass concentrations in the German Ultrafine Aerosol Network (GUAN). *Earth System Science Data*, *8*(2), 355–382. https://doi.org/10.5194/essd-8-355-2016

Birmili, W., Wiedensohler, A., Mueller, K., Birmili, W., Weinhold, K., Nordmann, S., Wiedensohler, A., Spindler, G., Müller, K., Herrmann, H., Gnauk, T., Pitz, M., Cyrys, J., Flentje, H., Nickel, C., J Kuhlbusch, T. A., Löschau, G., Haase, D., Meinhardt, F., F., Schwerin, A., Ries, L., Wirtz, K. (2009). *Atmospheric aerosol measurements in the German Ultrafine Aerosol Network (GUAN) Korngrößendifferenzierte Feinstaubbelastung in Straßennähe in Ballungsgebieten Sachsens (2003-2005) View project Chemistry, Air Quality and Climate View project Atmospheric aerosol measurements in the German Ultrafine Aerosol Network (GUAN) Part 1: Soot and particle number size distributions*. https://www.researchgate.net/publication/232089057

Bootstrap Methods: Another Look at the Jackknife on JSTOR. (1979). https://www.jstor.org/stable/2958830?origin=JSTOR-pdf

Bressi, M., Cavalli, F., Putaud, J. P., Fröhlich, R., Petit, J. E., Aas, W., Äijälä, M., Alastuey, A., Allan, J. D., Aurela, M., Berico, M., Bougiatioti, A., Bukowiecki, N., Canonaco, F., Crenn, V., Dusanter, S., Ehn, M., Elsasser, M., Flentje, H., M., Flentje, H., Graf, P., Green, D. C., Heikkinen, L., Hermann, H., Holzinger, R., Hueglin, C., Keernik, H., Kiendler-Scharr, A., Kubelova, L., Lunder, C., Maasikmets, M., Makes, O., Malaguti, A., Mihalopoulos, N., Nicolas, J.B., O'Dowd, C., Ovadnevaite, J., Petralia, E., Poulain, L., Priestman, M., Riffault, V., Ripoll, A., Schlag, P., Schwarz, J., Sciarec,, J., Slowik, J., Sosedova, Y., Stavroulas, I., Teinemaa, E., Via, M., Vodickar, P., Williams, P.I., Wiedensohler, A., Young, D.E., Zhang, S., Favez, O., Minguillon, M.C., Prevot, A. S. H. (2021). A European aerosol phenomenology–7: High-time resolution chemical characteristics of submicron particulate matter across Europe. *Atmospheric Environment: X*, *10*. https://doi.org/10.1016/j.aeaoa.2021.100108

Canagaratna, M. R., Jayne, J. T., Ghertner, D. A., Herndon, S., Shi, Q., Jimenez, J. L., Silva, P. J., Williams, P., Lanni, T., Drewnick, F., Demerjian, K. L., Kolb, C. E., & Worsnop, D. R. (2004). Chase studies of particulate emissions from in-use New York City vehicles. *Aerosol Science and Technology*, *38*(6), 555–573. https://doi.org/10.1080/02786820490465504

Canagaratna, M. R., Jimenez, J. L., Kroll, J. H., Chen, Q., Kessler, S. H., Massoli, P., Hildebrandt Ruiz, L., Fortner, E., Williams, L. R., Wilson, K. R., Surratt, J. D., Donahue, N. M., Jayne, J. T., & Worsnop, D. R. (2015). Elemental ratio measurements of organic compounds using aerosol mass spectrometry: Characterization, improved

calibration, and implications. *Atmospheric Chemistry and Physics*, *15*(1), 253–272. https://doi.org/10.5194/acp-15-253-2015

Canonaco, F., Crippa, M., Slowik, J. G., Baltensperger, U., & Prévôt, A. S. H. (2013). SoFi, an IGOR-based interface for the efficient use of the generalized multilinear engine (ME-2) for the source apportionment: ME-2 application to aerosol mass spectrometer data. *Atmospheric Measurement Techniques*, *6*(12), 3649–3661. https://doi.org/10.5194/amt-6-3649-2013

Canonaco, F., Slowik, J. G., Baltensperger, U., & Prévôt, A. S. H. (2015). Seasonal differences in oxygenated organic aerosol composition: Implications for emissions sources and factor analysis. *Atmospheric Chemistry and Physics*, *15*(12), 6993–7002. https://doi.org/10.5194/acp-15-6993-2015

Canonaco, F., Tobler, A., Chen, G., Sosedova, Y., Gates-Slowik, J., Bozzetti, C., Rudolf-Daellenbach, K., el Haddad, I., Crippa, M., Huang, R. J., Furger, M., Baltensperger, U., & Prévôt, A. S. H. (2021). A new method for long-term source apportionment with time-dependent factor profiles and uncertainty assessment using SoFi Pro: Application to 1 year of organic aerosol data. *Atmospheric Measurement Techniques*, *14*(2), 923–943. https://doi.org/10.5194/amt-14-923-2021

Canonaco, F., Tobler, A., Chen, G., Sosedova, Y., Slowik, J. G., Bozzetti, C., Daellenbach, K. R., ElHaddad, I., Crippa, M., Huang, R. J., Furger, M., Baltensperger, U., & Prévôt, A. S. H. (2020). A new method for long-term source apportionment with time-dependent factor profiles and uncertainty assessment using SoFi Pro: application to one year of organic aerosol data. *Atmospheric Measurement Techniques Discussions*, 1–39. https://doi.org/10.5194/amt-2020-204

Chazeau, B., el Haddad, I., Canonaco, F., Temime-Roussel, B., D'Anna, B., Gille, G., Mesbah, B., Prévôt, A. S. H., Wortham, H., & Marchand, N. (2022). Organic aerosol source apportionment by using rolling positive matrix factorization: Application to a Mediterranean coastal city. *Atmospheric Environment: X*, *14*. https://doi.org/10.1016/j.aeaoa.2022.100176

Chen, G., Canonaco, F., Tobler, A., Aas, W., Alastuey, A., Allan, J., Atabakhsh, S., Aurela, M., Baltensperger, U., Bougiatioti, A., de Brito, J. F., Ceburnis, D., Chazeau, B., Chebaicheb, H., Daellenbach, K. R., Ehn, M., el Haddad, I., Eleftheriadis, K., Favez, O., Flentje, H., Font, A., Fossum, K., Freney, E., Gini, M., Green, D.C., Heikkinen, L., Herrmann, H., Kalogridis, A., Keernik, H., Lhotka, R., Lin, C., Lunder, C., Maasikmets, M., Manousakas, M.I., Marchand, N., Marin, C., Marmureanu, L., Mihalopoulos, N., Mocnika, G., Nęckia, J., O'Dowd, C., Ovadnevaite, J., Petera, T., Petita, J.E., Pikridasa, M., Matthew Platt, S., Pokorna, P., Poulain, L., Priestman, M., Riffault, V., Rinaldia, M., Rozanskia, K., Schwarz, J., Sciarea, J., Simon, L., Skiba, A., Slowik, J.G., Sosedova, Y., Stavroulas, I., Styszkoa, K., Teinemaa, E., Timonen, H., Tremper, A., Vasilescu, J., Via, M., Vodicka, P., Wiedensohler, A., Zografou, O., Cruz Minguillon, M., Prévôt, A. S. H. (2022). European aerosol phenomenology – 8: Harmonised source apportionment of organic aerosol using 22 Year-long ACSM/AMS datasets. *Environment International*, *166*. https://doi.org/10.1016/j.envint.2022.107325

Chen, G., Sosedova, Y., Canonaco, F., Fröhlich, R., Tobler, A., Vlachou, A., Daellenbach, K., Bozzetti, C., Hueglin, C., Graf, P., Baltensperger, U., Slowik, J., el Haddad, I., & Prévôt, A. (2020). Time dependent source apportionment of submicron organic aerosol for a rural site in an alpine valley using a rolling PMF window. *Atmospheric Chemistry and Physics Discussions*, 1–52. https://doi.org/10.5194/acp-2020-1263

Chen, G., Sosedova, Y., Canonaco, F., Fröhlich, R., Tobler, A., Vlachou, A., Daellenbach, K. R., Bozzetti, C., Hueglin, C., Graf, P., Baltensperger, U., Slowik, J. G., el Haddad, I., & Prévôt, A. S. H. (2021). Time dependent source apportionment of submicron organic aerosol for a rural site in an alpine valley using a rolling positive matrix factorisation (PMF) window. *Atmospheric Chemistry and Physics*, *21*(19), 15081–15101. https://doi.org/10.5194/acp-21-15081-2021

Crippa, M., Canonaco, F., Lanz, V. A., Äijälä, M., Allan, J. D., Carbone, S., Capes, G., Ceburnis, D., Dall'Osto, M., Day, D. A., DeCarlo, P. F., Ehn, M., Eriksson, A., Freney, E., Ruiz, L. H., Hillamo, R., Jimenez, J. L., Junninen, H., Kiendler-Scharr, A., Kortelainen, A. M., Kulmala, M., Laaksonen, A., Mensah10, A.A., Mohr1, C., Nemitz, E., O'Dowd, C., Ovadnevaite, J., Pandis, S. N., Petäjä, T., Poulain, L., Saarikoski, S., Sellegri, K., Swietlicki, E., Tiitta, P., Worsnop, D. R., Baltensperger, U., Prévôt, A. S. H. (2014). Organic aerosol components derived from 25 AMS data sets across Europe using a consistent ME-2 based source apportionment approach. *Atmospheric Chemistry and Physics*, *14*(12), 6159–6176. https://doi.org/10.5194/acp-14-6159-2014

Crippa, M., Decarlo, P. F., Slowik, J. G., Mohr, C., Heringa, M. F., Chirico, R., Poulain, L., Freutel, F., Sciare, J., Cozic, J., di Marco, C. F., Elsasser, M., Nicolas, J. B., Marchand, N., Abidi, E., Wiedensohler, A., Drewnick, F., Schneider, J., Borrmann, S., Nemitz, E., Zimmermann, R., Jaffrezo, J. L., Prevot, A. S. H., Baltensperger, U. (2013). Wintertime aerosol chemical composition and source apportionment of the organic fraction in the metropolitan area of Paris. *Atmospheric Chemistry and Physics*, *13*(2), 961–981. https://doi.org/10.5194/acp-13-961-2013

Daellenbach, K. R., Uzu, G., Jiang, J., Cassagnes, L. E., Leni, Z., Vlachou, A., Stefenelli, G., Canonaco, F., Weber, S., Segers, A., Kuenen, J. J. P., Schaap, M., Favez, O., Albinet, A., Aksoyoglu, S., Dommen, J., Baltensperger, U., Geiser, M., el Haddad, I., Jaffrezo, J.L., Prévôt, A. S. H. (2020). Sources of particulate-matter air pollution and its oxidative potential in Europe. *Nature*, *587*(7834), 414–419. https://doi.org/10.1038/s41586-020-2902-8

Dall'Osto, M., Ovadnevaite, J., Ceburnis, D., Martin, D., Healy, R. M., O'Connor, I. P., Kourtchev, I., Sodeau, J. R., Wenger, J. C., & O'Dowd, C. (2013). Characterization of urban aerosol in Cork city (Ireland) using aerosol mass spectrometry. *Atmospheric Chemistry and Physics*, *13*(9), 4997–5015. https://doi.org/10.5194/acp-13-4997-2013

Draxler, R. R., & Hess, G. D. (2004). *NOAA Technical Memorandum ERL ARL-224 DESCRIPTION OF THE HYSPLIT_4 MODELING SYSTEM*.

Dudoitis, V., Byčenkiene, S., Plauškaite, K., Bozzetti, C., Fröhlich, R., Mordas, G., & Ulevičius, V. (2016). Spatial distribution of carbonaceous aerosol in the southeastern Baltic Sea region (event of grass fires). *Acta Geophysica*, *64*(3), 711–731. https://doi.org/10.1515/acgeo-2016-0018

Energy statistics an overview - Statistics Explained. (2022). https://ec.europa.eu/eurostat/statistics-explained/index.php?title=Energy_statistics_-_an_overview

Europe's coal exit - Europe Beyond Coal : Europe Beyond Coal. (2022). https://beyondcoal.eu/europes-coal-exit/

Fröhlich, R., Crenn, V., Setyan, A., Belis, C. A., Canonaco, F., Favez, O., Riffault, V., Slowik, J. G., Aas, W., Aijälä, M., Alastuey, A., Artiñano, B., Bonnaire, N., Bozzetti, C., Bressi, M., Carbone, C., Coz, E., Croteau, P. L., Cubison, M. J., Esser-Gietl, J. K., Green, D. C., Gros, V., Heikkinen, L., Herrmann, H., Jayne, J. T., Lunder, C. R., Minguillón, M. C., Močnik, G., O'Dowd, C. D., Ovadnevaite, J., Petralia, E., Poulain, L., Priestman, M., Ripoll, Sarda-Estève, A., R., Wiedensohler, A., Baltensperger, U., Sciare, J., Prévôt, A. S. H. (2015). ACTRIS ACSM intercomparison – Part 2: Intercomparison of ME-2 organic source apportionment results from 15 individual, co-located aerosol mass spectrometers. *Atmospheric Measurement Techniques*, *8*(6), 2555–2576. https://doi.org/10.5194/amt-8-2555-2015

Fröhlich, R., Cubison, M. J., Slowik, J. G., Bukowiecki, N., Prévôt, A. S. H., Baltensperger, U., Schneider, J., Kimmel, J. R., Gonin, M., Rohner, U., Worsnop, D. R., & Jayne, J. T. (2013). The ToF-ACSM: A portable aerosol chemical speciation monitor with TOFMS detection. *Atmospheric Measurement Techniques*, *6*(11), 3225–3241. https://doi.org/10.5194/amt-6-3225-2013

Gilardoni, S., Massoli, P., Paglione, M., Giulianelli, L., Carbone, C., Rinaldi, M., Decesari, S., Sandrini, S., Costabile, F., Gobbi, G. P., Pietrogrande, M. C., Visentin, M., Scotto, F., Fuzzi, S., & Facchini, M. C. (2016). Direct observation of aqueous secondary organic aerosol from biomass-burning emissions. *Proceedings of the National Academy of Sciences of the United States of America*, *113*(36), 10013–10018. https://doi.org/10.1073/pnas.1602212113

Heikkinen, L., Äijälä, M., Daellenbach, K., Chen, G., Garmash, O., Aliaga, D., Graeffe, F., Räty, M., Luoma, K., Aalto, P., Kulmala, M., Petäjä, T., Worsnop, D., & Ehn, M. (2020). Eight years of sub-micrometre organic aerosol composition data from the boreal forest characterized using a machine-learning approach. *Atmospheric Chemistry and Physics Discussions*, 1–47. https://doi.org/10.5194/acp-2020-868

Henry, R., Norris, G. A., Vedantham, R., & Turner, J. R. (2009). Source region identification using kernel smoothing. *Environmental Science and Technology*, *43*(11), 4090–4097. https://doi.org/10.1021/es8011723

Huang, S., Wu, Z., Poulain, L., van Pinxteren, M., Merkel, M., Assmann, D., Herrmann, H., & Wiedensohler, A. (2018). Source apportionment of the organic aerosol over the Atlantic Ocean from 53° N to 53° S: Significant contributions from marine emissions and long-range transport. *Atmospheric Chemistry and Physics*, *18*(24), 18043–18062. https://doi.org/10.5194/acp-18-18043-2018

Huang, W., Saathoff, H., Shen, X., Ramisetty, R., Leisner, T., & Mohr, C. (2019). Seasonal characteristics of organic aerosol chemical composition and volatility in Stuttgart, Germany. *Atmospheric Chemistry and Physics*, *19*(18), 11687–11700. https://doi.org/10.5194/acp-19-11687-2019

Hussein, T., Karppinen, A., Kukkonen, J., Härkönen, J., Aalto, P. P., Hämeri, K., Kerminen, V. M., & Kulmala, M. (2006). Meteorological dependence of size fractionated number concentrations of urban aerosol particles. *Atmospheric Environment*, *40*(8), 1427–1440. https://doi.org/10.1016/j.atmosenv.2005.10.061

Iapalucci, T. L., Demski, R. J., & Bienstock, D. (1969). *Report of Investigations - Google BookChlorine in Coal Combustion. United States Department of the Interior, Bureau of Mines Report of Investigation 7260s.* https://books.google.de/books?id=BmgiAQAAIAAJ&pg=RA9-PP5&lpg=RA9-PP5&dq=Iapalucci,+T.L.,+R.J.+Demski,+and+D.+Bienstock.+Chlorine+in+Coal+Combustion.+United+States+Department+of+the+Interior,+Bureau+of+Mines+Report+of+Investigation+7260,+May+1969.&source=bl&ots=6jvT4RW8xN&sig=ACfU3U2i9N0tWe9sohB1tyYQ9UfAH5pcQ&hl=en&sa=X&ved=2ahUKEwig78bQ2oH2AhXDQvEDHYcJCIUQ6AF6BAgCEAM#v=onepage&q=Iapalucci%2C%20T.L.%2C%20R.J.%20Demski%2C%20and%20D.%20Bienstock.%20Chlorine%20in%20Coal%20Combustion.%20United%20States%20Department%20of%20the%20Interior%2C%20Bureau%20of%20Mines%20Report%20of%20Investigation%207260%2C%20May%201969.&f=false

Iinuma, Y., Engling, G., Puxbaum, H., & Herrmann, H. (2009). A highly resolved anion-exchange chromatographic method for determination of saccharidic tracers for biomass combustion and primary bio-particles in atmospheric aerosol. *Atmospheric Environment*, *43*(6), 1367–1371. https://doi.org/10.1016/j.atmosenv.2008.11.020

Jayne, Danna C. Leard, Xuefeng Zhang, Paul Davidovits, Kenneth A. Smith, Charles E. Kolb, & Douglas R. Worsnop. (2000). *Development of an Aerosol Mass Spectrometer for Size and Composition Analysis of Submicron Particles Enhanced Reader.*

Jimenez, J. L., Canagaratna, M. R., Donahue, N. M., Prevot, A. S. H., Zhang, Q., Kroll, J. H., DeCarlo, P. F., Allan, J. D., Coe, H., Ng, N. L., Aiken, A. C., Docherty, K. S., Ulbrich, I. M., Grieshop, A. P., Robinson, A. L., Duplissy, J., Smith, J. D., Wilson, K. R., Lanz, V. A., … Worsnop, D. R. (2009). Evolution of organic aerosols in the atmosphere. *Science*, *326*(5959), 1525–1529. https://doi.org/10.1126/science.1180353

Katsanos, D., Bougiatioti, A., Liakakou, E., Kaskaoutis, D. G., Stavroulas, I., Paraskevopoulou, D., Lianou, M., Psiloglou, B. E., Gerasopoulos, E., Pilinis, C., & Mihalopoulos, N. (2019). Optical properties of near-surface urban aerosols and their chemical tracing in a mediterranean city (Athens). *Aerosol and Air Quality Research*, *19*(1), 49–70. https://doi.org/10.4209/aaqr.2017.11.0544

Kiendler-Scharr, A., Mensah, A. A., Friese, E., Topping, D., Nemitz, E., Prevot, A. S. H., Äijälä, M., Allan, J., Canonaco, F., Canagaratna, M., Carbone, S., Crippa, M., Dall Osto, M., Day, D. A., de Carlo, P., di Marco, C. F., Elbern, H., Eriksson, A., Freney, E., … Wu, H. C. (2016). Ubiquity of organic nitrates from nighttime chemistry in the European submicron aerosol. *Geophysical Research Letters*, *43*(14), 7735–7744. https://doi.org/10.1002/2016GL069239

Kumar, V., Giannoukos, S., Haslett, S. L., Tong, Y., Singh, A., Bertrand, A., Lee, C. P., Wang, D. S., Bhattu, D., Stefenelli, G., Dave, J. S., Puthussery, J. v., Qi, L., Vats, P., Rai, P., Casotto, R., Satish, R., Mishra, S., Pospisilova,

V., C., Bell, D.M., Ganguly, D., Verma, V., Rastogi, N., Baltensperger, U., Tripathi, S.N., Prévôt, A.S.H., Slowik, J. G. (2022). Highly time-resolved chemical speciation and source apportionment of organic aerosol components in Delhi, India, using extractive electrospray ionization mass spectrometry. *Atmospheric Chemistry and Physics*, *22*(11), 7739–7761. https://doi.org/10.5194/acp-22-7739-2022

Laborde, M., Crippa, M., Tritscher, T., Jurányi, Z., Decarlo, P. F., Temime-Roussel, B., Marchand, N., Eckhardt, S., Stohl, A., Baltensperger, U., Prévôt, A. S. H., Weingartner, E., & Gysel, M. (2013). Black carbon physical properties and mixing state in the European megacity Paris. *Atmospheric Chemistry and Physics*, *13*(11), 5831–5856. https://doi.org/10.5194/acp-13-5831-2013

Lanz, V. A., Alfarra, M. R., Baltensperger, U., Buchmann, B., Hueglin, C., & Prévôt, A. S. H. (2007). Source apportionment of submicron organic aerosols at an urban site by factor analytical modelling of aerosol mass spectra. In *Atmos. Chem. Phys* (Vol. 7). www.atmos-chem-phys.net/7/1503/2007/

Lanz, V. A., Alfarra, M. R., Baltensperger, U., Buchmann, B., Hueglin, C., Szidat, S., Wehrli, M. N., Wacker, L., Weimer, S., Caseiro, A., Puxbaum, H., & Prevot, A. S. H. (2008). Source attribution of submicron organic aerosols during wintertime inversions by advanced factor analysis of aerosol mass spectra. *Environmental Science and Technology*, *42*(1), 214–220. https://doi.org/10.1021/es0707207

Li, G., Lei, W., Bei, N., & Molina, L. T. (2012). Contribution of garbage burning to chloride and PM-2.5 in Mexico City. *Atmospheric Chemistry and Physics*, *12*(18), 8751–8761. https://doi.org/10.5194/acp-12-8751-2012

Lin, C., Ceburnis, D., Hellebust, S., Buckley, P., Wenger, J., Canonaco, F., Prévôt, A. S. H., Huang, R. J., O'Dowd, C., & Ovadnevaite, J. (2017). Characterization of Primary Organic Aerosol from Domestic Wood, Peat, and Coal Burning in Ireland. *Environmental Science and Technology*, *51*(18), 10624–10632. https://doi.org/10.1021/acs.est.7b01926

Liu, P. S. K., Deng, R., Smith, K. A., Williams, L. R., Jayne, J. T., Canagaratna, M. R., Moore, K., Onasch, T. B., Worsnop, D. R., & Deshler, T. (2007). Transmission efficiency of an aerodynamic focusing lens system: Comparison of model calculations and laboratory measurements for the aerodyne aerosol mass spectrometer. *Aerosol Science and Technology*, *41*(8), 721–733. https://doi.org/10.1080/02786820701422278

Ma, N., Birmili, W., Müller, T., Tuch, T., Cheng, Y. F., Xu, W. Y., Zhao, C. S., & Wiedensohler, A. (2014). Tropospheric aerosol scattering and absorption over central Europe: A closure study for the dry particle state. *Atmospheric Chemistry and Physics*, *14*(12), 6241–6259. https://doi.org/10.5194/acp-14-6241-2014

Middlebrook, A. M., Bahreini, R., Jimenez, J. L., & Canagaratna, M. R. (2012). Evaluation of composition-dependent collection efficiencies for the Aerodyne aerosol mass spectrometer using field data. *Aerosol Science and Technology*, *46*(3), 258–271. https://doi.org/10.1080/02786826.2011.620041

Ng, N. L., Canagaratna, M. R., Zhang, Q., Jimenez, J. L., Tian, J., Ulbrich, I. M., Kroll, J. H., Docherty, K. S., Chhabra, P. S., Bahreini, R., Murphy, S. M., Seinfeld, J. H., Hildebrandt, L., Donahue, N. M., Decarlo, P. F., Lanz, V. A., Prévôt, A. S. H., Dinar, E., Rudich, Y., & Worsnop, D. R. (2010). Organic aerosol components observed in

Northern Hemispheric datasets from Aerosol Mass Spectrometry. *Atmospheric Chemistry and Physics*, *10*(10), 4625–4641. https://doi.org/10.5194/acp-10-4625-2010

Ng, N. L., Herndon, S. C., Trimborn, A., Canagaratna, M. R., Croteau, P. L., Onasch, T. B., Sueper, D., Worsnop, D. R., Zhang, Q., Sun, Y. L., & Jayne, J. T. (2011a). An Aerosol Chemical Speciation Monitor (ACSM) for routine monitoring of the composition and mass concentrations of ambient aerosol. *Aerosol Science and Technology*, *45*(7), 780–794. https://doi.org/10.1080/02786826.2011.560211

O'Dowd, C., Ceburnis, D., Ovadnevaite, J., Vaishya, A., Rinaldi, M., & Facchini, M. C. (2014). Do anthropogenic, continental or coastal aerosol sources impact on a marine aerosol signature at Mace Head? *Atmospheric Chemistry and Physics*, *14*(19), 10687–10704. https://doi.org/10.5194/acp-14-10687-2014

Ovadnevaite, J., Ceburnis, D., Leinert, S., Dall'Osto, M., Canagaratna, M., O'Doherty, S., Berresheim, H., & O'Dowd, C. (2014). Submicron NE Atlantic marine aerosol chemical composition and abundance: Seasonal trends and air mass categorization. *Journal of Geophysical Research*, *119*(20), 11,850-11,863. https://doi.org/10.1002/2013JD021330

Paatero, P. (1997). Least squares formulation of robust non-negative factor analysis. In *Chemometrics and Intelligent Laboratory Systems* (Vol. 37).

Paatero, P. (1999). The Multilinear Engine—A Table-Driven, Least Squares Program for Solving Multilinear Problems, Including the n-Way Parallel Factor Analysis Model. *Journal of Computational and Graphical Statistics*, *8*(4), 854–888. https://doi.org/10.1080/10618600.1999.10474853

Paatero, P., & Tappert, U. (1994). POSITIVE MATRIX FACTORIZATION: A NON-NEGATIVE FACTOR MODEL WITH OPTIMAL UTILIZATION OF ERROR ESTIMATES OF DATA VALUES*. In *ENVIRONMETRICS* (Vol. 5).

Paglione, M., Gilardoni, S., Rinaldi, M., Decesari, S., Zanca, N., Sandrini, S., Giulianelli, L., Bacco, D., Ferrari, S., Poluzzi, V., Scotto, F., Trentini, A., Poulain, L., Herrmann, H., Wiedensohler, A., Canonaco, F., Prévôt, A. S. H., Massoli, P., Carbone, C., C., Bell, D.M., Ganguly, D., Verma, V., Rastogi, N., Baltensperger, U., Tripathi, S.N., Prévôt, A.S.H., Fuzzi, S. (2020). The impact of biomass burning and aqueous-phase processing on air quality: A multi-year source apportionment study in the Po Valley, Italy. *Atmospheric Chemistry and Physics*, *20*(3), 1233–1254. https://doi.org/10.5194/acp-20-1233-2020

Parworth, C., Fast, J., Mei, F., Shippert, T., Sivaraman, C., Tilp, A., Watson, T., & Zhang, Q. (2015). Long-term measurements of submicrometer aerosol chemistry at the Southern Great Plains (SGP) using an Aerosol Chemical Speciation Monitor (ACSM). *Atmospheric Environment*, *106*, 43–55. https://doi.org/10.1016/j.atmosenv.2015.01.060

Petit, J.-E., Favez, O., Sciare, J., Crenn, V., Sarda-Esteve, R., Bonnaire, N., Mocnik, G., Dupont, J. C., Haeffelin, M., Leoz-Garziandia, E., Sarda, R., Petit, J. E., Favez, O., Sciare, J., Crenn, V., Sarda-Estève, R., Bonnaire, N., Močnik, G., Dupont, J. C., Haeffelin., M., Leoz-Garziandia, E. (2015). Two years of near real-time chemical

composition of submicron aerosols in the region of Paris using an Aerosol Chemical Speciation Monitor (ACSM) and a multi wavelength Aethalometer. *European Geosciences Union*, *15*(6), 2985–3005. https://doi.org/10.5194/acpd-14-24221-2014ï

Petzold, A., & Schönlinner, M. (2004). Multi-angle absorption photometry—A new method for the measurement of aerosol light absorption and atmospheric black carbon. *Journal of Aerosol Science*, *35*(4), 421–441. https://doi.org/10.1016/j.jaerosci.2003.09.005

Poulain, L., Birmili, W., Canonaco, F., Crippa, M., Wu, Z. J., Nordmann, S., Spindler, G., Prévôt, A. S. H., Wiedensohler, A., & Herrmann, H. (2014). Chemical mass balance of 300 °c non-volatile particles at the tropospheric research site Melpitz, Germany. *Atmospheric Chemistry and Physics*, *14*(18), 10145–10162. https://doi.org/10.5194/acp-14-10145-2014

Poulain, L., Fahlbusch, B., Spindler, G., Müller, K., van Pinxteren, D., Wu, Z., Iinuma, Y., Birmili, W., Wiedensohler, A., & Herrmann, H. (2020). Source apportionment and impact of long-range transport on carbonaceous aerosol particles in Central Germany during HCCT-2010. *Atmospheric Chemistry and Physics*, 1–33. https://doi.org/10.5194/acp-2020-626

Poulain, L., Fahlbusch, B., Spindler, G., Müller, K., van Pinxteren, D., Wu, Z., Iinuma, Y., Birmili, W., Wiedensohler, A., & Herrmann, H. (2021). Source apportionment and impact of long-range transport on carbonaceous aerosol particles in central Germany during HCCT-2010. *Atmospheric Chemistry and Physics*, *21*(5), 3667–3684. https://doi.org/10.5194/acp-21-3667-2021

Poulain, L., Spindler, G., Birmili, W., Plass-Dülmer, C., Wiedensohler, A., & Herrmann, H. (2011). Seasonal and diurnal variations of particulate nitrate and organic matter at the IfT research station Melpitz. *Atmospheric Chemistry and Physics*, *11*(24), 12579–12599. https://doi.org/10.5194/acp-11-12579-2011

Poulain, L., Spindler, G., Grüner, A., Tuch, T., Stieger, B., Pinxteren, D. van, Petit, J. E., Favez, O., Herrmann, H., & Wiedensohler, A. (2020). Multi-year ACSM measurements at the central European research station Melpitz (Germany)–Part 1: Instrument robustness, quality assurance, and impact of upper size cutoff diameter. *Atmospheric Measurement Techniques*, *13*(9), 4973–4994. https://doi.org/10.5194/amt-13-4973-2020

Qi, L., Vogel, A. L., Esmaeilirad, S., Cao, L., Zheng, J., Jaffrezo, J. L., Fermo, P., Kasper-Giebl, A., Daellenbach, K. R., Chen, M., Ge, X., Baltensperger, U., Prévôt, A. S. H., & Slowik, J. G. (2020). A 1-year characterization of organic aerosol composition and sources using an extractive electrospray ionization time-of-flight mass spectrometer (EESI-TOF). *Atmospheric Chemistry and Physics*, *20*(13), 7875–7893. https://doi.org/10.5194/acp-20-7875-2020

Schlag, P., Kiendler-Scharr, A., Johannes Blom, M., Canonaco, F., Sebastiaan Henzing, J., Moerman, M., Prévôt, A. S. H., & Holzinger, R. (2016). Aerosol source apportionment from 1-year measurements at the CESAR tower in Cabauw, the Netherlands. *Atmospheric Chemistry and Physics*, *16*(14), 8831–8847. https://doi.org/10.5194/acp-16-8831-2016

Seinfeld and Pandis. (2006). *Atmospheric Chemistry and Physics: From Air Pollution to Climate Change, 3rd Edition* |*Wiley*.https://www.wiley.com/enus/Atmospheric+Chemistry+and+Physics:+From+Air+Pollution+to+Climate+Change,+3rd+Edition-p-9781118947401

Shi, Y., Chen, J., Hu, D., Wang, L., Yang, X., & Wang, X. (2014). Airborne submicron particulate (PM1) pollution in Shanghai, China: Chemical variability, formation/dissociation of associated semi-volatile components and the impacts on visibility. *Science of the Total Environment*, *473–474*, 199–206. https://doi.org/10.1016/j.scitotenv.2013.12.024

Shrivastava, M., Cappa, C. D., Fan, J., Goldstein, A. H., Guenther, A. B., Jimenez, J. L., Kuang, C., Laskin, A., Martin, S. T., Ng, N. L., Petaja, T., Pierce, J. R., Rasch, P. J., Roldin, P., Seinfeld, J. H., Shilling, J., Smith, J. N., Thornton, J. A., Volkamer, R., Wang, J., Worsnop, D.R., Zaveri, R.A., Zelenyuk, A., Zhang, Q. (2017). Recent advances in understanding secondary organic aerosol: Implications for global climate forcing. *Reviews of Geophysics*, *55*(2), 509–559. https://doi.org/10.1002/2016RG000540

Simoneit, B. R. T., & Elias, V. O. (2001). *Detecting Organic Tracers from Biomass Burning in the Atmosphere q*.

Simoneit, B. R. T., Schauer, J. J., Nolte, C. G., Oros, D. R., Elias, V. O., Fraser, M. P., Rogge, W. F., & Cass, G. R. (1999). Levoglucosan, a tracer for cellulose in biomass burning and atmospheric particles. In *Atmospheric Environment* (Vol. 33).

Spindler, G., Brüggemann, E., Gnauk, T., Grüner, A., Müller, K., & Herrmann, H. (2010). A four-year size-segregated characterization study of particles PM10, PM2.5 and PM1 depending on air mass origin at Melpitz. *Atmospheric Environment*, *44*(2), 164–173. https://doi.org/10.1016/j.atmosenv.2009.10.015

Spindler, G., Gnauk, T., Grüner, A., Iinuma, Y., Müller, K., Scheinhardt, S., & Herrmann, H. (2012). Size-segregated characterization of PM10 at the EMEP site Melpitz (Germany) using a five-stage impactor: A six year study. *Journal of Atmospheric Chemistry*, *69*(2), 127–157. https://doi.org/10.1007/s10874-012-9233-6

Spindler, G., Grüner, A., Müller, K., Schlimper, S., & Herrmann, H. (2013). Long-term size-segregated particle (PM10, PM2.5, PM1) characterization study at Melpitz – Influence of air mass inflow, weather conditions and season. *Journal of Atmospheric Chemistry*, *70*(2), 165–195. https://doi.org/10.1007/s10874-013-9263-8

Spindler, G., Müller, K., Brüggemann, E., Gnauk, T., & Herrmann, H. (2004). Long-term size-segregated characterization of PM-10, PM-2.5, and PM-1 at the IfT research station Melpitz downwind of Leipzig (Germany) using high and low volume filter samplers. *Atmospheric Environment*, *38*(31), 5333–5347. https://doi.org/10.1016/j.atmosenv.2003.12.047

Stavroulas, I., Bougiatioti, A., Grivas, G., Paraskevopoulou, D., Tsagkaraki, M., Zarmpas, P., Liakakou, E., Gerasopoulos, E., & Mihalopoulos, N. (2019a). Sources and processes that control the submicron organic aerosol composition in an urban Mediterranean environment (Athens): A high temporal-resolution chemical composition measurement study. *Atmospheric Chemistry and Physics*, *19*(2), 901–919. https://doi.org/10.5194/acp-19-901-2019

Stavroulas, I., Bougiatioti, A., Grivas, G., Paraskevopoulou, D., Tsagkaraki, M., Zarmpas, P., Liakakou, E., Gerasopoulos, E., & Mihalopoulos, N. (2019b). Sources and processes that control the submicron organic aerosol composition in an urban Mediterranean environment (Athens): A high temporal resolution chemical composition measurement study. *Atmospheric Chemistry and Physics*, *19*(2), 901–919. https://doi.org/10.5194/acp-19-901-2019

Stieger, B., Spindler, G., Fahlbusch, B., Müller, K., Grüner, A., Poulain, L., Thöni, L., Seitler, E., Wallasch, M., & Herrmann, H. (2018). Measurements of PM10 ions and trace gases with the online system MARGA at the research station Melpitz in Germany – A five-year study. *Journal of Atmospheric Chemistry*, *75*(1), 33–70. https://doi.org/10.1007/s10874-017-9361-0

Sun, J., Birmili, W., Hermann, M., Tuch, T., Weinhold, K., Merkel, M., Rasch, F., Müller, T., Schladitz, A., Bastian, S., Löschau, G., Cyrys, J., Gu, J., Flentje, H., Briel, B., Asbach, C., Kaminski, H., Ries, L., Sohmer, R., … Wiedensohler, A. (2020). Decreasing trends of particle number and black carbon mass concentrations at 16 observational sites in Germany from 2009 to 2018. *Atmospheric Chemistry and Physics*, *20*(11), 7049–7068. https://doi.org/10.5194/acp-20-7049-2020

Sun, Y., Xu, W., Zhang, Q., Jiang, Q., Canonaco, F., Prévôt, A. S. H., Fu, P., Li, J., Jayne, J., Worsnop, D. R., & Wang, Z. (2018). Source apportionment of organic aerosol from 2-year highly time-resolved measurements by an aerosol chemical speciation monitor in Beijing, China. *Atmospheric Chemistry and Physics*, *18*(12), 8469–8489. https://doi.org/10.5194/acp-18-8469-2018

Tiitta, P., Leskinen, A., Hao, L., Yli-Pirilä, P., Kortelainen, M., Grigonyte, J., Tissari, J., Lamberg, H., Hartikainen, A., Kuuspalo, K., Kortelainen, A. M., Virtanen, A., Lehtinen, K. E. J., Komppula, M., Pieber, S., Prévôt, A. S. H., Onasch, T. B., Worsnop, D. R., Czech, H., … Sippula, O. (2016). Transformation of logwood combustion emissions in a smog chamber: Formation of secondary organic aerosol and changes in the primary organic aerosol upon daytime and nighttime aging. *Atmospheric Chemistry and Physics*, *16*(20), 13251–13269. https://doi.org/10.5194/acp-16-13251-2016

Tobler, A., Skiba, A., Canonaco, F., Močnik, G., Rai, P., Chen, G., Bartyzel, J., Zimnoch, M., Styszko, K., Nęcki, J., Furger, M., Różański, K., Baltensperger, U., Slowik, J., & Prévôt, A. (2021). Characterization of NR-PM1 and source apportionment of organic aerosol in Krakow, Poland. *Atmospheric Chemistry and Physics*, 1–22. https://doi.org/10.5194/acp-2021-197

Ulbrich, I. M., Canagaratna, M. R., Zhang, Q., Worsnop, D. R., & Jimenez, J. L. (2009). Interpretation of organic components from Positive Matrix Factorization of aerosol mass spectrometric data. In *Atmos. Chem. Phys* (Vol. 9). www.atmos-chem-phys.net/9/2891/2009/

van Pinxteren, D., Fomba, K. W., Spindler, G., Müller, K., Poulain, L., Iinuma, Y., Löschau, G., Hausmann, A., & Herrmann, H. (2016). Regional air quality in Leipzig, Germany: Detailed source apportionment of size-resolved

aerosol particles and comparison with the year 2000. *Faraday Discussions*, *189*, 291–315. https://doi.org/10.1039/c5fd00228a

van Pinxteren, D., Mothes, F., Spindler, G., Fomba, W., Cuesta, A., Tuch, T., Müller, T., Wiedensohler, A., & Herrmann, H. (2020). *Zusatzbelastung aus Holzheizungen*.

van Pinxteren, D., Engelhardt, V., Mothes, F., Poulain, L., Spindler, G., Cuesta, A., Tuch, T., Müller, T., Wiedensohler, A., Herrmann, H. (2022). Residential wood combustion in Germany: A twin site study of local village contributions to particulate pollutants. (in preparation)

Via, M., Minguillón, M. C., Reche, C., Querol, X., & Alastuey, A. (2020). Increase of secondary organic aerosol over four years in an urban environment. *Atmospheric Chemistry and Physics Discussions*, 1–20. https://doi.org/10.5194/acp-2020-1244

Vlachou, A., Daellenbach, K., Bozzetti, C., Chazeau, B., Salazar, G., Szidat, S., Jaffrezo, J. L., Hueglin, C., Baltensperger, U., Haddad, I. el, Daellenbach, K. R., Salazar, G. A., & Prévôt, A. S. H. (2018). Advanced source apportionment of carbonaceous aerosols by coupling offline AMS and radiocarbon size-segregated measurements over a nearly 2-year period. *Atmos. Chem. Phys*, *18*(9), 6187–6206. https://doi.org/10.5194/acp-18-6187-2018ï

Vlachou, A., Tobler, A., Lamkaddam, H., Canonaco, F., Daellenbach, K. R., Jaffrezo, J. L., Minguillón, M. C., Maasikmets, M., Teinemaa, E., Baltensperger, U., el Haddad, I., & Preávôt, A. S. H. (2019). Development of a versatile source apportionment analysis based on positive matrix factorization: a case study of the seasonal variation of organic aerosol sources in Estonia. *Atmospheric Chemistry and Physics*, *19*(11), 7279–7295. https://doi.org/10.5194/acp-19-7279-2019

Wang, T., Fu, T., Chen, K., Cheng, R., Chen, S., Liu, J., Mei, M., Li, J., & Xue, Y. (2020). Co-combustion behavior of dyeing sludge and rice husk by using TG-MS: Thermal conversion, gas evolution, and kinetic analyses. *Bioresource Technology*, *311*. https://doi.org/10.1016/j.biortech.2020.123527

Wehner, B., Philippin, S., & Wiedensohler, A. (2002). Design and calibration of a thermodenuder with an improved heating unit to measure the size-dependent volatile fraction of aerosol particles. In *Aerosol Science* (Vol. 33). www.elsevier.com/locate/jaerosci

WHO, Expert Consultation. (2019). https://www.who.int/news-room/events/detail/2019/02/12/default-calendar/expert-consultation-risk-communication-and-intervention-to-reduce-exposure-and-to-minimize-the-health-effects-of-air-pollution

Wierońska-Wiśniewska, F., Makowska, D., & Strugała, A. (2022). Arsenic in polish coals: Content, mode of occurrence, and distribution during coal combustion process. *Fuel*, *312*. https://doi.org/10.1016/j.fuel.2021.122992

Xu, W., He, Y., Qiu, Y., Chen, C., Xie, C., Lei, L., Li, Z., Sun, J., Li, J., Fu, P., Wang, Z., Worsnop, D. R., & Sun, Y. (2020). Mass spectral characterization of primary emissions and implications in source apportionment of organic aerosol. *Atmospheric Measurement Techniques*, *13*(6), 3205–3219. https://doi.org/10.5194/amt-13-3205-2020

Yuan, J., Lewis Modini, R., Zanatta, M., Herber, A. B., Müller, T., Wehner, B., Poulain, L., Tuch, T., Baltensperger, U., & Gysel Beer, M. (2021). Variability in the mass absorption cross section of black carbon (BC) aerosols is driven by BC internal mixing state at a central European background site (Melpitz, Germany) in winter. *Atmospheric Chemistry and Physics*, *21*(2), 635–655. https://doi.org/10.5194/acp-21-635-2021

Yudovich, Y. E., & Ketris, M. P. (2006). Chlorine in coal: A review. In *International Journal of Coal Geology* (Vol. 67, Issues 1–2, pp. 127–144). https://doi.org/10.1016/j.coal.2005.09.004

Zhang, Q., Jimenez, J. L., Canagaratna, M. R., Ulbrich, I. M., Ng, N. L., Worsnop, D. R., & Sun, Y. (2011). Understanding atmospheric organic aerosols via factor analysis of aerosol mass spectrometry: A review. In *Analytical and Bioanalytical Chemistry* (Vol. 401, Issue 10, pp. 3045–3067). https://doi.org/10.1007/s00216-011-5355-y

Zhang, Q., Rami Alfarra, M., Worsnop, D. R., Allan, J. D., Coe, H., Canagaratna, M. R., & Jimenez, J. L. (2005). Deconvolution and quantification of hydrocarbon-like and oxygenated organic aerosols based on aerosol mass spectrometry. *Environmental Science and Technology*, *39*(13), 4938–4952. https://doi.org/10.1021/es048568l

Zhang, Y., Favez, O., Petit, J. E., Canonaco, F., Truong, F., Bonnaire, N., Crenn, V., Amodeo, T., Prévôt, A. S. H., Sciare, J., Gros, V., & Albinet, A. (2019). Six-year source apportionment of submicron organic aerosols from near-continuous highly time-resolved measurements at SIRTA (Paris area, France). *Atmospheric Chemistry and Physics*, *19*(23), 14755–14776. https://doi.org/10.5194/acp-19-14755-2019

Zhang, Y. J., Tang, L. L., Wang, Z., Yu, H. X., Sun, Y. L., Liu, D., Qin, W., Canonaco, F., Prévôt, A. S. H., Zhang, H. L., & Zhou, H. C. (2015). Insights into characteristics, sources, and evolution of submicron aerosols during harvest seasons in the Yangtze River delta region, China. *Atmospheric Chemistry and Physics*, *15*(3), 1331–1349. https://doi.org/10.5194/acp-15-1331-2015

Zhu, Q., Huang, X. F., Cao, L. M., Wei, L. T., Zhang, B., He, L. Y., Elser, M., Canonaco, F., Slowik, J. G., Bozzetti, C., El Haddad, I., & Prévôt, A. S. H. (2018). Improved source apportionment of organic aerosols in complex urban air pollution using the multilinear engine (ME-2). *Atmospheric Measurement Techniques*, *11*(2), 1049–1060. https://doi.org/10.5194/amt-11-1049-2018

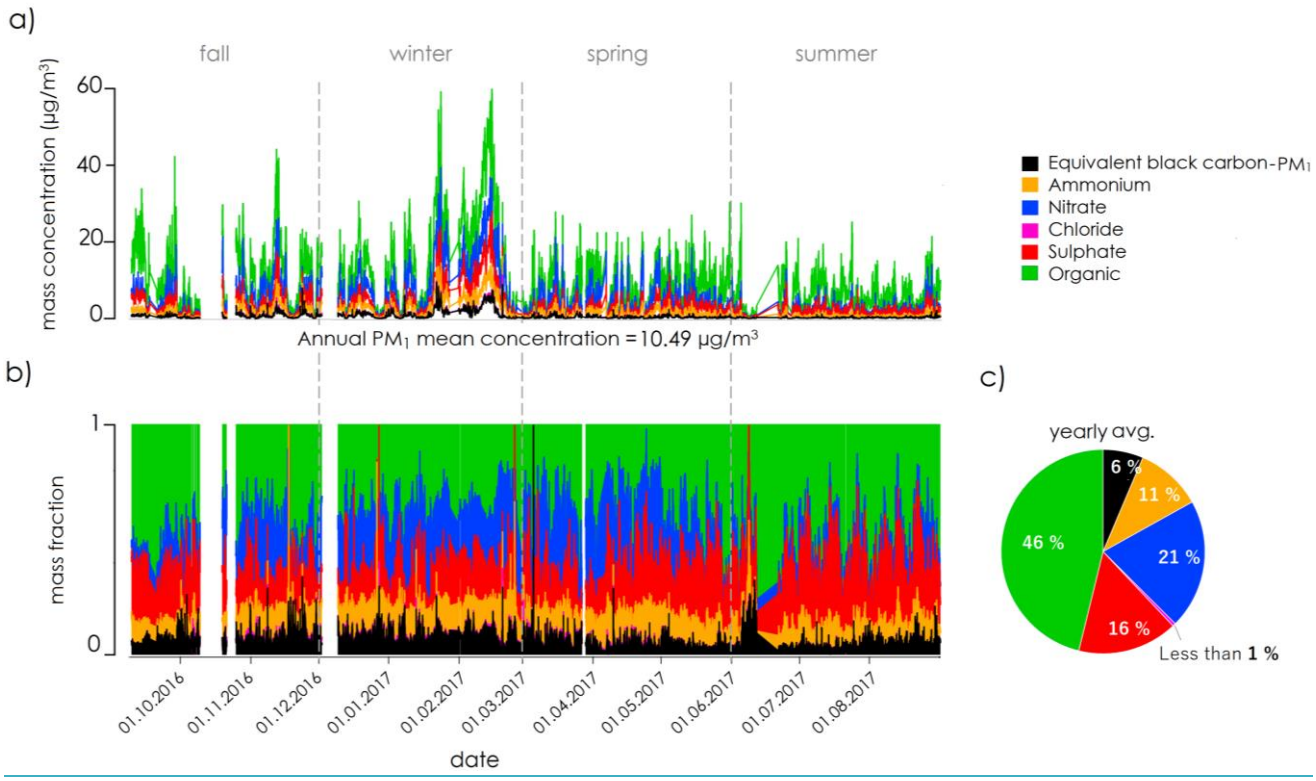
a)
fall
winter
spring
summer
mass concentration (µg/m³)
60
40
20
0
Annual PM1 mean concentration =10.49 µg/m³
Equivalent black carbon-PM1
Ammonium
Nitrate
Chloride
Sulphate
Organic
b)
mass fraction
1
0
01.10.2016
01.11.2016
01.12.2016
01.01.2017
01.02.2017
01.03.2017
01.04.2017
01.05.2017
01.06.2017
01.07.2017
01.08.2017
date
c)
yearly avg.
6 %
11 %
21 %
16 %
46 %
Less than 1 %

1711

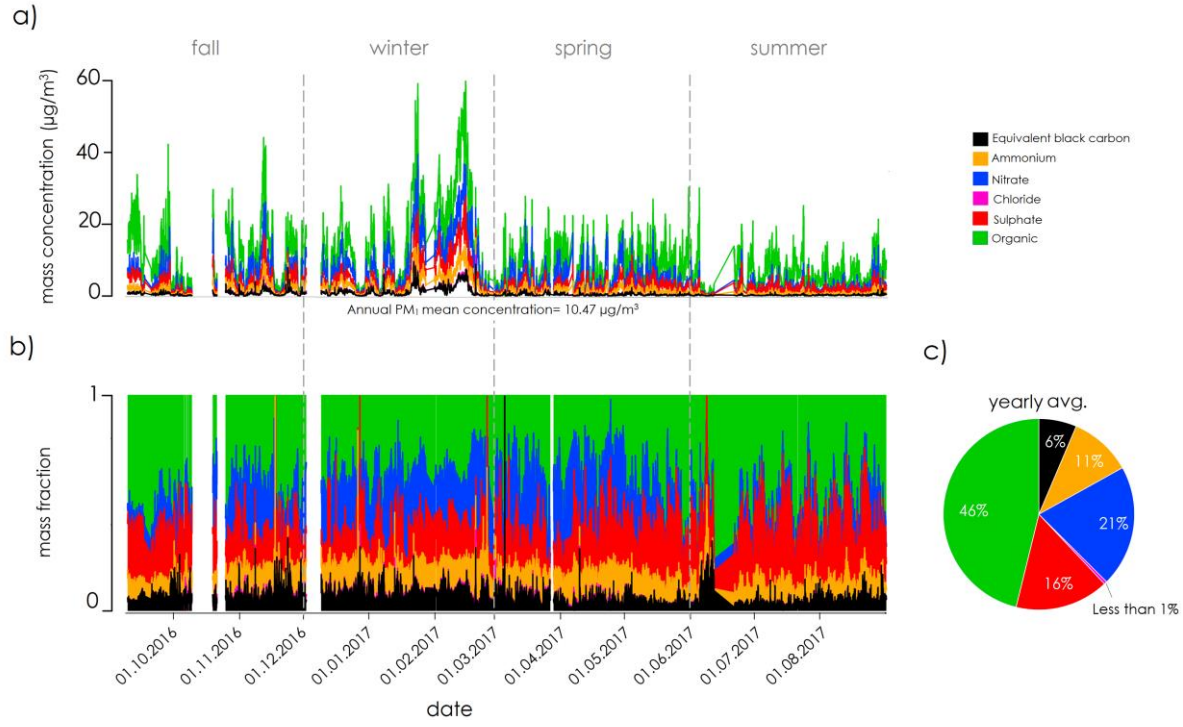
a)
fall
winter
spring
summer
mass concentration (µg/m³)
60
40
20
0
Annual PM1 mean concentration= 10.47 µg/m³
Equivalent black carbon
Ammonium
Nitrate
Chloride
Sulphate
Organic
b)
mass fraction
1
0
01.10.2016
01.11.2016
01.12.2016
01.01.2017
01.02.2017
01.03.2017
01.04.2017
01.05.2017
01.06.2017
01.07.2017
01.08.2017
date
c)
yearly avg.
6%
11%
21%
16%
46%
Less than 1%

1712

Fig. 1: Time series of a) the particulate PM_1 chemical composition, b) the corresponding mass fraction and c) average contribution of each chemical component (~~Time~~ time is in UTC).

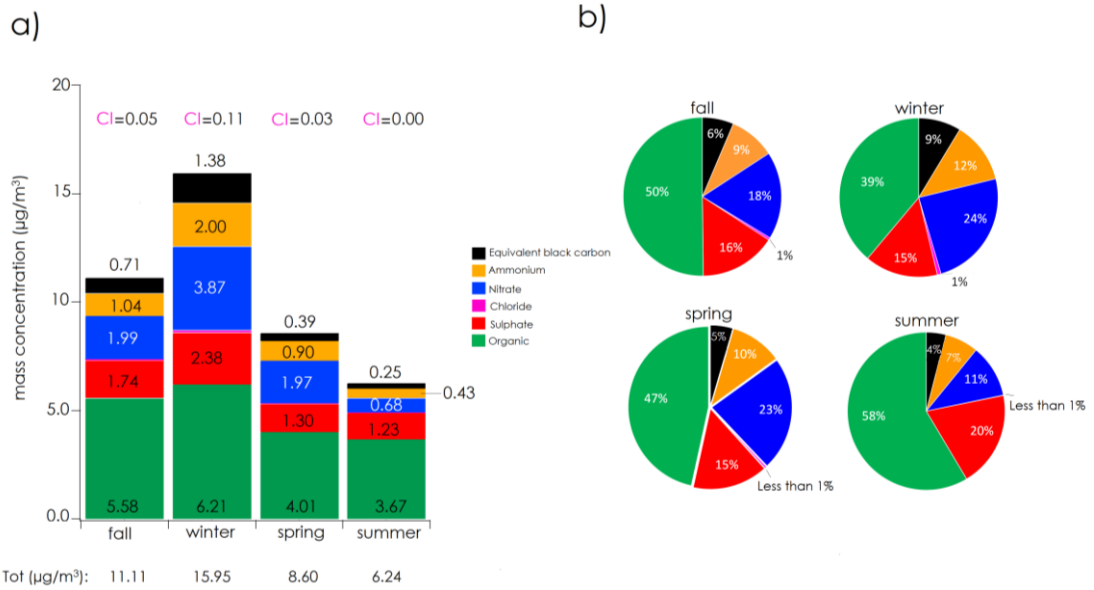

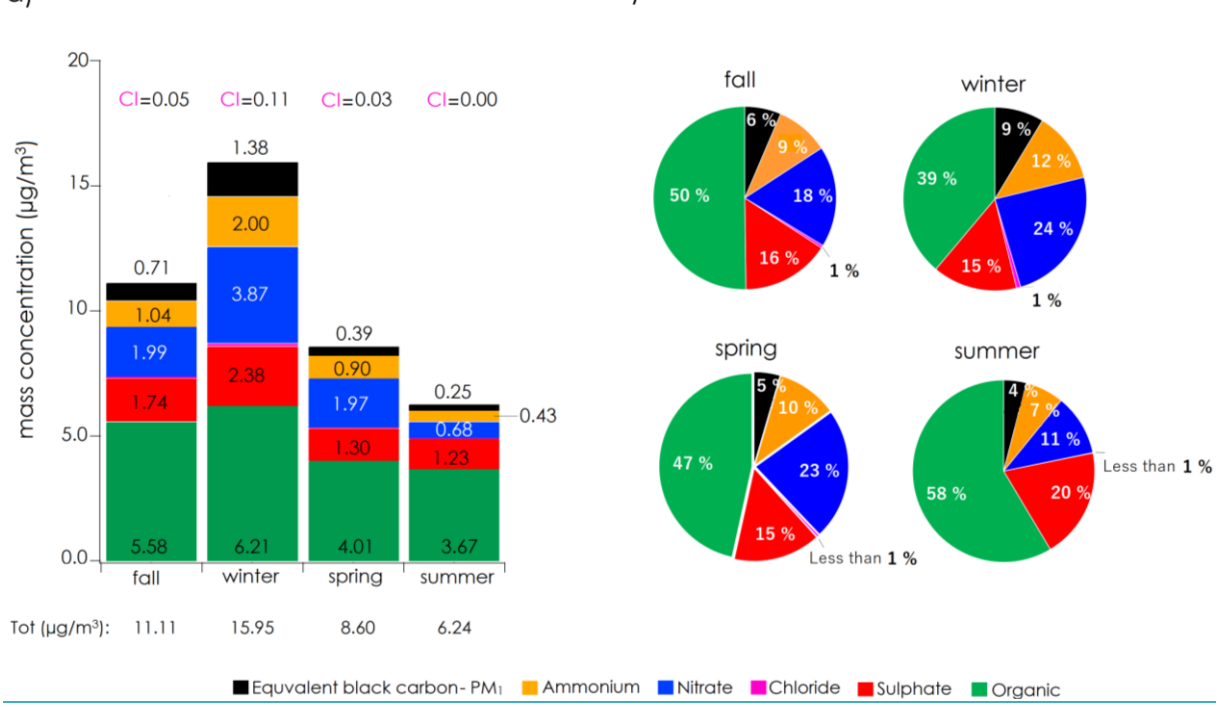

Fig. 2: seasonal variation of PM_1 a) absolute mass concentration and b) mass fraction.

1720

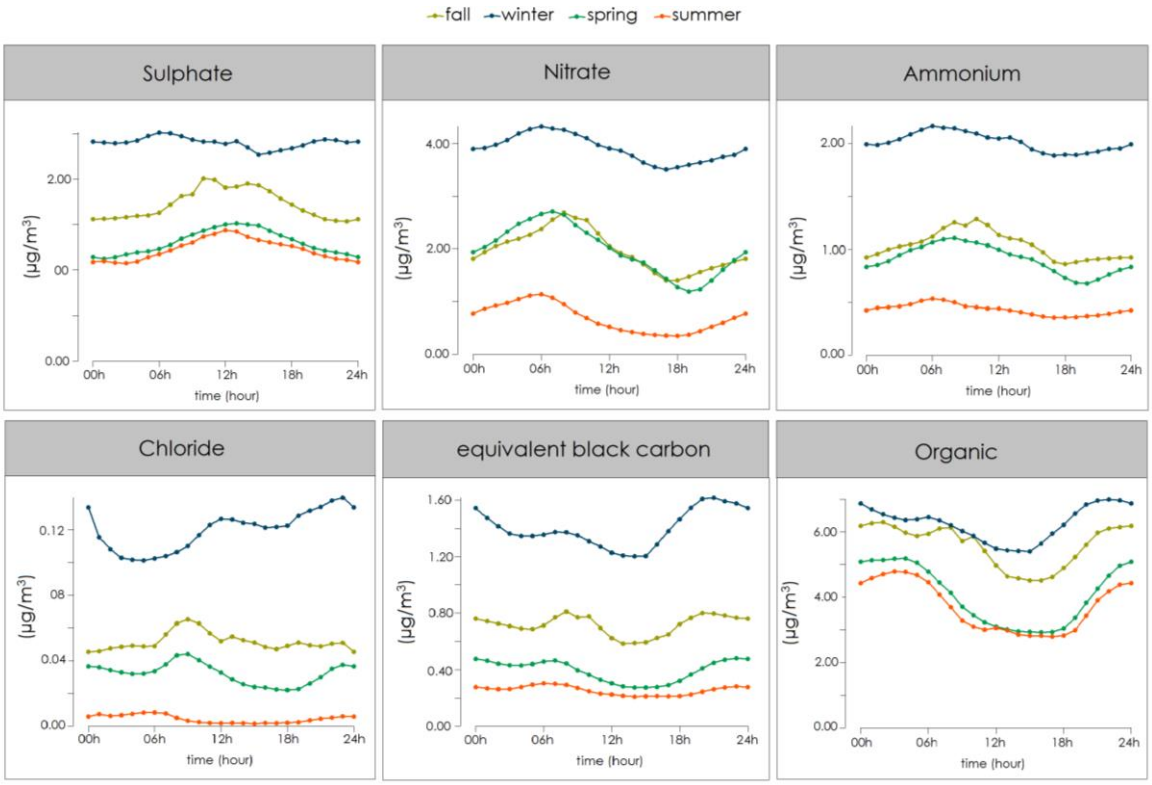
fall
winter
spring
summer
Sulphate
Nitrate
Ammonium
Chloride
equivalent black carbon
Organic
(µg/m³)
time (hour)
00h
06h
12h
18h
24h

1721

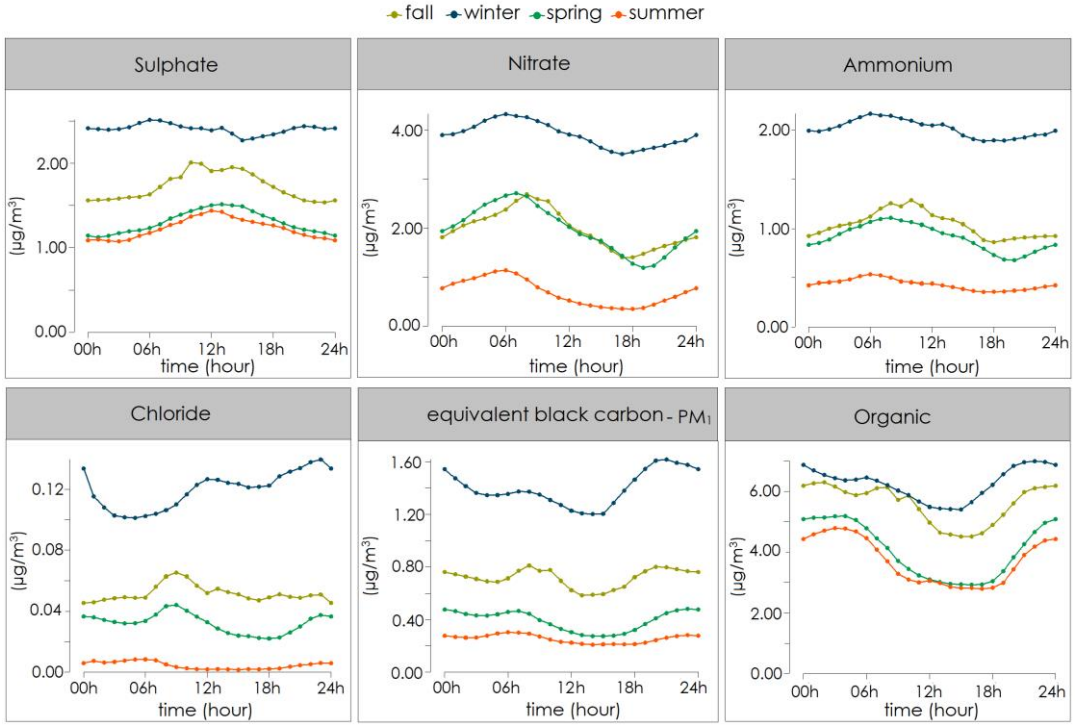
fall
winter
spring
summer
Sulphate
Nitrate
Ammonium
Chloride
equivalent black carbon - PM1
Organic
(µg/m³)
time (hour)
00h
06h
12h
18h
24h

1722

Fig. 3: Seasonal diurnal cycle of PM_1 for ACSM organic and inorganic species (~~Time~~ time is in UTC).

Table. 1: Seasonal/yearly mass concentration of each ACSM species, each PMF factors, contribution of the different POA-PMF-eBC-PM_1~~eBC~~, and correlation of each factors with related species; PM_1.

Species/ Factors		Fall	Winter	Spring	Summer	Yearly
ACSM (µg/m³)	Org	5.58	6.21	4.01	3.67	4.84
	SO_4^{2-}	1.74	2.38	1.30	1.23	1.67
	NO_3^-	1.99	3.87	1.97	0.68	2.16
	NH_4^+	1.04	2.00	0.90	0.43	1.11
	Cl^-	0.05	0.11	0.03	0.00	0.05
MAAP (µg/m³)	eBC -PM_1~~eBC~~	0.71	1.38	0.39	0.25	0.66
PMF (µg/m³)	HOA	0.35	0.36	0.27	0.23	0.30
	BBOA	0.36	0.72	0.27	0.21	0.39
	CCOA	0.72	1.58	0.47	0.30	0.77
	LO-OOA	2.13	1.95	1.24	1.26	1.62
	MO-OOA	2.21	2.25	1.82	1.44	1.92
eBC-PM_1~~eBC~~ (µg/m³)	eBC-PM_1~~eBC~~-HOA	0.16	0.19	0.03	0.04	0.05
	eBC-PM_1~~eBC~~-BBOA	0.34	0.38	0.17	0.15	0.25
	eBC-PM_1~~eBC~~-CCOA	0.23	0.74	0.16	0.02	0.37
eBC-PM_1~~eBC~~ (%)	eBC-PM_1~~eBC~~-HOA	22	15	9	18	8
	eBC-PM_1~~eBC~~-BBOA	47	29	47	69	37
	eBC-PM_1~~eBC~~-CCOA	31	56	44	13	55
Correlation (R^2)	HOA/ eBC-PM_1~~eBC~~	0.49	0.52	0.34	0.24	0.33
	HOA/NO_x	0.23	0.12	0.32	0.23	0.17
	BBOA/Levo.	0.19	0.59	0.09	0.07	0.54
	BBOA/ eBC-PM_1~~eBC~~	0.62	0.81	0.48	0.42	0.77
	CCOA/ eBC-PM_1~~eBC~~	0.65	0.85	0.49	0.30	0.82
	CCOA/Cl^-	0.40	0.41	0.18	0.15	0.46
	LO-OOA/ NO_3^-	0.22	0.59	0.01	0.12	0.19
	LO-OOA/ SO_4^2	0.36	0.55	0.00	0.02	0.23
	MO-OOA / SO_4^2	0.58	0.47	0.34	0.42	0.44
	MO-OOA/ NO_3^-	0.24	0.47	0.16	0.24	0.31

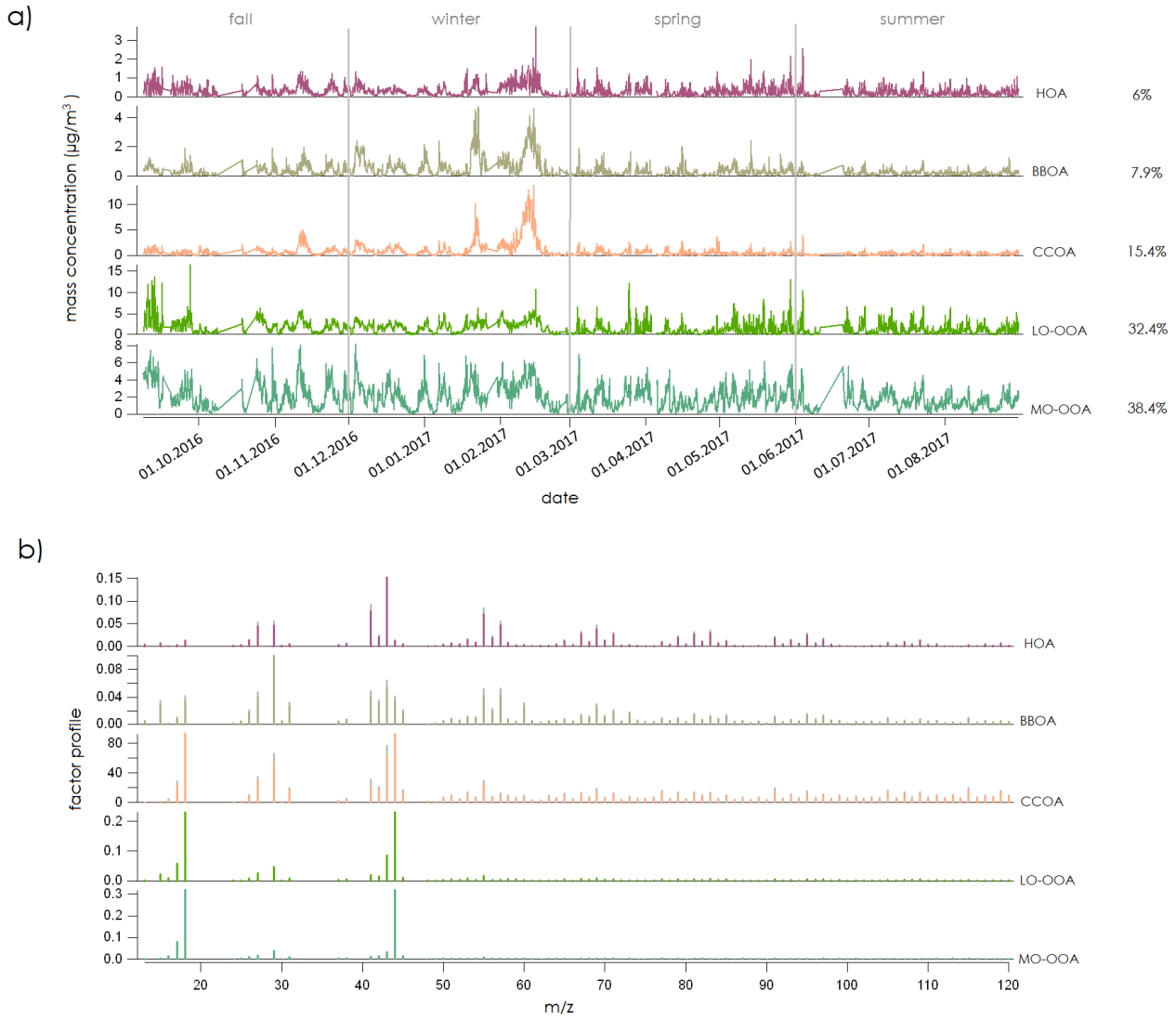
a)
fall
winter
spring
summer
mass concentration (µg/m³)
HOA
6%
BBOA
7.9%
CCOA
15.4%
LO-OOA
32.4%
MO-OOA
38.4%
01.10.2016
01.11.2016
01.12.2016
01.01.2017
01.02.2017
01.03.2017
01.04.2017
01.05.2017
01.06.2017
01.07.2017
01.08.2017
date
b)
factor profile
HOA
BBOA
CCOA
LO-OOA
MO-OOA
m/z

1729

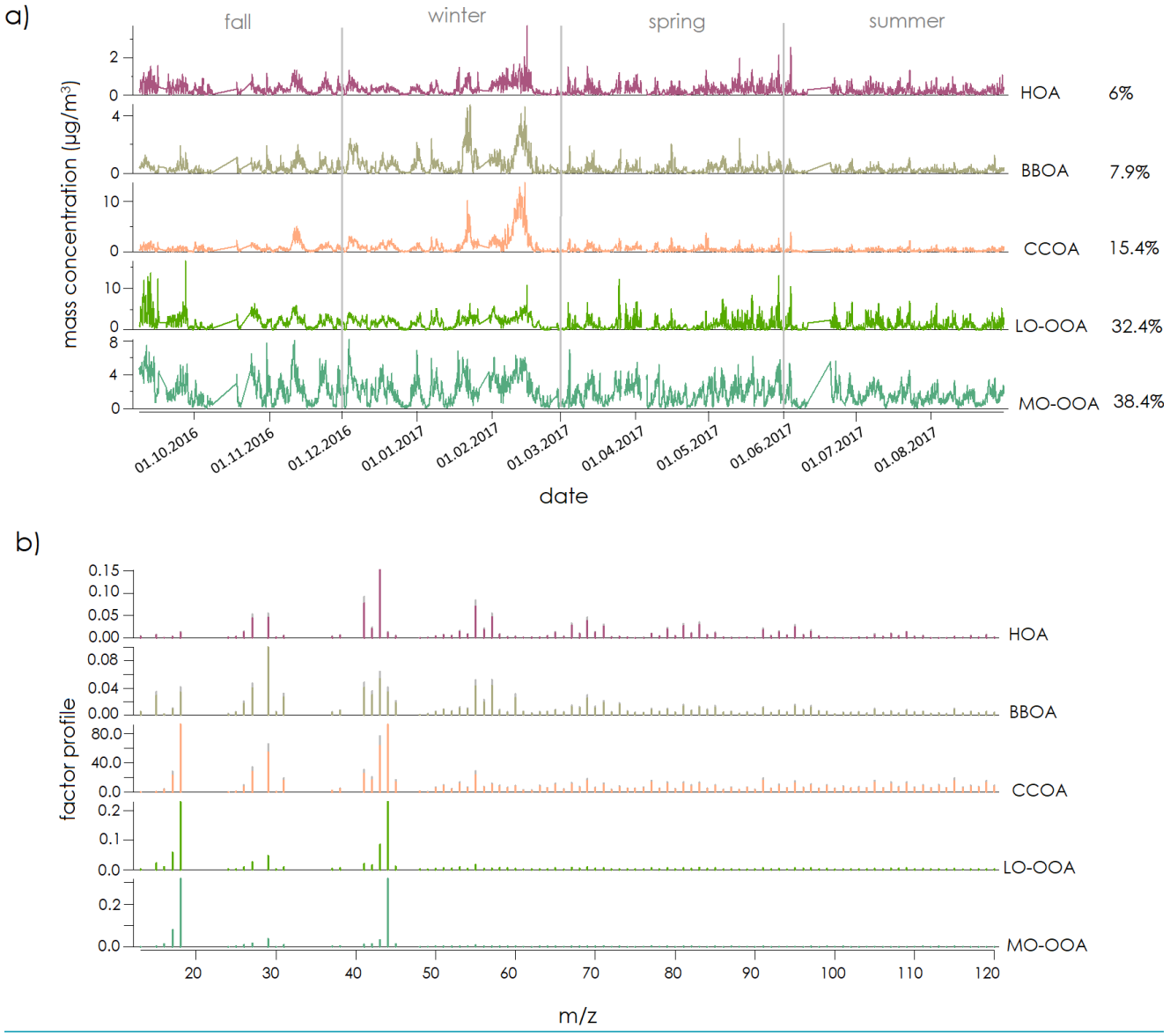

**Fig. 4: Overview of averaged PMF (ME-2) results, a) time series, and b) mass spectral profile of organic PMF factors~~.~~ (~~Time~~ time is in UTC).

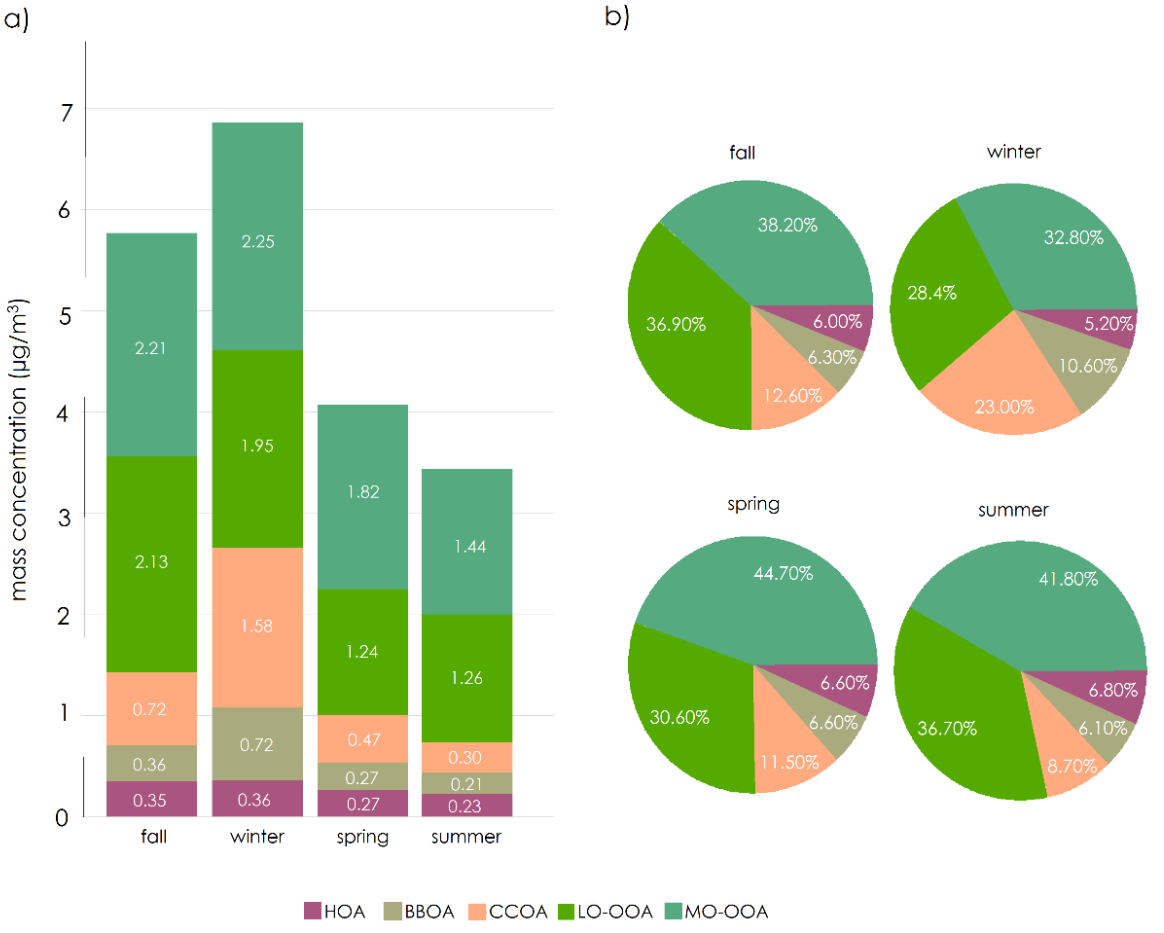
a)
b)
mass concentration (µg/m³)
0
1
2
3
4
5
6
7
2.21
2.13
0.72
0.36
0.35
2.25
1.95
1.58
0.72
0.36
1.82
1.24
0.47
0.27
0.27
1.44
1.26
0.30
0.21
0.23
fall
winter
spring
summer
fall
38.20%
36.90%
6.00%
6.30%
12.60%
winter
32.80%
28.4%
5.20%
10.60%
23.00%
spring
44.70%
30.60%
6.60%
6.60%
11.50%
summer
41.80%
36.70%
6.80%
6.10%
8.70%
HOA
BBOA
CCOA
LO-OOA
MO-OOA

1733

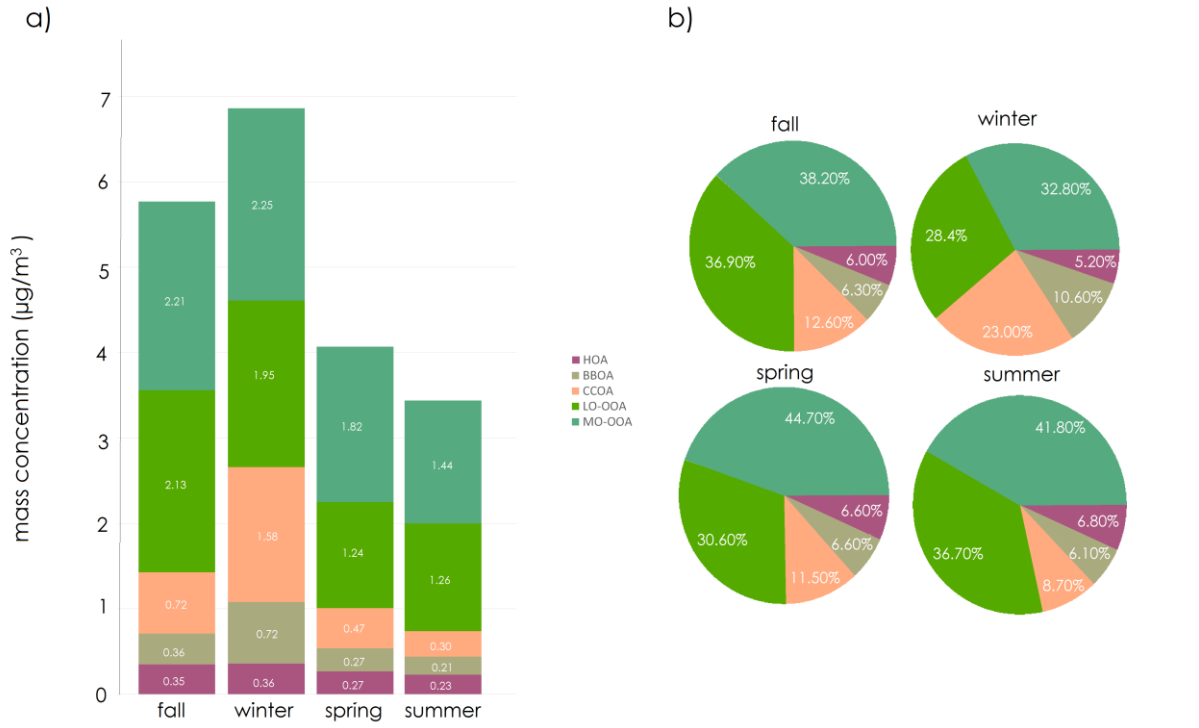

Fig. 5: Seasonal variation of a) mass concentration, b) mass fraction of PMF source factors.


HOA
BBOA
CCOA
LO-OOA
MO-OOA
µg/m³
time (hour)
00h
06h
12h
18h
24h
fall
winter
spring
summer

1736

Fig. 6: Seasonal diurnal cycle (hourly averages) of the organic components HOA, BBOA, CCOA, LO-OOA and MO-OOA in UTC time.

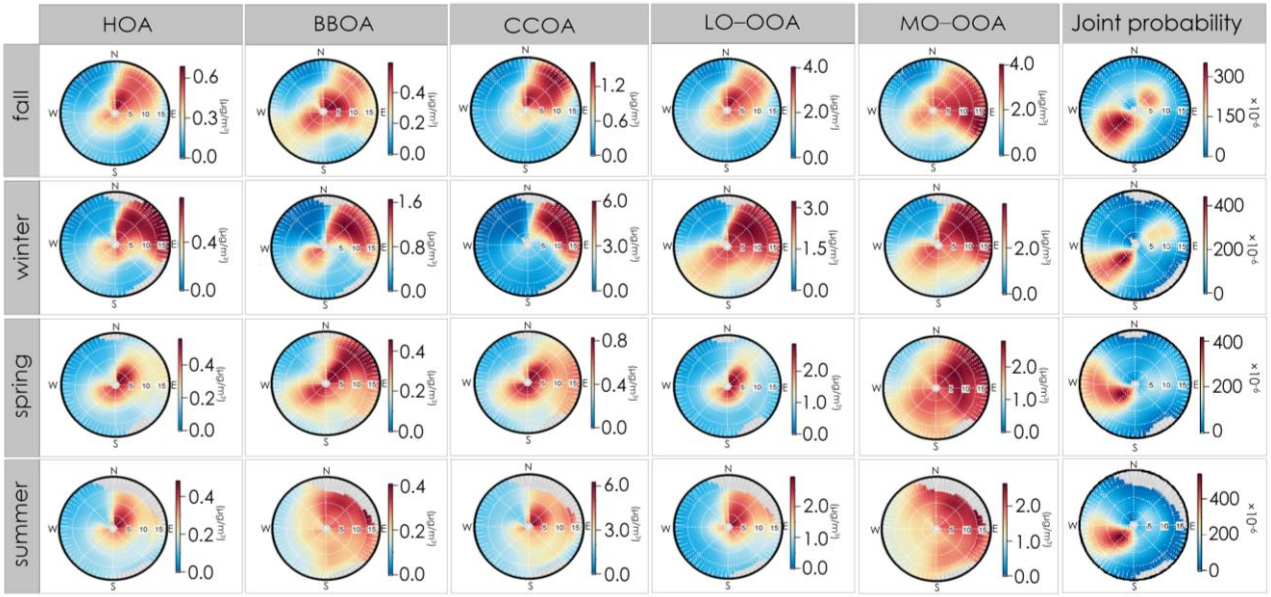

Fig. 7: Seasonal ~~wind roses and~~ NWR plots for the different PMF factors (in µg/m³).

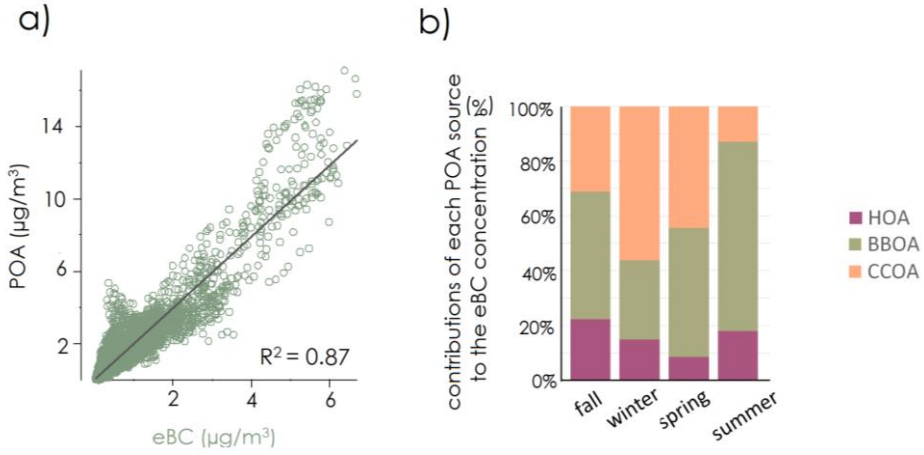

Fig. 8: Contribution of the three POA factors to the mass concentration of eBC-PM$_1$ ~~eBC~~, a) scatter plots POA vs eBC-PM$_1$ ~~eBC~~ and b) contributions of sources to the eBC-PM$_1$ ~~eBC~~ mass concentration.

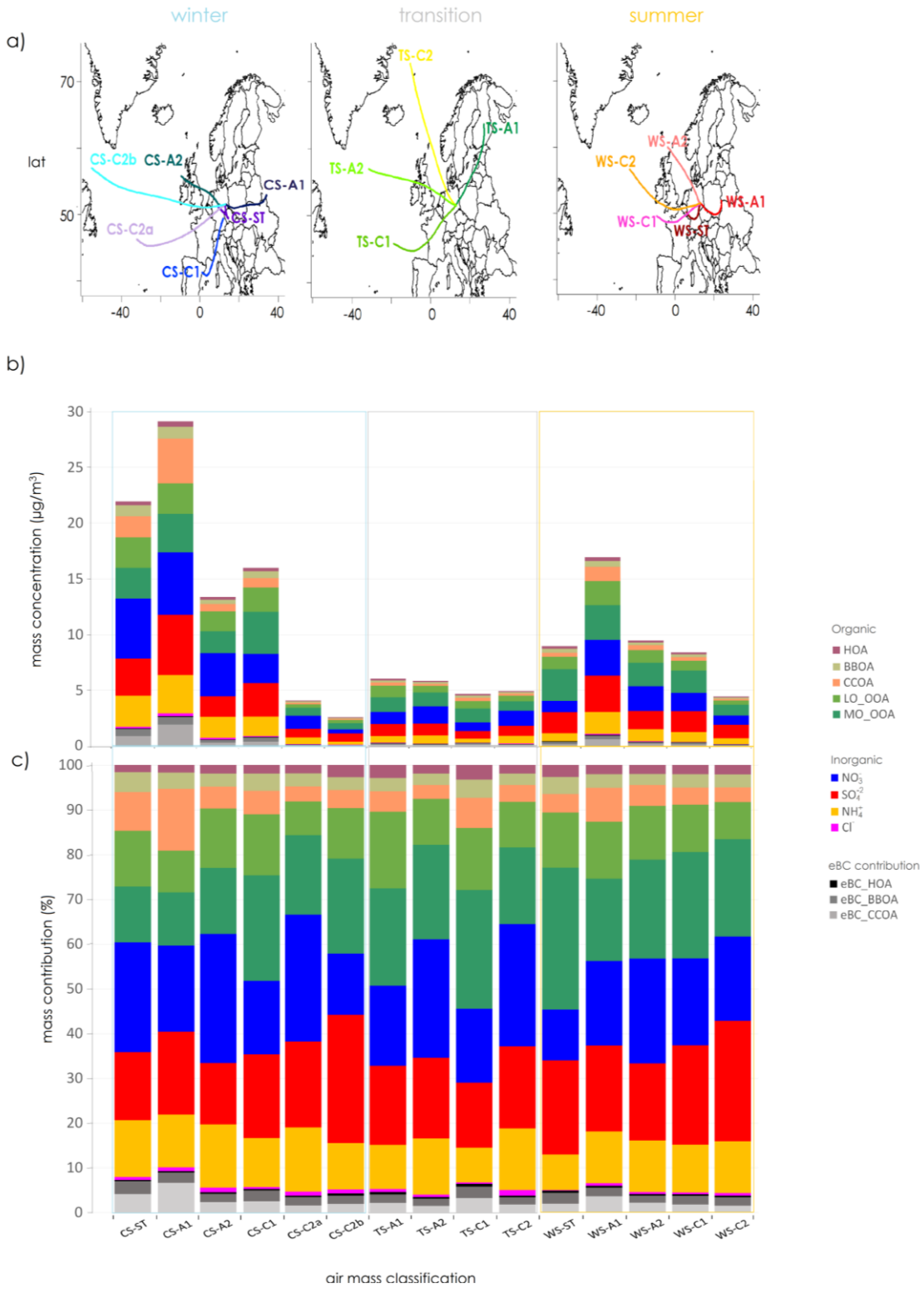
a)
winter
transition
summer
lat
70
50
CS-C2b
CS-A2
CS-A1
CS-ST
CS-C2a
CS-C1
TS-C2
TS-A1
TS-A2
TS-C1
WS-A2
WS-C2
WS-A1
WS-C1
WS-ST
-40
0
40
b)
mass concentration (µg/m³)
30
25
20
15
10
5
0
c)
mass contribution (%)
100
90
80
70
60
50
40
30
20
10
0
CS-ST
CS-A1
CS-A2
CS-C1
CS-C2a
CS-C2b
TS-A1
TS-A2
TS-C1
TS-C2
WS-ST
WS-A1
WS-A2
WS-C1
WS-C2
air mass classification
Organic
HOA
BBOA
CCOA
LO_OOA
MO_OOA
Inorganic
NO3
SO4-2
NH4
Cl
eBC contribution
eBC_HOA
eBC_BBOA
eBC_CCOA

1749

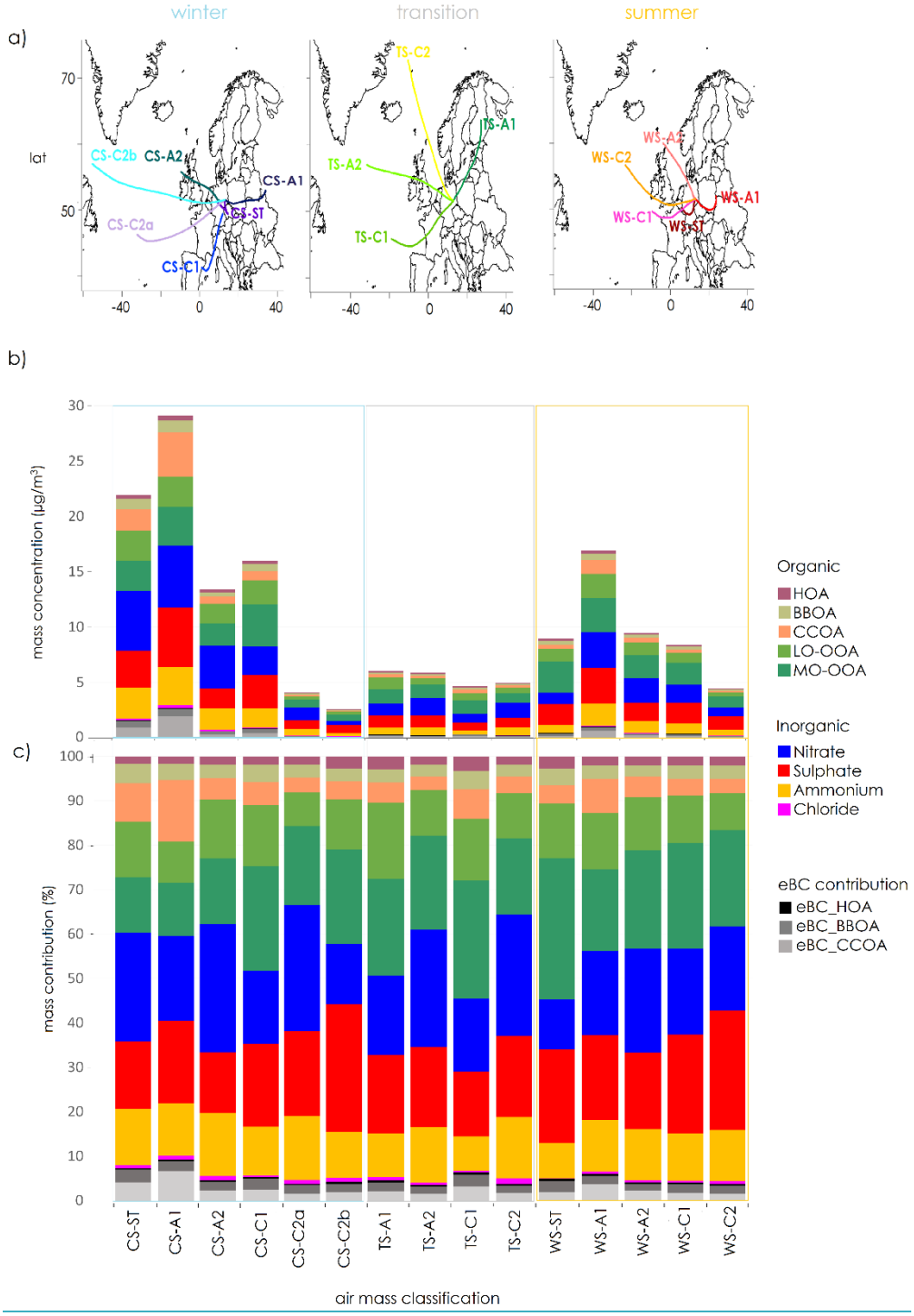

Fig. 9: a) air mass classification based on one-year ~~13 years~~ backward trajectories cluster analysis at 12:00 UTC, b) influence of air mass to the PM_1 data and PMF factors, and c) contribution of them which averaged from 10:00 to 14:00 UTC.

Table. 2: Main statistical details of the 15 air mass types for total PM_1 (CS=Cold Season, WS=Warm Season, ST=Stagnant, A=Anticyclonic, C=Cyclonic).

Main season	Airmass type	Wind direction	Vorticity	Frequency (%)	Total mean ($\mu g/m^3$)
Winter	CS-ST	Stagnating	Anticyclonic	14	21.95
	CS-A1	East	Anticyclonic	18	29.14
	CS-A2	West	Anticyclonic	8	13.39
	CS-C1	South	Cyclonic	10	15.99
	CS-C2a	South West	Cyclonic	3	04.09
	CS-C2b	West	Cyclonic	2	02.60
Transition (Spring/ Fall)	TS-A1	North East	Anticyclonic	4	06.06
	TS-A2	West	Anticyclonic	4	05.86
	TS-C1	South West	Cyclonic	3	04.69
	TS-C2	North West	Cyclonic	4	04.94
Summer	WS-ST	Stagnating	Anticyclonic	6	08.97
	WS-A1	South East	Anticyclonic	11	16.95
	WS-A2	North West	Anticyclonic	6	09.48
	WS-C1	West	Cyclonic	5	08.41
	WS-C2	West	Cyclonic	3	04.46